Flavor Physics at CEPC: a General Perspective

Peter Athron[1], **Lorenzo Calibbi**[2], **Yuzhi Che**[3], **Long Chen**[4], **Mingshui Chen**[3], **Shanzhen Chen**[3], **Shan Cheng**[5], **Hanhua Cui**[3], **Xiaokang Du**[6], **Zhi-Hui Guo**[7], **Jibo He**[8], **Geng Li**[9], **Haibo Li**[3], **Honglei Li**[10], **Lingfeng Li**[11], **Qiang Li**[12], **Xin-Qiang Li**[13], **Yiming Li**[3], **Hao Liang**[3], **Libo Liao**[14], **Tao Liu**[11], **Peng-Cheng Lu**[4], **Hong-Hao Ma**[15], **Kai Ma**[16], **Juan-Juan Niu**[15], **Wenbin Qian**[8], **Qin Qin**[17], **Manqi Ruan**[3], **Xiaoyan Shen**[3], **Zong-Guo Si**[4], **Cristian Sierra**[1], **Huayang Song**[18], **Wei Su**[14], **Fei Wang**[19], **Hengyu Wang**[3], **Jianchun Wang**[3], **Wei Wang**[20], **Yuexin Wang**[3,21], **Xing-Gang Wu**[22], **Yongcheng Wu**[1], **Yuehong Xie**[13], **Zijun Xu**[3], **Haijun Yang**[20], **Hongtao Yang**[23], **Changzheng Yuan**[3], **Xing-Bo Yuan**[13], **Xi-Jie Zhan**[22], **Liming Zhang**[24], **Yang Zhang**[19], **Yanxi Zhang**[25], **Yu Zhang**[26], **Zhen-Hua Zhang**[27], **Zhong Zhang**[28], **Xu-Chang Zheng**[22], **Pengxuan Zhu**[18]

[1] *Nanjing Normal University*
[2] *Nankai University*
[3] *Institute of High Energy Physics, Chinese Academy of Sciences*
[4] *Shandong University*
[5] *Hunan University*
[6] *Institute of Physics, Henan Academy of Sciences*
[7] *Hebei Normal University*
[8] *University of Chinese Academy of Sciences*
[9] *Hangzhou Institute for Advanced Study, University of Chinese Academy of Sciences*
[10] *University of Jinan*
[11] *Hong Kong University Of Science And Technology*
[12] *Northwestern Polytechnical University*
[13] *Central China Normal University*
[14] *Sun Yat-Sen University*
[15] *Guangxi Normal University*
[16] *Shaanxi University of Technology*
[17] *Huazhong University of Science and Technology*
[18] *Institute of Theoretical Physics, Chinese Academy of Sciences*
[19] *Zhengzhou University*
[20] *Shanghai Jiao Tong University*
[21] *China Center of Advanced Science and Technology*
[22] *Chongqing University*
[23] *University of Science and Technology of China*
[24] *Tsinghua University*
[25] *Peking University*
[26] *Hefei University of Technology*
[27] *University of South China*
[28] *University College London*

Contents

1 Introduction

The Circular Electron Positron Collider (CEPC) [1] was proposed in 2012 by the Chinese high-energy physics community to function primarily as a Higgs factory at a center-of-mass energy of 240 GeV. Additionally, it is also set to operate as a Z factory at the Z-pole, conduct precise WW threshold scans, and potentially be upgraded to a center-of-mass energy of 360 GeV, above the $t\bar{t}$ threshold. In the proposed nominal operation scenario [2], the CEPC is anticipated to produce significant quantities of Higgs and Z bosons, W boson pairs and, potentially, top quarks. With respect to accelerator design, the development of key technologies has led to significantly enhancement in instantaneous luminosities compared to those repeoted in the Conceptual Design Report (CDR), as shown in Figure 1. Based on this progress, the CEPC study group proposes a new nominal operation scenario, which would allow for precision measurements of Higgs boson couplings, electroweak observables, QCD differential rates, and provide ample opportunities to search for rare decays and new physics (NP) signals, as seen in Table 1. Moreover, the large quantities of bottom quarks, charm quarks, and tau leptons from the decays of Z bosons create opportunities for numerous critical flavor physics measurements. It should be noted that the results presented here are based on the updated running scenario using a 50 MW synchrotron radiation (SR) power beam.

Flavor physics, as a well-developed area of investigation in particle physics, has contributed substantially to the establishment of the Standard Model (SM) over recent decades. This has been achieved through the examination of the properties of SM fermion flavors in a myriad of experiments and has yielded significant findings and discoveries. CEPC can serve as a flavor factory, and its flavor physics program enhances the CEPC's overarching
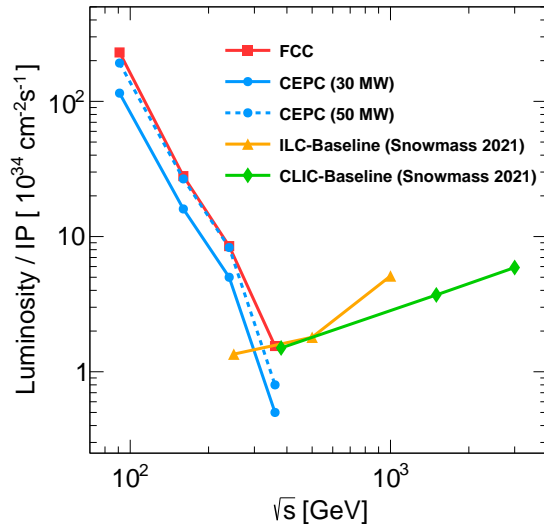

Figure 1: Updated run plan of the CEPC, with the baseline and upgrade shown in solid and dashed blue curves, respectively. The run plans for several other proposals of e^+e^- colliders are also shown for comparison. See [2] for details.

Operation mode	Z factory	WW threshold	Higgs factory	$t\bar{t}$
$\sqrt{s}$ (GeV)	91.2	160	240	360
Run time (year)	2	1	10	5
Instantaneous luminosity ($10^{34}\mathrm{cm}^{-2}\mathrm{s}^{-1}$, per IP)	191.7	26.7	8.3	0.83
Integrated luminosity (ab^{-1}, 2 IPs)	100	6.9	21.6	1
Event yields	4.1×10^{12}	2×10^7	4.3×10^6	6×10^5

Table 1: Nominal CEPC operation schemes of four different modes. See [2] for details.

physics objectives. The flavor sector provides substantial motivation for CEPC operation, given the existing multitude of unknowns within the SM.

Understanding the flavor physics potential of the CEPC is not an isolated field of study, but also influences other primary fields to be explored at the CEPC, including Higgs physics, electroweak (EW) physics, QCD physics, and Beyond the Standard Model (BSM) physics. For instance, within the SM, the fermion mixing, specifically the Cabibbo-Kobayashi-Maskawa (CKM) matrix [3, 4] and its hierarchical structure, originates from the Yukawa couplings between the Higgs field and the fermion gauge eigenstates. While some of the fermion Yukawa couplings will be pinned down by the CEPC [5], studying the origin of the off-diagonal flavor mixing terms and their CP-violating phases remains the main goal of flavor physics. Conversely, while most heavy-flavored particles decay via EW transitions at the tree level, many rare processes are induced by EW one-loop effects. Their measurements may also serve as an alternative test of the EW sector at a lower energy scale. Meanwhile, many electroweak precision observables (EWPOs) necessitate precise flavor tagging and reconstruction for high precision, $e.g.$, the forward-backward asymmetry of c and b quarks. Furthermore, most flavor physics studies involve QCD, since all quarks are colored and the τ can decay to hadronic final states. In fact, most flavor physics studies rely on the theory of QCD, either perturbatively or non-perturbatively, to provide insights into the corresponding production, spectroscopy, and decay of hadronic states. In turn, the plethora of flavor measurements could provide crucial inputs to, and calibration of, QCD theories in multiple ways. It is also noteworthy that flavor physics provides a set of probes sensitive to BSM physics. For instance, the decay width of a fermion f is suppressed by the small factor $G_F^2 m_f^4 \lesssim 10^{-7}$, and thus f becomes long-lived. Therefore, even minor BSM effects could reveal themselves on top of such extremely narrow SM widths. Finally, the ambitious goals of flavor physics studies push the frontier of instrumentation, demanding enhanced detector performance in vertexing, tracking, particle identification (PID), and calorimetry.

The successful realization of the flavor physics program at the CEPC relies on a number of key factors:

- One of these is the significant luminosity of the Z pole run of the CEPC, which yields substantial heavy flavor statistics. With a high integrated luminosity and

Particle	BESIII	Belle II (50 ab^{-1} on $\Upsilon(4S)$)	LHCb (300 fb^{-1})	CEPC (4×Tera-Z)
B^0, $\bar{B}^0$	-	5.4×10^{10}	3×10^{13}	4.8×10^{11}
$B^{\pm}$	-	5.7×10^{10}	3×10^{13}	4.8×10^{11}
B_s^0, $\bar{B}_s^0$	-	6.0×10^8 (5 ab^{-1} on $\Upsilon(5S)$)	1×10^{13}	1.2×10^{11}
$B_c^{\pm}$	-	-	1×10^{11}	7.2×10^8
Λ_b^0, $\bar{\Lambda}_b^0$	-	-	2×10^{13}	1×10^{11}
D^0, $\bar{D}^0$	1.2×10^8	4.8×10^{10}	1.4×10^{15}	8.3×10^{11}
$D^{\pm}$	1.2×10^8	4.8×10^{10}	6×10^{14}	4.9×10^{11}
$D_s^{\pm}$	1×10^7	1.6×10^{10}	2×10^{14}	1.8×10^{11}
$\Lambda_c^{\pm}$	0.3×10^7	1.6×10^{10}	2×10^{14}	6.2×10^{10}
$\tau^{\pm}$	3.6×10^8	4.5×10^{10}		1.2×10^{11}

Table 2: Expected yields of b-hadrons, c-hadrons, and τ leptons at BESIII, Belle II, LHCb Upgrade II, and CEPC (4×Tera-Z, namely 4×10^{12} Z bosons). For b- and c-hadrons, their yields include both charge conjugates, while the yield of τ leptons refers to the $\tau^+\tau^-$ events, namely the number of τ pairs. The cross sections for $b\bar{b}$ and $c\bar{c}$ productions at $E_{\rm cm}(\Upsilon(4S))$ and $E_{\rm cm}(\Upsilon(5S))$ are taken from [6]. The b-quark production cross section in the acceptance of LHCb is taken from [7]. We use the production fractions of B_s^0 and Λ_b^0 in [8] and assume $f_u + f_d + f_s + f_{\rm baryon} = 1$, $f_u = f_d$, and $f_{\Lambda_b^0} = f_{\rm baryon}$ to estimate the production fractions of B^0 and $B^{\pm}$ at LHCb. The production fractions of B^0, $B^{\pm}$, B_s^0, and Λ_b^0 in Z decays are taken from [9]. As for the B_c meson, its production fraction at the Z-pole (including the contribution from B_c^* decays) is taken from [10], while its production fraction at LHCb is taken from [11]. For inclusive charm meson production at the Z pole including b-hadron decay products, see [12–16]. Yields of τ leptons at CEPC 4×Tera-Z scenario are scaled from [1].

large $\sigma(e^+e^- \to Z \to b\bar{b}, c\bar{c}, \tau^+\tau^-)$, the Tera-$Z$ will generate extensive statistics of flavored hadrons and τ leptons, rivaling other proposed flavor physics experiments [1]. This is demonstrated by the expected yields of b-hadrons in Belle II, LHCb and a representative future Z factory, as listed in Table 2, with the Tera-Z yields reaching approximately 4.8×10^{11} $B^0/\bar{B}^0$ or $B^{\pm}$ mesons, almost one order of magnitude larger than that in Belle II [6].

- The clean environment of e^+e^- collisions constitutes another cornerstone, substantially diminishing the background level and systematic uncertainties associated with neutral particles. This environment is particularly beneficial in studying flavor physics involving heavy b-hadrons, especially given the significantly limited event reconstruction efficiency in the noisy data environment of the LHCb [17].

- The heavy $m_Z \gg m_{b,c,\tau,s}$ and $\Lambda_{\rm QCD}$ also underpin the success of the project, facilitating the production of a wide array of species. Even soft decay products of flavored particles are expected to be boosted to higher energies and larger displacements,

augmenting measurement precision.

- Lastly, state-of-the-art detector technologies and algorithms under development today will be crucial when deployed in the CEPC era. These technologies will enhance the investigation of extremely rare decay modes that contain neutral or invisible particles, as the cleanliness of a lepton collider enables such studies. The evolving field of advanced algorithms, especially deep learning ones, could also benefit flavor physics at the CEPC in almost all aspects by fully utilizing the large amount of data recorded from the hardware.

While the flavor physics program at the CEPC simultaneously benefits from the various advantages above, it also confronts new challenges. The first of these challenges is related to the significant increase in event statistics at the CEPC, which is expected to be greater by a factor $\gtrsim \mathcal{O}(10^5)$ than the LEP run at the Z pole. Given the improved detector systems and electronics, the volume of data to be processed will increase substantially. Concurrently, the precision goals of flavor physics, driven by theoretical interests, will also reach an elevated level in the CEPC era. Therefore, it becomes essential to enhance understanding of backgrounds and to control systematic effects in order to prevent dominance by systematic uncertainties, which could potentially undermine the benefits of the CEPC's high luminosity.

A second challenge arises from the abundance of viable channels for study at the CEPC. Compared to proposed future flavor physics experiments or upgrades of current ones, the relative improvement achievable by the CEPC or other future lepton colliders varies. Initial studies indicate that while the CEPC could enhance the precision of measurements by orders of magnitude in many instances, the improvement could be marginal in others. Therefore, identifying the most valuable systems, or "golden channels" - those with the highest potential for significant discoveries - for investigation in the CEPC context could substantially conserve future resources. As it stands, some of these golden modes at the CEPC may be overlooked as they are not suitable for existing experiments.

Lastly, numerous direct observables require interpretation via an appropriate theory before they can augment knowledge of flavor physics. Theoretical inputs come in multiple forms, such as: the non-perturbative theory of hadronization; perturbative QCD and EW corrections of fermion production; lattice extrapolation of heavy flavor form factors; the relation between the CKM matrix elements and observed CP asymmetries; as well as the proper modeling of the electron beam and detector system. In order to accurately scrutinize the SM or to search for NP, the precision of theoretical tools must align with experimental outputs.

Given the aforementioned challenges and still incomplete community contributions to the project, the principal objective of this document is to provide a stage summary of current advancements across multiple aspects of flavor physics. Special attention is devoted to phenomenological analyses and sensitivity projections that utilize Monte Carlo (MC) simulations to substantiate their conclusions. Due to the occasional unavailability of corresponding theory tools, discussions concerning theoretical uncertainties are deferred to future studies. Additionally, this document aims to offer guidance and recommendations

for forthcoming individual studies. The suggestion of some candidate golden channels is intended to stimulate further research targeting relevant channels, thereby maximizing the physics outputs.

During the compilation of this white paper, simultaneous efforts were dedicated to promoting flavor physics programs for other proposed future lepton colliders, such as the Future Circular Collider (FCC-*ee*) [18, 19] and the Internation Linear Collider (ILC) [20], both of which also include a Z-factory phase and higher energy operations. In particular, the FCC-*ee* Z pole run has a similar integrated luminosity ($150\,\text{ab}^{-1}$) to the current CEPC proposal, and the higher-energy runs are likewise comparable. Since both proposals share similar detector performances [1, 21], and both adopt a particle flow oriented detector design [1] and IDEA detector design [22], relevant FCC-*ee* studies were also incorporated into the current summaries, with only minimal rescaling applied as necessary. It is hoped that the content of this white paper, especially its suggestions for the future, could aid forthcoming studies in the FCC-*ee* context and also in other e^+e^- factories.

This document is structured as follows. In Section 2, we provide an overview of the CEPC facility, delineating key features of the collider and detector that are crucial for flavor physics. Additionally, the simulation methods utilized at the CEPC are explained. Section 3 delves into Flavor Changing Charged Current (FCCC)-mediated semileptonic and leptonic b decays, discussing their theoretical framework, recent progress and future research directions. Rare b decays mediated by Flavor Changing Neutral Current (FCNC) are explored in Section 4, featuring a preliminary theoretical interpretation and discussion of dileptonic, neutrino and radiative modes. Section 5 is dedicated to the measurement of CP asymmetries, followed by Section 6 which discusses tests of the SM global symmetries. Prospects of hadron spectroscopy and exotic states are covered in Section 11, while Sections 7 and 8 focus on charm/strange and τ physics respectively. Section 10 extends the discussion to flavor physics at higher energies, including exclusive hadronic decays of heavy bosons and $|V_{cb}|$ measurements from on-shell W decays, as well as touches upon other possibilities. Finally, the production of BSM states from heavy flavor interactions forms the central theme of Section 12. All discussions are summarized in Section 13.

2   Description of the CEPC Facility

2.1   Key Collider Features for Flavor Physics

As an e^+e^- collider operating around the EW scale, flavor physics studies at the CEPC are affected by three major features. Firstly, as $\sqrt{s} \gg m_{b,c,\tau}$, the CEPC produces highly relativistic heavy flavor quarks or leptons. Their boosted decay products allow for precise momentum and lifetime measurements. This is in contradistinction to the situations at low energy e^+e^- colliders such as Belle II [6], BaBar [23], BESIII [24], and other future proposals, such as the Super Tau-Charm Factory (STCF) [25]. Secondly, as an e^+e^- collider, the CEPC provides a clean environment for flavor physics studies with low QCD backgrounds, negligible pileup events, and an almost fixed E_{cm}. Compared to hadron collider experiments, such as the LHCb [26], the CEPC enables more effective identification and reconstruction of final states that include neutral or invisible particles. The above

Operation mode	Z factory	WW threshold	Higgs factory	$t\bar{t}$
$\sqrt{s}$ (GeV)	91.2	160	240	360
Beam size σ_x (μm)	6	13	15	39
Beam size σ_y (μm)	0.035	0.042	0.036	0.113
Bunch length (total, mm)	8.7	4.9	3.9	2.9
Crossing angle at IP (mrad)		33		

Table 3: Beam size, bunch length, and crossing angle at different operation modes of the CEPC [2].

arguments show the uniqueness of CEPC flavor physics studies. Thanks to advanced accelerator design grants, the large instantaneous luminosity will allow to collect $\mathcal{O}(10^5)$ times more statistics than the LEP Z-pole run [27]. As a consequence, the search and analysis strategies may differ significantly from those employed in relevant studies at LEP. For instance, high signal statistics allows sharper cuts to reduce backgrounds. At the same time, one needs to carefully address other systematic uncertainty sources using the plethora of data. Hence, the large luminosity of the CEPC brings new challenges and invalidates several luminosity projections from LEP. Such challenges are especially severe for precision measurements.

According to the CEPC CDR [1], the beam energy spread could typically be controlled to the level of 0.1%. This, together with a detector that can reconstruct precisely the hadronic events – allowing for precise determination of missing energy/momentum – thus enables relevant physics measurements with high precision; for instance, tagging leptonic heavy quark decay and searching for dark matter candidates in hadronic events, especially at the Z factory mode.

The CEPC uses a nano beam scenario and therefore the typical beam spot sizes are of order μm in the x direction, order nm in the y direction, and correspondingly of order a few hundred μm in the z direction. The beam sizes at different operation modes of the CEPC are summarized in Table 3. The accelerator could stabilize the collision area with a typical size of order μm in the transverse direction and of order $\sim \mathcal{O}(100)$ μm along the beam direction. The spatial uncertainty of the interaction point could therefore be limited, enabling high precision measurements with τ final states – for example, in dark matter searches with $Z \to \tau^+\tau^-$ events at Z factory.

2.2 Key Detector Features for Flavor Physics

Flavor physics program at Tera-Z is enormously rich and extremely demanding on detector performance. In general, a Tera-Z detector would have a large acceptance with a solid angle coverage of at least $|\cos\theta| < 0.99$. This detector would also have a low energy/momentum threshold at the 100 MeV level in order to record and recognize low energy objects that characterize certain hadron decays, $e.g.$, soft photons and pions generated from excited heavy hadrons, as well as some low energy hadrons that are essential for understanding relevant QCD processes [28].
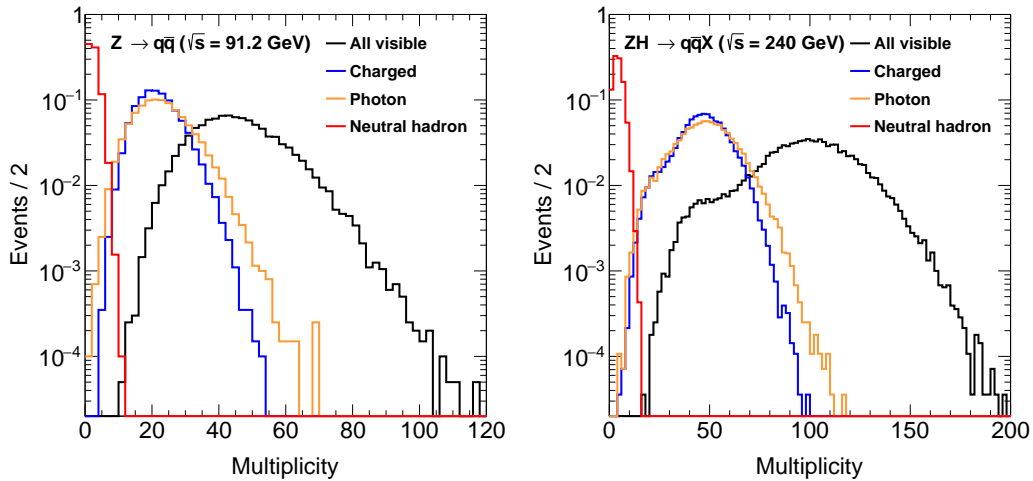
Figure 2: Multiplicities of different types of final state particles in $Z \rightarrow q\bar{q}$ (91.2 GeV) and $Z(\rightarrow q\bar{q})H(\rightarrow \text{inclusive})$ (240 GeV) events.

To efficiently separate signal events from background, it is essential to identify the relevant physics objects and to precisely reconstruct their properties – especially their energy/momentum. For a Tera-Z detector, a typical benchmark is to reconstruct the intermediate particles, such as $\pi^0 \rightarrow \gamma\gamma$, $K_S^0 \rightarrow \pi^+\pi^-$, $\phi \rightarrow K^+K^-$, $\Lambda \rightarrow p\pi^-$, etc, inside hadronic Z events. A more challenging case would be to identify the decay products of a target heavy flavor hadron which may decay into $\mathcal{O}(10)$ particles with a complicated and rich decay cascading order inside a jet. These decay products include not only charged final state particles (leptons and charged hadrons), but also photons, neutral hadrons, and the missing energy/momentum induced by neutrinos. A hadronic Z event could has upto 100 final state particles, as shown in Figure 2. To successfully separate and reconstruct the relevant final state particles of the target particle is a key challenge for the measurements performed in hadronic Z events, and it is necessary to employ the particle flow method [29, 30], which emphasizes the separation of final state particles and has been proven capable of providing better reconstruction of both the hadronic system and of the missing energy/momentum.

In addition, good intrinsic resolution of sub-detectors, (*i.e.*, momentum reconstruction by the tracker and energy measurement by the calorimeter), is always critical for flavor physics measurements. It not only leads to the precise reconstruction of physics properties such as particle masses, but also significantly reduces the combinatory background especially present in physics measurements with narrow resonances. In particular, determining how to achieve an excellent electromagnetic (EM) energy resolution with a particle flow oriented high-granularity calorimeter is indeed challenging but necessary for the flavor physics program, since photons and neutral pions are common decay products in many fundamental flavor physics measurements. The benchmark analysis of CKM angle α measurement via $B \rightarrow \pi\pi$ [31] suggests an EM resolution of order $\mathcal{O}(3\%/\sqrt{E})$ in order to fulfill the requirement of 3σ separation between B^0 and B_s^0 with a 30 MeV B-meson mass
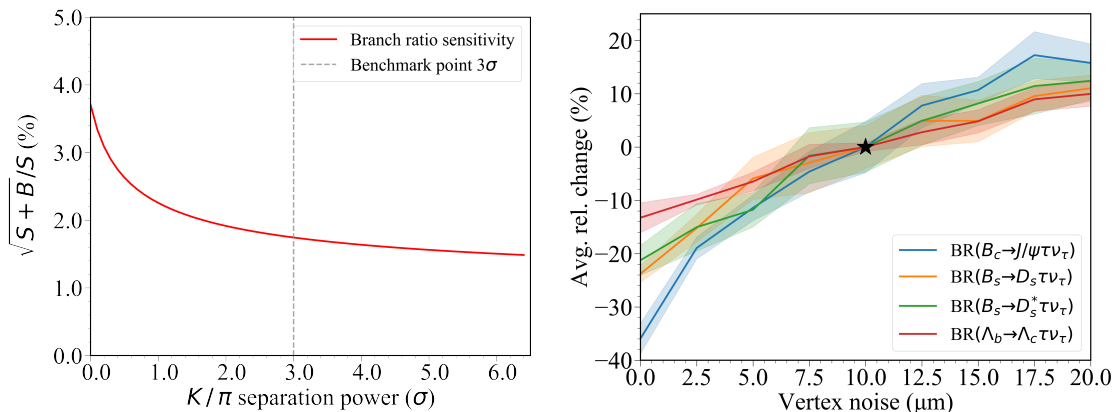
Figure 3: **LEFT:** Sensitivity of measuring $\mathrm{BR}(B_s \to \phi\nu\bar{\nu})$ as a function of PID performance, parameterized by the K/π separation power [35]. **RIGHT:** Precision variance of measuring $\mathrm{BR}(H_b \to H_c\tau\nu_\tau)$ as a function of detector vertex noise [38], with stared reference point set by a vertex noise of 10 μm.

resolution.

Most of the flavor physics measurements are relevant to hadronic events, especially di-jet events at the Z pole. It is essential to identify the origin of a jet, i.e., to determine whether it is originated from a quark, an anti-quark, or even a gluon. The jet origin identification [32], to a certain extend, shall be regarded as a natural extension of jet flavor tagging, quark-gluon jet separation, and jet charge measurements, which is indispensable in flavor physics measurements such as CKM and CP violation measurements.

A successful flavor physics program also needs a high efficiency/purity PID. An efficient PID not only suppresses the combinatory background induced by misidentified particles, but also separates decays with similar topologies in final states, such as $B^0_{(s)} \to \pi^+\pi^-$, $B^0_{(s)} \to K^+K^-$, and $B^0_{(s)} \to K^\pm\pi^\pm$ [33]. A decent PID is also critical for the jet origin identification [32, 34] and relevant physics measurements such as the Higgs rare/exotic decay measurement [32]. The benchmark analysis of $B_s \to \phi\nu\bar{\nu}$ [35] shows that a relative sensitivity of $\mathrm{BR}(B_s \to \phi\nu\bar{\nu})$ less than 2% at a Tera-Z collider requires a $3\,\sigma$ K/π separation for the identification of charged hadrons, see the left panel of Figure 3. This requirement can be addressed by multiple PID technologies. For instance, the CEPC baseline detector can separate different species of hadrons using dE/dx information measured by TPC and TOF information provided by either an dedicated TOF device, or combining TOF and ECAL together. Detector optimization study[36] suggests that dE/dx needs to reach 3% with combination of a TOF resolution of 50 ps to statisfy this PID requirement. In addition, the dN/dx technology proposed by drift chamber of IDEA concept [37] is promising to further improve the PID performance.

A high-precision and low-material vertex system is vital for the CEPC flavor physics program. Precise vertex measurements provide pivotal information to distinguish the species of the initial quark that fragments into a jet, namely the jet origin identification. Precise vertex information is also critical for determining the decay time or lifetime
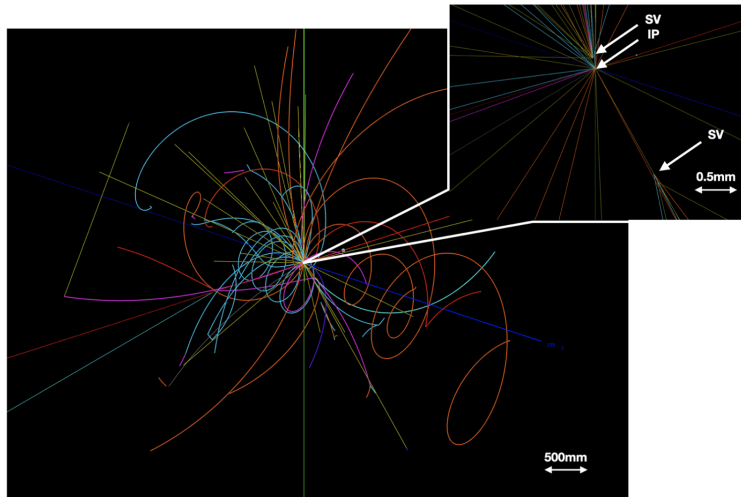
Figure 4: Display of a $Z \to b\bar{b}$ event with typical secondary vertices (SV).

of heavy flavor hadrons with high precision. To match the characteristic timescales such as those of $B_s - \bar{B}_s$ mixing (~ 56 fs), of D_s decay (~ 500 fs), and of τ decay (~ 290 fs), the lifetime resolution is required to reach order $\mathcal{O}(10)$ fs. This accurate lifetime measurement also benefits flavor tagging and time-dependent CP violation measurements. In addition, a high-performance vertex system can provide a precise reconstruction of the secondary vertices that characterize some heavy flavor hadron decays, such as the example shown in Figure 4. Such a system can also help to suppress the background, especially from the IP. One concrete application can be the measurements of FCCC-mediated $\mathrm{BR}(H_b \to H_c \tau \nu_\tau)$, where the H_b reconstruction can significantly rely on the determination of the H_c decay vertex and the measurement of the muon track originating from the τ decay [38]. As shown in the right panel of Figure 3, the reduced noise of vertex system can uniformly benefit these measurements, yielding an improvement in precision of $\mathcal{O}(10\%)$ level.

The above-mentioned requirements are also highly beneficial for physics programs at higher center-of-mass energies, *i.e.* the 160 GeV W^+W^- threshold scan, the 240 GeV Higgs run, and the 360 GeV top operation. On top of their core physics programs, such as W mass and precise Higgs/top properties measurements, the data samples and key detector features also support an intensive flavor physics program, see Section 10.

To address these physics requirements, intensive efforts on detector conceptual design, on physics performance study, and on key technology R&D have been performed. We refer to two benchmark detector concepts in this white paper. These concepts are used in the simulations in this manuscript, providing reference performance for relevant physics potential studies.

The starting point of our discussion is the CEPC baseline detector as delineated in its CDR study [1]. Guided by the particle flow principle, the CEPC baseline design features a high-precision tracking system, a high-granularity calorimeter system, and a high magnetic field. Shown in detail in Figure 5, the CEPC baseline detector consists, from inside
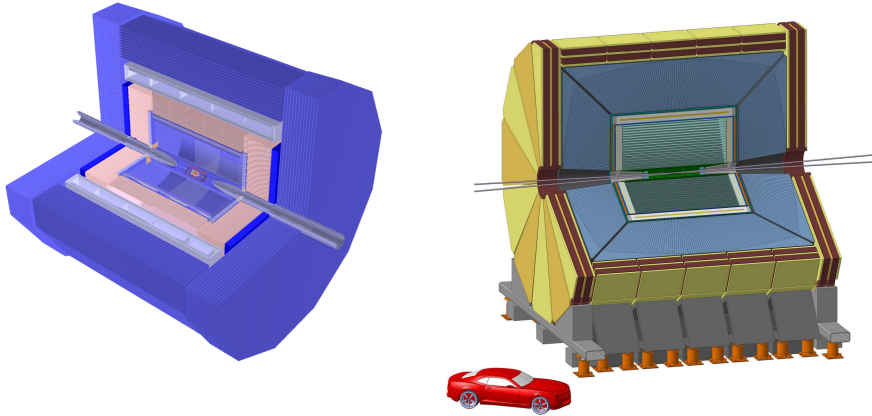
Figure 5: Schematic layouts of the CEPC baseline detector [1] (left) and the IDEA detector [39] (right).

to outside, of a silicon pixel vertex detector, a silicon tracker, a time projection chamber (TPC), a silicon-tungsten sampling EM calorimeter (Si-W ECAL), a steel-glass resistive plate chambers sampling hadronic calorimeter (SDHCAL), a superconducting solenoid providing a magnetic field of 3 Tesla, and a flux return yoke embedded with a muon detector. Additionally, the Si-W ECAL could also be instrumented with a few timing layers to enable time-of-flight (TOF) measurements with precision of 50 ps or even better [1, 40].

Alongside the CEPC baseline detector, an alternative detector concept known as IDEA (Innovative Detector for Electron-positron Accelerator) [39] is also utilized in various studies covered in this white paper. The IDEA detector also serves as a reference detector for the FCC-*ee* project. In comparison to the CEPC baseline detector, the IDEA detector incorporates a dual readout calorimeter system to attain superior energy resolution for both EM and hadronic showers. Moreover, the IDEA detector operates with a reduced magnetic field of 2 Tesla while compensating for this reduction by offering a larger tracking volume. The overall structure of the IDEA detector can be seen in Figure 5.

By virtue of the particle flow oriented design, the CEPC baseline detector performs well in efficient tracking, lepton identification, and precise reconstruction of hadronic systems. These excellent features of the CEPC baseline detector provide a solid basis for flavor physics studies. The achieved performance of the CEPC baseline detector during its CDR phase is summarized in Table 4. Notably, the baseline tracking system demonstrates an efficiency close to 100% and a relative momentum resolution approaching $\mathcal{O}(10^{-3})$ for individual tracks with momenta exceeding 1 GeV within the barrel region, as illustrated in Figure 6. As depicted in left panel of Figure 7, the baseline photon energy resolution is $17\%/\sqrt{E} \oplus 1\%$, achieved by the sampling Si-W ECAL, which features the high granularity critical for particle flow reconstruction. In terms of PID performance, the CEPC baseline design achieves a K/π separation better than 2σ in the momentum range up to 20 GeV by effectively combining TOF and dE/dx information, as shown in Figure 8. The inclusive $Z \to q\bar{q}$ sample exhibits an overall $K^{\pm}$ identification efficiency and purity exceeding

Item	Baseline [1]	Objective	Comments
Basic Performance			
Acceptance	$\lvert\cos\theta\rvert < 0.99$ [1]		
Threshold	200 MeV [41, 42]	100 MeV	For tracks & photons
Beam energy spread	$\mathcal{O}(0.1\%)$ [1]		
Tracker momentum resolution	$\mathcal{O}(0.1\%)$ [1]		
ECAL energy resolution	$17\%/\sqrt{E}\oplus 1\%$ [1]	$3\%/\sqrt{E}$ [31]	
HCAL energy resolution	$60\%/\sqrt{E}\oplus 1\%$ [1]		
Vertex resolution	10–200 μm [1]		
Jet energy resolution	3–5% [1, 43]		For 20–100 GeV
$\ell - \pi$ mis-ID	$< 1\%$ [44]		In jet, $\lvert\vec{p}\rvert > 2$ GeV
$\pi - K$ separation	$> 2\sigma$ [1]	$> 3\sigma$ [35]	In jet, $\lvert\vec{p}\rvert > 1$ GeV, TOF+dE/dx
Flavor Physics Benchmarks (Depending on the Above)			
$\sigma(m_{H,W,Z})$	3.7% [1]		Hadronic decays
b-jet efficiency×purity	$\sim 70\%$ [1]		In Z hadronic decays
c-jet efficiency×purity	$\sim 40\%$ [1]		In Z hadronic decays
b-jet charge tagging $\epsilon_{\mathrm{eff}} = \epsilon(1-2\omega)^2$	-	15–25% [34, 45]	For B_s
π^0 efficiency×purity	$\gtrsim 70\%$ [42]	$\gtrsim 80\%$ [31]	In Z hadronic decays, $\lvert\vec{p}_{\pi^0}\rvert > 5$ GeV
K_S^0, Λ , D efficiency	60%-85% [46]		In Z hadronic decays, all tracks
τ efficiency×purity	70% [47]		In $WW \to \tau\nu q\bar{q}'$, inclusive
τ mis-ID	$\mathcal{O}(1\%)$ [47]		In $WW \to \tau\nu q\bar{q}'$, inclusive

Table 4: Summary of detector performance of the CEPC baseline detector and some objectives for flavor physics benchmarks.
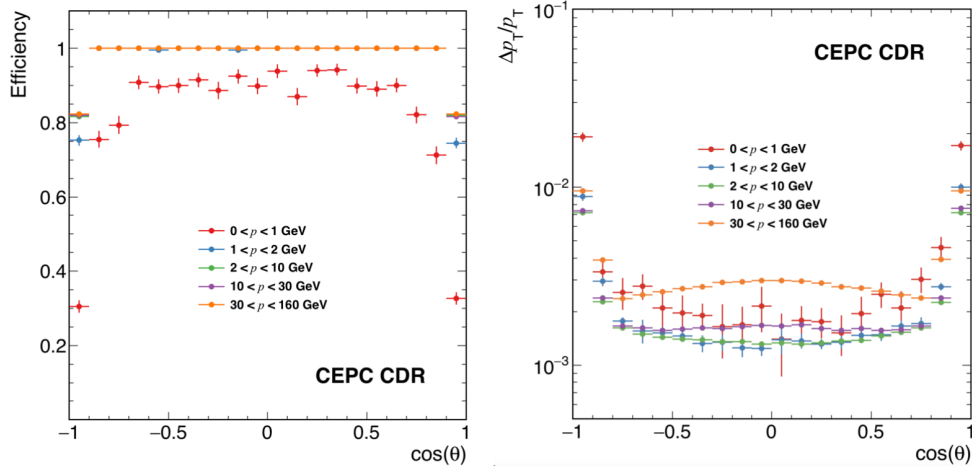

Figure 6: Single track reconstruction efficiency (left) and momentum resolution (right) of the CEPC baseline detector [1].

95% [36]. Regarding hadronic systems, the CEPC baseline detector attains a boson mass resolution (BMR) better than 4% for hadronically decaying W, Z, and Higgs bosons, as illustrated in right panel of Figure 7. This not only enables a separation exceeding $2\,\sigma$ between W and Z bosons in their hadronic decays, but also enhances the precision of missing energy/momentum measurements, which are vital for flavor physics investigations.
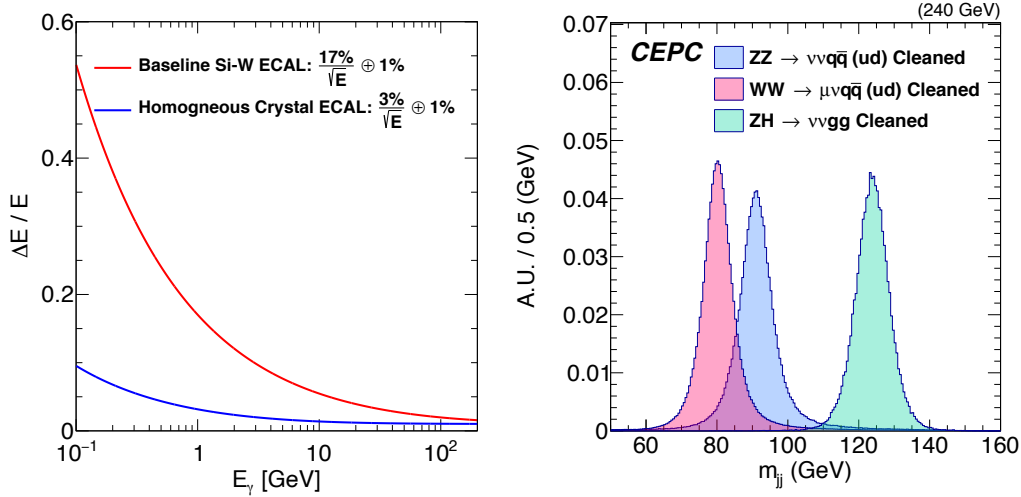
Figure 7: **LEFT:** Comparison of the CEPC baseline photon energy resolution achieved by the sampling Si-W ECAL [1] and expected photon energy resolution of homogeneous crystal ECAL. **RIGHT** Reconstructed boson masses of cleaned $\nu\bar{\nu}q\bar{q}$, $l\nu q\bar{q}$, and $\nu\bar{\nu}H$, $H \to gg$ events [43].
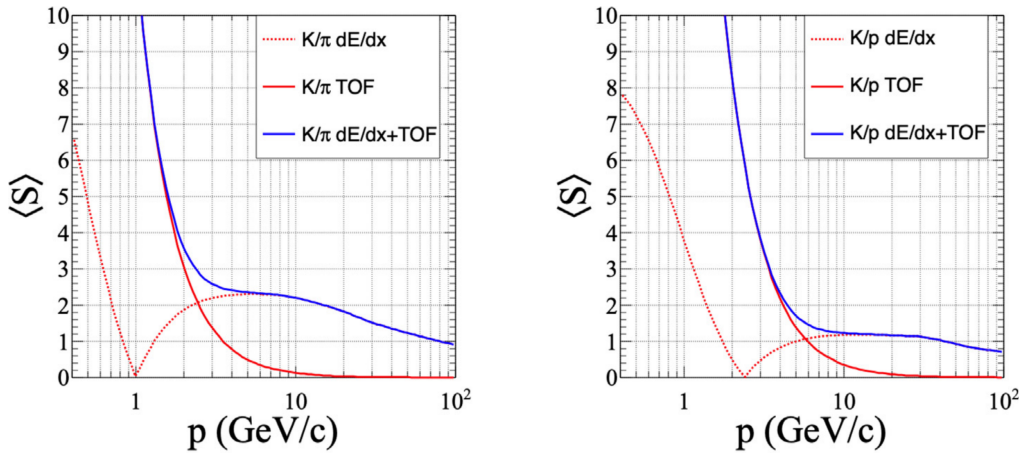

Figure 8: Separation power of K/π (left) and K/p (right) using different techniques [36].

Following the completion of the CEPC CDR, there are still ongoing research efforts focused on the detector design to further optimize the baseline performance parameters and to cater to the requirements for the CEPC flavor physics program. These optimization efforts primarily concentrate on three key aspects: EM energy resolution, PID performance, and jet charge measurements. To address the demand for improved separation of B^0 and B_s^0 with EM final states, a significantly enhanced EM energy resolution of $3\%/\sqrt{E}$ [31] is pursued, as compared to the baseline resolution of $17\%/\sqrt{E} \oplus 1\%$ shown in left panel of Figure 7. Accompanying this resolution enhancement, a corresponding photon energy threshold of 100 MeV is envisioned. To attain this level of EM resolution while maintaining compatibility with PFA performance, novel concepts for high-resolution
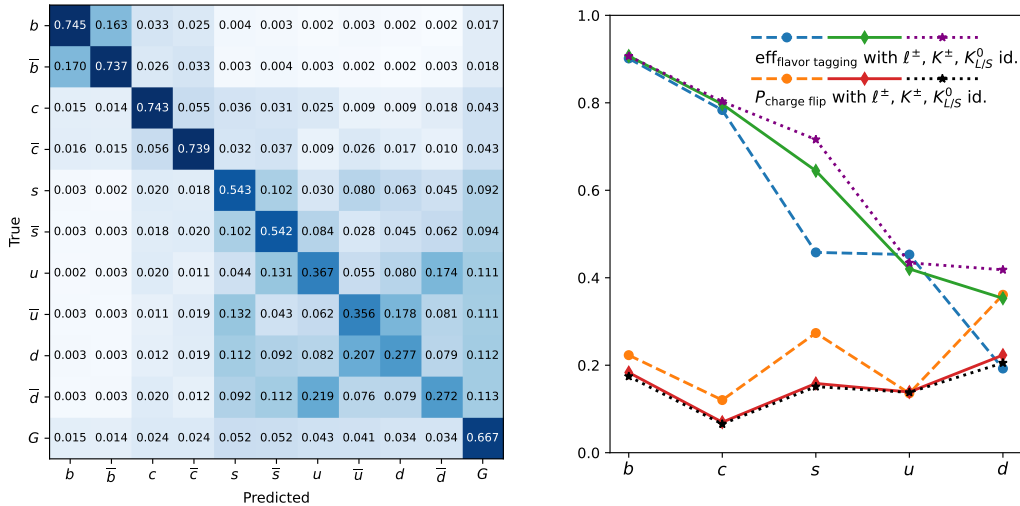
Figure 9: Jet origin identification performance [32] of full simulated Higgs/Z to di-jet processes with CEPC conceptual detector. **LEFT:** The confusion matrix M_{11} with perfect identification of leptons and charged hadrons. **RIGHT:** Jet flavor tagging efficiency and charge flip rate for S vs. U or D with identification of leptons, plus identification of charged hadrons and neutral kaons.

and high-granularity crystal ECAL designs have been proposed [48–50], and relevant R&D studies [51] are progressing. For PID performance, a K/π separation better than 3 σ is suggested. This improved PID capability can be achieved by combining various techniques, including TOF [52, 53], dE/dx [36, 54], and dN/dx [37] measurements. The performance of jet charge measurement is typically characterized by the effective tagging efficiency (power) $\epsilon_{\text{eff}} \equiv \epsilon_{\text{tag}}(1 - 2\omega)^2$, where ϵ_{tag} is the flavor tagging efficiency and ω is the wrong tagging fraction. The study [34] develops a Leading Particle Jet Charge method (LPJC) and combines it with a Weighted Jet Charge (WJC) method to form a Heavy Flavor Jet Charge method (HFJC). This study evaluates the effective tagging power for c/b jets at the CEPC Z pole operation and finds it to be 39%/20%. Additionally, by implementing benchmark IP cuts of 0.02/0.04 mm to distinguish the origin of the leading charged particle (whether from the decay of the leading heavy hadron or QCD fragmentation), the effective tagging power for c/b jets was found to be 39.0%/26.8%. Furthermore, a dedicated b-jet charge tagging algorithm developed specifically for the study of $B_s^0 \to J/\psi\phi$ at the CEPC [45] achieved an effective tagging power of 20%. Consequently, a range of $\epsilon_{\text{eff}} \in [15, 25]\%$ is determined for the future b-jet charge tagging power at the Tera-Z. These advancements in performance parameters are also summarized in Table 4.

In addition, the conceptual detector of CEPC has a large geometric acceptance, a decent performance in identifying final state particles, especially charged hadrons, as well as a precise low-material vertex system located close to the interaction point. These detector properties are of great significance in the identification of jet origins. Furthermore, recent advancements in machine learning algorithms, such as the ParticleNet algorithm [55] developed in the CMS experiments, provide necessary tools for this multi-category identification.
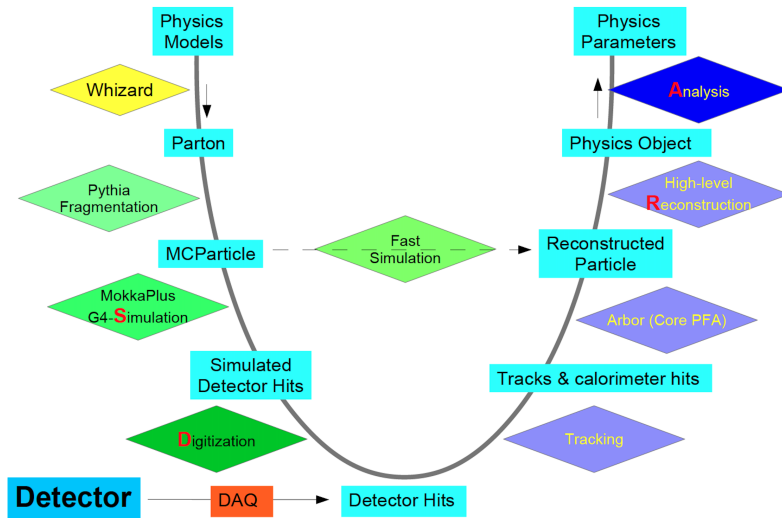
Figure 10: The CEPC official software chain and analysis flow [56]. More detailed information can be found in the CEPC CDR [1].

Through full simulated sample of Higgs/Z to di-jet processes with CEPC conceptual detector, ParticleNet can simultaneously identify $b/\bar{b}$, $c/\bar{c}$, and $s/\bar{s}$ quarks with flavor tagging efficiencies of 90%, 80%, and 60%, respectively [32]. Meanwhile, the misidentification rate for jet charge can be controlled at 18%, 7%, and 16%, correspondingly. The corresponding performance is shown in Figure 9. By applying this jet origin identification method, we further estimate the upper limits of rare ($H \to ss, uu, dd$) and flavor-changing neutral current ($H \to sb, sd, db, uc$) hadronic Higgs decays, as illustrated in Section 10.2. Moreover, the jet origin identification can also contribute to the measurement of V_{cb} from W boson decay and facilitate FCNC measurements, see Section 10.1.

2.3 Simulation Method

To explore the flavor physics potential of the CEPC, various benchmark analyses that have been evaluated at the simulation level are covered in this manuscript. Many of them are performed in the CEPC official software framework, shown in Figure 10, with full simulation and reconstruction of the baseline detector. For flavor physics measurements carried out at Tera-Z, a dataset of $\mathcal{O}(10^9)$ generator level inclusive $Z \to q\bar{q}$ events is available. Since the full simulation of the whole dataset is computationally expensive and time-consuming, pre-selections are generally applied to refine the dataset into core subsets. The analysis of $B_c \to \tau\nu_\tau$ in Section 3, the study of $B_s \to \phi\nu\bar{\nu}$ in Section 4, and the ϕ_s measurement via $B_s \to J/\psi\phi$ in Section 5 are three typical examples.

For some studies, especially those that are oriented towards phenomenology and detector requirements, fast simulation is usually adopted. Based on the understanding of detector responses and validated by the full simulation results, key detector performance is parameterized and modelled, and its effect on final physics observables is evaluated accordingly. This evaluation is used in studies such as the measurement of the α angle via

$B^0_{(s)} \to \pi\pi$ channels discussed in Section 5. In this way, we can investigate the whole parameter space as much as possible with fast convergence.

To make the physics picture complete, we also list many benchmarks that have not been fully explored and recommend them for future studies of the CEPC flavor physics program. Guesstimates are made for some benchmarks, such as τ relevant studies in Section 8 and exclusive hadronic Z decays in Section 9.

3 Charged Current Semileptonic and Leptonic b Decays

Historically, FCCC-mediated β decays have resulted in the discovery of weak interactions. As for heavy flavors, semileptonic and leptonic b decays are intensively explored in ongoing experiments and will continue to be a vital topic within flavor physics in the CEPC era. Measuring the signal rates of these channels can help determine the values of CKM matrix elements such as V_{cb} and V_{ub} [57]. Moreover, by measuring different leptonic modes, one can test lepton flavor universality (LFU), one of the most important hypothetical principles in the SM. In this way, FCCC measurements can serve as an efficient way to probe NP particles that couple with different strength to different lepton families. For instance, given a relative deviation δ_{SL} in signal rate from the SM prediction, the energy scale probed can reach

$$\Lambda^{\mathrm{SL}}_{\mathrm{NP}} \sim (G_F|V_{cb}|\delta_{\mathrm{SL}})^{-\frac{1}{2}} \sim (1.5~\mathrm{TeV}) \times \delta^{-\frac{1}{2}}_{\mathrm{SL}} \tag{3.1}$$

for $b \to c\ell\nu$ transitions and

$$\Lambda^{\mathrm{SL}}_{\mathrm{NP}} \sim (G_F|V_{ub}|\delta_{\mathrm{SL}})^{-\frac{1}{2}} \sim (5~\mathrm{TeV}) \times \delta^{-\frac{1}{2}}_{\mathrm{SL}} \tag{3.2}$$

for $b \to u\ell\nu$ transitions. Notice that here the NP effective couplings have been assumed agnostic about the SM flavor structure and have strengths of $\mathcal{O}(1)$.

The operation of the CEPC at the Z pole enables the detector to access a full spectrum of b hadrons with high statistics, including multiple-flavored mesons like B_c and baryons like Λ_b. Measuring their (semi)leptonic decays would cross-validate our current understanding of FCCCs and further reveal hitherto unexplored physics. Particularly interesting among the list of expected measurements are the ones involving τ decays. These measurements are crucial for, *inter alia*, achieving a full test of LFU. However the multi-body decays for τ leptons complicate the event topology and kinematics. The decay products tend to be soft in B-factories, while the signature of neutrinos as missing momentum is inaccessible at hadron colliders. Therefore, the event reconstruction becomes a challenging task. In contrast, the reconstruction of these events including the τ leptons and various intermediate particles may greatly benefit from the excellent collider environment of the CEPC and the high-performance of its detector. These measurements thus define one of the most representative "golden" cases for flavor physics at the CEPC.

Note, the discussions above can also be applied to measuring the FCNC-mediated processes. As such processes are suppressed at tree level in the SM, these channels are capable of probing NP (see detailed discussions in Section 4). The results obtained from both classes of measurements can be directly interpreted in various NP models. In a simplified

Figure 11: Illustrative Feynman diagrams for $B_c^+ \to \tau^+ \nu_\tau$ decay. **LEFT**: SM example. **RIGHT**: BSM example.

NP model, these processes can arise from either colorless or colored flavor mediators. The simplest colorless example might be a family non-universal Z' boson, which can couple to both quark and lepton flavors off-diagonally, yielding FCNC processes, see, *e.g.*, [58]. This possibility can be extended to a framework with an extra $SU(2)$ gauge triplet, where the additional flavor mediator W' will contribute to the FCCC processes [59]. A colored example is provided by leptoquarks, scalar or vector bosons that couple to quarks and leptons simultaneously. Leptoquarks are predicted by a wide range of ultraviolet (UV) theories such as grand unified theories, supersymmetry, composite Higgs models, etc. – for a review see [60]. Such interpretations are model-dependent, and hence often limited in their applicability.

Alternatively, one can interpret the results in an Effective Field Theory (EFT). The EFT is usually defined to parameterize the NP effects by integrating out the short distance physics. As a manifestation of physics at a low energy scale, the EFT is insensitive to the concrete format of UV physics in general. Here let us consider low-energy EFT (LEFT) [61], with a natural cutoff at the electroweak-breaking scale. For $b \to c\ell\nu$ transitions, we have the LEFT Hamiltonian

$$\mathcal{H}_{b \to c\ell\nu}^{\text{eff}} = \frac{4G_F}{\sqrt{2}} V_{cb} \sum_i C_i O_i + \text{h.c.} \,, \tag{3.3}$$

where O_i denotes the left(right)-handed scalar and vector currents and the tensor current, namely

$$\begin{aligned}
O_{S_{L(R)}} &= (\bar{c} P_{L(R)} b)(\bar{\ell} P_L \nu) \,, \\
O_{V_{L(R)}} &= (\bar{c} \gamma^\mu P_{L(R)} b)(\bar{\ell} \gamma_\mu P_L \nu) \,, \\
O_T &= (\bar{c} \sigma^{\mu\nu} b)(\bar{\ell} \sigma_{\mu\nu} P_L \nu) \,,
\end{aligned} \tag{3.4}$$

and C_i represents the corresponding Wilson coefficients. The only SM contribution is to C_{V_L} via the exchange of a W boson. Any deviation from that will indicate the presence of NP, and the specific pattern of such deviation may carry a message on the nature of the NP. For example, the $B_c \to \tau\nu$ process, shown in Figure 11, is sensitive to the axial vector $(C_{V_L} - C_{V_R})$ and pseudoscalar $(C_{S_L} - C_{S_R})$ Wilson coefficients.

For the $B_c \to \tau\nu$ decay, its branching ratio (BR) is predicted to be $\simeq 2.3 \times 10^{-2}$ [62] in the SM, but it is currently constrained very weakly by the experiments to be $(\text{BR} \lesssim 30\%)$. Some detailed examinations of this mode indicate that a Tera-Z factory can measure this BR with a precision of $\mathcal{O}(10^{-4})$ [62–64]. To this effect, the CEPC study in [63] employs
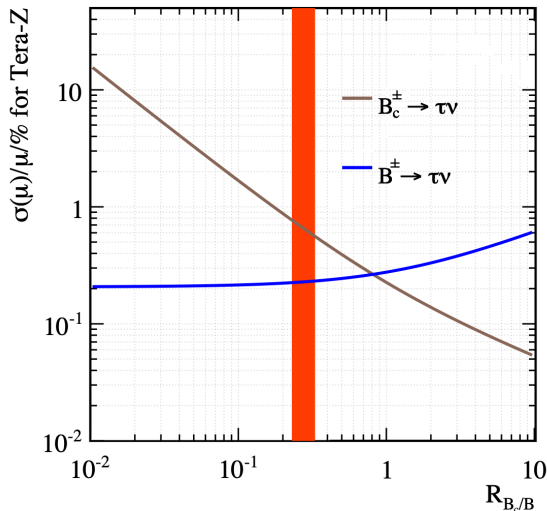
Figure 12: Relative accuracy of measuring the $B_{(c)}^{\pm} \to \tau\nu$ signal strength at Tera-Z, as a function of $R_{B_c/B} \equiv N(B_c^{\pm} \to \tau\nu)/N(B^{\pm} \to \tau\nu)$, with the red band showing the SM predicted range of $R_{B_c/B}$ at the CEPC Tera-Z operation [63].

a full simulation and incorporates leptonic τ decays of $\tau^{\pm} \to \ell^{\pm}\nu\bar{\nu}$, whereas the FCC-$ee$ studies in [62, 64] employ a fast simulation and use the 3-prong decay of $\tau^{\pm} \to \pi^{\pm}\pi^{\pm}\pi^{\mp}\nu$. As shown in Figure 12, a relative accuracy as low as $\mathcal{O}(1\%)$ for measuring the $B_c \to \tau\nu$ signal strength can be achieved. Such a precision level would also allow for $|V_{cb}|$ to be measured with a comparable accuracy during the Tera-Z phase of CEPC.

As mentioned above, one can test LFU by employing the $b \to c\ell\nu$ measurements. As LFU demands that the three generations of leptons have the same quantum numbers, therefore any difference between their interacting modes thus can arise from the mass only. For performing these tests of LFU, one usually introduces a ratio

$$R_{H_c} = \frac{\mathrm{BR}(H_b \to H_c\tau\nu_\tau)}{\mathrm{BR}(H_b \to H_c\ell'\nu_{\ell'})}, \tag{3.5}$$

where $H_{b(c)}$ represents a $b(c)$-hadron, and $\ell' = e, \mu$ unless stated otherwise. For such an observable, a large portion of systematics, such as the uncertainties from CKM matrix elements and form factors, could be cancelled. As a demonstration, we show the Feynman diagrams for the SM and BSM contributions to the $H_b \to H_c\ell^+\nu_\ell$ transitions in Figure 13.

For the test of LFU at the Z pole, a variety of R_{H_c} observables (R_{D_s}, $R_{D_s^*}$, $R_{J/\psi}$, and R_{Λ_c}) have been investigated recently [38] with the fast simulation template of the CEPC. The relative precisions, with the statistical errors being considered only, are summarized in Table 5. This study indicates that at Tera-Z, a relative precision of $\lesssim 5\%$ for $R_{J/\psi}$, as well as $\lesssim 0.4\%$ and $\sim 0.1\%$ for $R_{D_s^{(*)}}$ and R_{Λ_c}, respectively, could be reached. Due to the complex topology and dynamics, these outcomes rely heavily on a vertex-based strategy for event reconstruction. Thus, they benefit from a higher performance of detector in general. Concretely, the $R_{J/\psi}$ measurement benefits the most from the improvement of
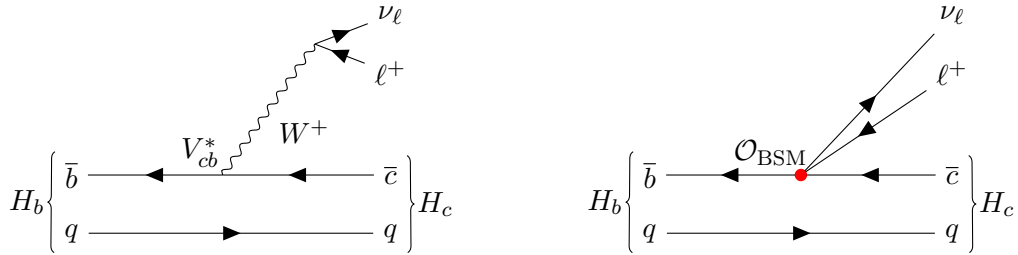
Figure 13: Illustrative Feynman diagrams for the $H_b \to H_c \ell^+ \nu_\ell$ transitions. **LEFT**: SM example. **RIGHT**: BSM example.

R_{H_c}	SM Value	Tera-Z	$4 \times$Tera-Z	$10 \times$Tera-Z
$R_{J/\psi}$	0.289	4.25×10^{-2}	2.13×10^{-2}	1.35×10^{-2}
R_{D_s}	0.393	4.09×10^{-3}	2.05×10^{-3}	1.30×10^{-3}
$R_{D_s^*}$	0.303	3.26×10^{-3}	1.63×10^{-3}	1.03×10^{-3}
R_{Λ_c}	0.334	9.77×10^{-4}	4.89×10^{-4}	3.09×10^{-4}

Table 5: SM predictions for the R_{H_c} observables and relative precision for their measurements at Tera-Z, $4 \times$Tera-Z, and $10 \times$Tera-Z [38].

tracker resolution, (see right panel of Figure 3 also), in reconstructing the $B_c^\pm$ vertex as an identity of the J/ψ one, while the $R_{D_s^{(*)}}$ measurements gain more from the increase of soft photon identification efficiency in distinguishing the D_s^* and D_s modes via the decay $D_s^* \to D_s \gamma$.

Note, these measurements cover a variety of $b \to c\tau\nu$ transitions: such as the ones from pseudoscalar ($B_{s,c}$) to vector (D_s^*, J/ψ) or pseudoscalar (D_s); those from baryon (Λ_b) to another baryon (Λ_c); and the decay of a pseudoscalar (B_c) to fermion pair. Consequently, they can be applied to constrain the $b \to c\tau\nu$ LEFT in different dimensions. Following the approach in [38], we present in Figure 14 the marginalized constraints on the Wilson coefficients of $b \to c\tau\nu$ LEFT at the CEPC, based on the results of [38, 63]. In this context, these Wilson coefficients can be universally constrained to a level of $\mathcal{O}(10^{-3})$ [1].

Concurrently, several untouched topics of FCCC physics deserve further exploration. Firstly, in view of the scientific significance of testing LFU, it is necessary to establish the CEPC sensitivity for a full list of R_{H_c} measurements including the traditional R_D and R_{D^*}, higher-resonant $R_{D^{**}}$ [65], remaining baryonic modes such as R_{Ξ_c}, etc., and their corresponding differential measurements. Also, to provide an LFU test for all three generations, it is natural to extend the studies to the measurements of $\frac{\text{BR}(b \to c + \mu\nu)}{\text{BR}(b \to c + e\nu)}$, where it might be crucial to reduce the systematics to a level comparable to that of statistical errors. The relevant benchmark channels that can be investigated at CEPC are listed in Table 6. Secondly, the superior precision of measuring the B meson lifetime at the CEPC creates a new space for the measurement of time-dependent CP-violation in semileptonic $b \to c\ell\nu$

---

[1]In this analysis, the operator O_{V_R} has been turned off, as it can not be generated by UV physics respecting the $SU(2)_L$ gauge symmetry.
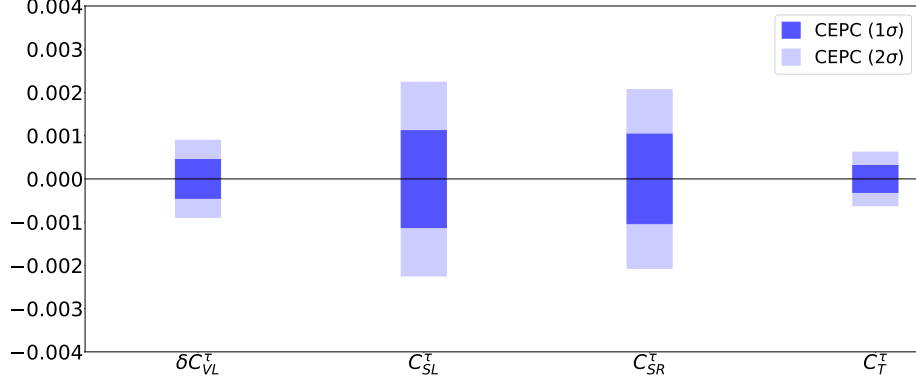
Figure 14: Marginalized constraints on the Wilson coefficients of $b \to c\tau\nu$ LEFT at the CEPC, with $\delta C_{V_L}^\tau = C_{V_L}^\tau - \delta C_{V_L,\mathrm{SM}}^\tau$. This plot is adapted from [38].

Process	Observable
$b \to cl\nu, b \to ul\nu$	LFU
$b \to cl\nu$	$R_{H_c}(R_{J/\psi}, R_{D_s^{(*)}}, R_{\Lambda_c})$
$B_c \to \tau\nu$	$|V_{cb}|$

Table 6: List of benchmark FCCC-mediated Semileptonic and Leptonic b-decay channels that can be investigated at CEPC.

decays. With this approach, the CP-violating markers in $B_{(s)}^0 - \bar{B}_{(s)}^0$ mixing, which are encoded as $\mathcal{A}_{\mathrm{SL}}^d$ and $\mathcal{A}_{\mathrm{SL}}^s$ [66, 67] respectively, can be extracted by measuring the B_d and B_s decays. As these measurements can contribute significantly to the global constraints on the parameters β and β_s [68, 69], where the current experimental precision remains far from the SM predictions, it is of high value to perform a more dedicated sensitivity analysis with either fast or full simulations.

4 Rare/Penguin and Forbidden b Decays

FCNC-mediated transitions such as $b \to s$ and $b \to d$ are theoretically prohibited at tree level in the SM. Instead, these transitions are catalyzed by EW penguin or box diagrams (see Figure 15), which are subjected to a joint suppression by off-diagonal CKM matrix elements and loop factors, and thus are rare. Because of this feature, the FCNC-mediated processes emerge uniquely sensitive to weak NP effects that may otherwise evade detection. Given a relative deviation of δ_{rare} in signal rate from the SM prediction, the energy scale probed can reach [70]

$$\Lambda_{\mathrm{NP}}^{\mathrm{rare}} \sim \left(\frac{\alpha}{4\pi} \frac{m_t^2}{m_W^2} G_F |V_{tb} V_{ts}^*| \delta_{\mathrm{rare}} \right)^{-\frac{1}{2}} \sim (30 \text{ TeV}) \times \delta_{\mathrm{rare}}^{-\frac{1}{2}} \tag{4.1}$$

and

$$\Lambda_{\mathrm{NP}}^{\mathrm{rare}} \sim \left(\frac{\alpha}{4\pi} \frac{m_t^2}{m_W^2} G_F |V_{tb} V_{td}^*| \delta_{\mathrm{rare}} \right)^{-\frac{1}{2}} \sim (67 \text{ TeV}) \times \delta_{\mathrm{rare}}^{-\frac{1}{2}} \tag{4.2}$$
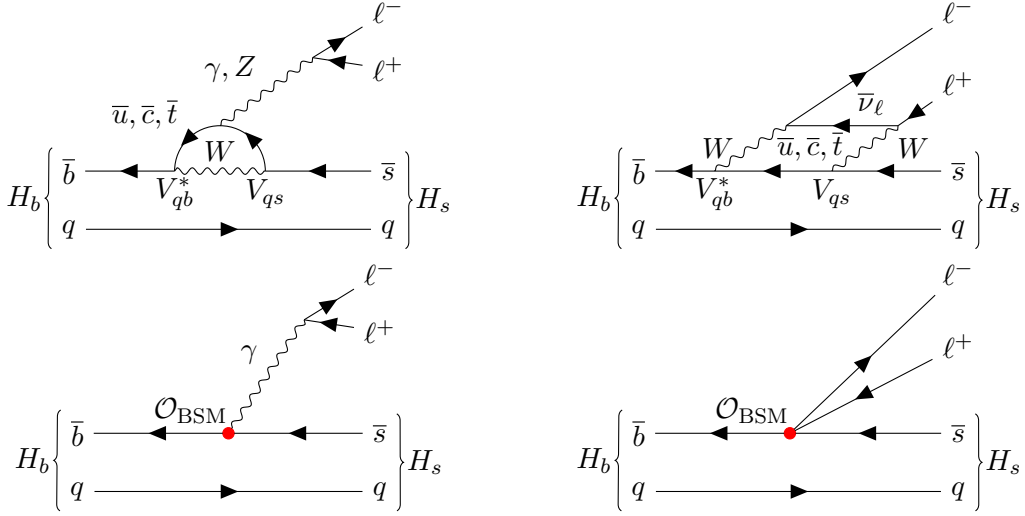
Figure 15: Illustrative Feynman diagrams for the $H_b \to H_s \ell^+ \ell^-$ transitions. **UPPER**: SM examples. **BOTTOM**: BSM examples.

for the $b \to s$ and $b \to d$ transitions, respectively. Notably, while the FCNC-mediated processes are rarer than the FCCC-mediated ones in the SM, $\Lambda_{\text{NP}}^{\text{rare}}$ can be comparable to, or even higher than, $\Lambda_{\text{NP}}^{\text{SL}}$ as long as $\delta_{\text{rare}} \lesssim 100\delta_{\text{SL}}$ is achieved.

Similar to the $b \to c\ell\nu$ transitions investigated in Section 3, we have the LEFT Hamiltonian for the $b \to s$ transitions:

$$\mathcal{H}_{b \to s}^{\text{eff}} = -\frac{4G_F}{\sqrt{2}} V_{tb} V_{ts}^* \sum_j (C_j O_j + C_j' O_j') + (C_L O_L + C_R O_R) + \text{h.c.,} \qquad (4.3)$$

where the operators of interest include

$$O_S^{(\prime)} = \frac{\alpha}{4\pi}(\bar{s} P_{L(R)} b)(\bar{\ell}\ell), \qquad O_P^{(\prime)} = \frac{\alpha}{4\pi}(\bar{s} P_{L(R)} b)(\bar{\ell}\gamma^5\ell),$$

$$O_9^{(\prime)} = \frac{\alpha}{4\pi}(\bar{s}\gamma^\mu P_{L(R)} b)(\bar{\ell}\gamma_\mu\ell), \qquad O_{10}^{(\prime)} = \frac{\alpha}{4\pi}(\bar{s}\gamma^\mu P_{L(R)} b)(\bar{\ell}\gamma_\mu\gamma^5\ell),$$

$$O_{T(T5)} = \frac{\alpha}{4\pi}(\bar{s}\sigma_{\mu\nu} b)(\bar{\ell}\sigma^{\mu\nu}(\gamma^5)\ell), \qquad O_7^{(\prime)} = \frac{e}{16\pi^2} m_b(\bar{s}\sigma^{\mu\nu} P_{R(L)} b)F_{\mu\nu},$$

$$O_{L(R)} = \frac{e^2}{8\pi^2}(\bar{s}\gamma^\mu P_{L(R)} b)(\bar{\nu}\gamma_\mu P_L \nu).$$

Among these operators, the first five ones encode the scalar, vector and tensor-mediated $b \to s$ transitions with a pair of charged leptons. Being with and without "prime" denotes a $b \to s$ factor subject to right and left-chiral projections respectively – this is also true for the operator $O_7^{(\prime)}$. $O_{L(R)}$ encodes the vector-mediated $b \to s$ transitions with a pair of neutrinos. $O_7^{(\prime)}$ is an EM dipole operator which can either yield an on-shell photon or contribute to the $b \to s\ell\ell$ transitions, (see the bottom-left panel in Figure 15). Note that the SM contributes to O_9, O_{10}, O_L and O_7 only.

In this section, we will focus on the measurements of $b \to s\tau\tau$, $b \to s\nu\nu$ and $b \to s\gamma$ transitions. The CEPC offers a great platform for these studies, particularly during its

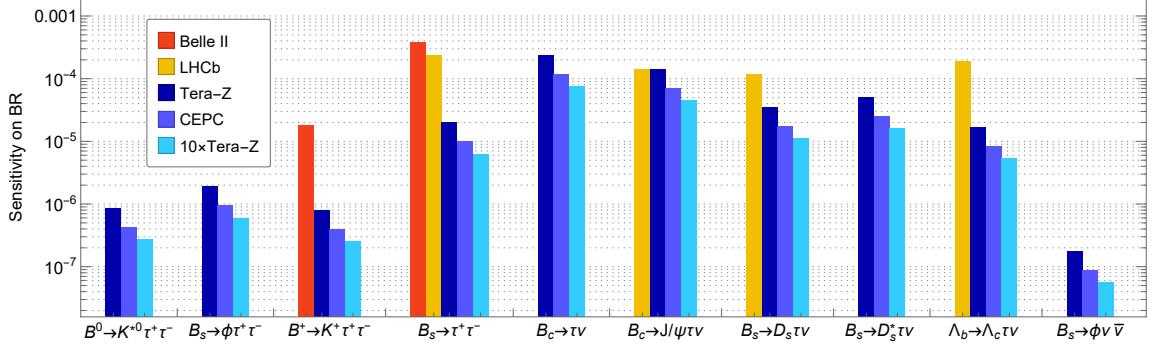**Figure 16**: Projected sensitivities of measuring the $b \to s\tau\tau$ [71], $b \to s\nu\bar\nu$ [35] and $b \to c\tau\nu$ [38, 63] transitions at the Z pole. The sensitivities at Belle II @ 50 ab^{-1} [6] and LHCb Upgrade II [17, 72] have also been provided as a reference. Note, the LHCb sensitivities are generated by combining the analyses of $\tau^+ \to \pi^+\pi^-\pi^-(\pi^0)\nu$ and $\tau \to \mu\nu\bar\nu$. This plot is adapted from [38].

Z-pole run. The extraordinarily high luminosity delivered by the CEPC ensures considerable signal statistics for even the most elusive decay modes with BRs typically $\lesssim 10^{-5}$. Moreover, as compared to the LHCb detector, the detector of the CEPC is better suited to the measurement of $b \to s\tau\tau$ in reconstructing the τ lepton, (and hence the b-meson resonance), to the measurement of $b \to s\nu\nu$ in calculating the missing energy, and to the measurement of $b \to s\gamma$ in identifying the photon. A combination of these advantages yields an enhanced sensitivity for both testing the SM and probing the NP. The CEPC thus represents an ideal facility for investigating these rare FCNC decays and their underlying physics. For the convenience of discussions below, we summarize the projected sensitivities for measuring the $b \to s\tau\tau$ and $b \to s\nu\bar\nu$ transitions, together with the $b \to c\tau\nu$ processes discussed in Section 3, Figure 16.

4.1 Dilepton Modes

In general, the reconstruction of $b \to s\tau\tau$ is more involved as compared to the reconstruction of $b \to see, s\mu\mu$. As the τ decays are accompanied by neutrino production, the $b \to s\tau\tau$ events are not fully visible to a detector. This difficulty, however, can be well-addressed at a machine like the CEPC. In a recent study [71] (for discussions on $B^0 \to K^{*0}\tau^+\tau^-$, also see [73]), the sensitivity for measuring a set of benchmark $b \to s\tau\tau$ transitions, including $B^0 \to K^{*0}\tau^+\tau^-$, $B_s \to \phi\tau^+\tau^-$, $B^+ \to K^+\tau^+\tau^-$ and $B_s \to \tau^+\tau^-$, at the Z pole has been systematically analyzed. To utilize the machine's capability, a tracker-based scheme to reconstruct the signal B mesons that works for these $b \to s\tau\tau$ channels has been developed, achieved by using the decay modes of $\tau^\pm \to \pi^\pm\pi^\pm\pi^\mp\nu$. Such a tracker-based scheme also benefits from the particle kinematics at the Z pole. Due to their boost, the signal b hadrons tend to displace more (compared to, e.g., Belle II) before their decay, which benefits the relevant tracker measurements. The predominant backgrounds for these measurements are anticipated to be the Cabibbo-favored $b \to c + X$ processes. Recall that both $D^\pm$ and $D_s^\pm$ mesons have a mass and lifetime comparable to those of τ leptons and thus may decay to
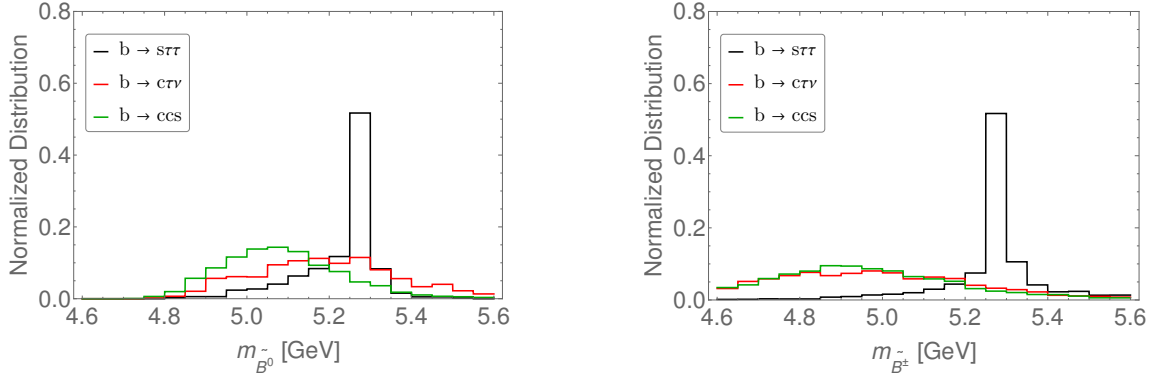
Figure 17: Mass reconstruction for the signal b-mesons in the measurements of $b \to s\tau\tau$ at the Z pole, with $\tau^\pm \to \pi^\pm\pi^\pm\pi^\mp\nu$ [71]. **LEFT:** $B^0 \to K^{*0}\tau^+\tau^-$. **RIGHT:** $B^+ \to K^+\tau^+\tau^-$. The major backgrounds arise from the $b \to c\tau\nu$ and $b \to ccs$ transitions and are both reconstructed.

a vertex of $\pi^\pm\pi^\pm\pi^\mp$ with extra particles. Therefore, they can fake the τ leptons in the signal. In Figure 17 we demonstrate the mass reconstruction for the signal b-mesons in the measurements of $B^0 \to K^{*0}\tau\tau$ and $B^+ \to K^+\tau^+\tau^-$ at the Z pole. These two channels involve the decay of b-mesons into vector and pseudoscalar mesons respectively. They are sensitive to the LEFT in approximately orthogonal ways and thus are complementary in probing the NP [71].

As demonstrated in Figure 16, the Tera-Z and $10\times$Tera-Z machines are able to measure $B^0 \to K^{*0}\tau^+\tau^-$, $B_s \to \phi\tau^+\tau^-$ and $B^+ \to K^+\tau^+\tau^-$ with a precision (with respect to their BRs) of $\mathcal{O}(10^{-7} - 10^{-6})$, as well as $B_s \to \tau^+\tau^-$ with a precision (with respect to its BR) of $\mathcal{O}(10^{-6} - 10^{-5})$. In comparison, Belle II and LHCb either have no sensitivity to these measurements or can only yield a sensitivity one to two orders of magnitude weaker. With the baseline luminosity, this indicates that the CEPC will be able to recognize $\sim \mathcal{O}(1)$ deviations from the SM predictions. These measurements can be further applied to probe the $b \to s\tau\tau$ LEFT. Figure 18 shows the marginalized constraints on the corresponding Wilson coefficients in the presence of the vector-mediated operators only.

In spite of this progress, the study of FCNC-mediated b rare decays at CEPC should be extended in multiple directions. Firstly, the CEPC constraints on its LEFT must be improved. The relatively weak constraints on the LEFT as shown in Figure 18 indicate the existence of degenerate directions in the theory parameter space. This can be understood as $B^0 \to K^{*0}\tau^+\tau^-$ and $B_s \to \phi\tau^+\tau^-$ both involve the decays of b-mesons into vector mesons and hence share similar capabilities in probing the NP. To improve the constraints on the relevant LEFT, one can consider: (1) introducing differential observables, such as forward-backward asymmetry and τ polarimetry [73]; and (2) incorporating $b \to s\tau\tau$ transitions of a different nature, like the baryonic decay of $\Lambda_b \to \Lambda\tau^+\tau^-$.

A second area of improvement would be to advance the study of LFU tests at the CEPC. The CEPC analysis in [71] focuses on the di-τ mode of $b \to s$ transitions. To paint a full picture in this context, it is of high value to extend the analysis to $b \to$
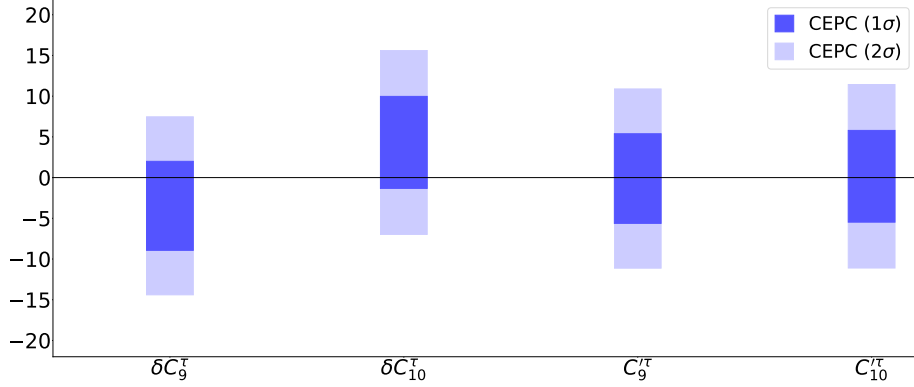
Figure 18: Marginalized constraints on the Wilson coefficients of $b \to s\tau\tau$ LEFT (vector current only) at the CEPC, with $\delta C_9^\tau = C_9^\tau - C_{9,\mathrm{SM}}^\tau$ and $\delta C_{10}^\tau = C_{10}^\tau - C_{10,\mathrm{SM}}^\tau$. This plot is adapted from [71].

$s\ell\ell$. The measurements of, $e.g.$, $R_{K^{(*)}}$, R_{pK} [74], R_ϕ [75], $R_{f_2'}$ [75] and even R_Λ could provide an important message about LFU. For some of these measurements, the systematic uncertainties induced by PID could be dominant. The superior electron- and muon-ID capabilities of future detectors are anticipated to offer an edge over the LHCb. Notably, the luminosity advantage of the CEPC in measuring the $b \to s\tau\tau$ transitions could be extended to ultra-rare channels such as $B_s \to \mu^+\mu^-$. The measurement of $\mathrm{BR}(B_s \to \mu^+\mu^-)$ in the SM is known to be statistically limited, due to its tiny value of around $\sim 3.0 \times 10^{-9}$ [76]. With a yield of $\sim 1.2 \times 10^{11}$ for B_s^0 mesons at the CEPC, about 360 $B_s \to \mu^+\mu^-$ events are expected to be produced, which provides a good opportunity to improve the precision of its measurement.

Finally, the sensitivity studies should be extended to the $b \to d\ell^+\ell^-$ transitions at the CEPC. The $b \to d\ell^+\ell^-$ transitions represent another independent category of FCNC-mediated rare b-decays, and hence play a role complementary to the $b \to s\ell^+\ell^-$ transitions in exploring flavor physics. Interestingly, the measurements of these channels including both signal rate and CP asymmetry [77, 78] may share difficulties similar to those of $b \to s\ell^+\ell^-$ decays, and hence would impose similar requirements for the detector performance at the CEPC. All of these issues deserve further detailed examinations.

4.2 Neutrino Modes

The $b \to s\nu\bar{\nu}$ decay is immune from non-factorizable corrections and photonic contributions. Therefore, the theoretical calculation for its SM rate is cleaner than that for the $b \to s\ell\ell$ transitions, which yields $\mathrm{BR}(B_s \to \phi\nu\bar{\nu})_{\mathrm{SM}} = (9.93 \pm 0.72) \times 10^{-6}$ [35]. The $b \to s\nu\bar{\nu}$ decay can be applied to probe light dark sectors, such as dark photons, sterile neutrinos, axions/axion-like-particles, or neutral scalars, which may significantly alter the kinematics of visible particles [79, 80], (for discussions on the light dark sectors at CEPC, also see Section 12). Also, due to the constraints of $SU(2)_L$ symmetry, the impacts of NP on the $b \to s\nu\bar{\nu}$ and $b \to s\ell^+\ell^-$ decays could be interconnected. Thus, the measurement of $b \to s\nu\bar{\nu}$ offers a complementary probe to look into the underlying physics [81, 82].
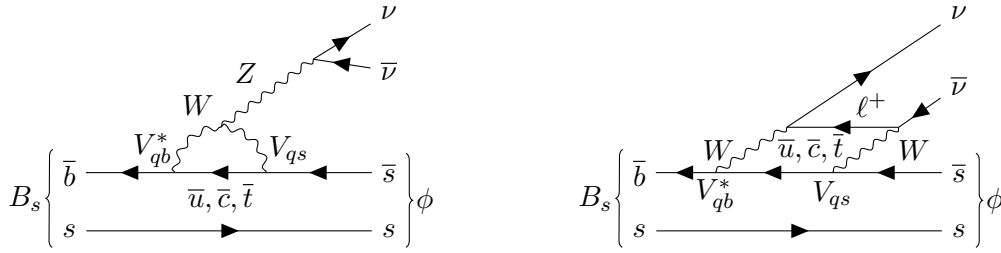
Figure 19: Illustrative Feynman diagrams for the $B_s \to \phi\nu\bar{\nu}$ transitions in the SM. **LEFT**: EW penguin diagram. **RIGHT**: EW box diagram.

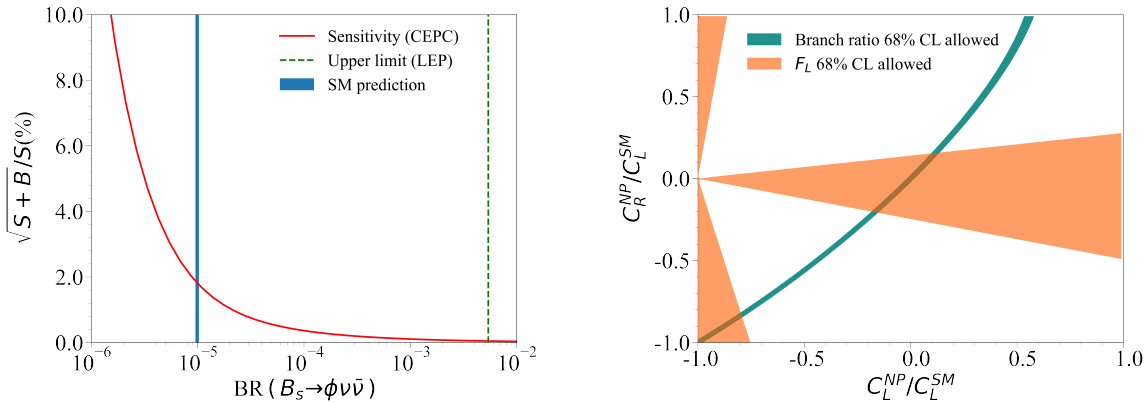**Figure 20**: **LEFT**: Relative precision for measuring the signal strength of $B_s \to \phi\nu\bar{\nu}$ at Tera-Z, as a function of its BR. **RIGHT**: Constraints on the LEFT coefficients $C_L^{\mathrm{NP}} \equiv C_L - C_L^{\mathrm{SM}}$ and C_R with the measurements of the overall $B_s \to \phi\nu\bar{\nu}$ decay rate (green band) and the ϕ polarization F_L (orange regions). These plots are taken from [35].

A dedicated study on the $B_s \to \phi\nu\bar{\nu}$ decay (see Figure 19) at the Z pole has been conducted, using full simulation samples aligned with the CEPC detector profile [35]. This study, facilitated by the large B_s statistics at the CEPC (see Table 2), suggests that a precise measurement of such a rare decay is possible. Explicitly, the accurate ϕ and B_s reconstructions in this analysis reduce the $Z \to q\bar{q}$ events by a factor $\sim \mathcal{O}(10^{-8})$, with a signal efficiency $\sim 3\%$, leaving primarily the $Z \to b\bar{b}$ events as the backgrounds. As a result, a relative precision $\lesssim 2\%$ can be achieved for measuring the SM $B_s \to \phi\nu\bar{\nu}$ signal, as shown in the left panel of Figure 20. Particularly, with a high signal-to-background ratio of $\simeq 77\%$, the robustness of this measurement against potential systematic uncertainties is largely assured. This study has also shown that the constraints obtained from this measurement can contribute pivotally to the global determination of NP effects, *e.g.*, the ones encoded in the LEFT, (see the right panel of Figure 20).

In addition to the $B_s \to \phi\nu\bar{\nu}$ decay, there exist a set of other physical processes which can be applied to study the $b \to s\nu\bar{\nu}$ transitions at the CEPC. One example is $B^0 \to K^{0*}\nu\bar{\nu}$. Despite the challenges of reconstructing the secondary vertex in these events, Belle II is expected to measure this channel with a precision of 10% [6]. Yet, by

leveraging its advantages in reconstructing the missing energy and producing b-hadrons, the CEPC may push this precision to a much higher level. For these possibilities, the baryonic processes such as $\Lambda_b \to \Lambda \nu \bar{\nu}$ and $\Xi_b^{\pm} \to \Xi^{\pm} \nu \bar{\nu}$ are particularly interesting. The long life time of Λ and $\Xi^{\pm}$ may generate a signature of displacement or track of $\mathcal{O}(10)\,\mathrm{cm}$ in the detector. However, both channels are not dynamically accessible in the B-factory experiments such as Belle II. In contract, the high-production rate at the Z pole and the high performance in track measurement and vertex reconstruction jointly put the CEPC in a great position for their measurements.

4.3 Radiative Modes

The third category of FCNC-mediated rare B decays are radiative, such as $b \to s\gamma, d\gamma$. They are sensitive to the EM dipole operators O_7 and O_7'. A wealth of data, including the inclusive $B \to X_{s,d}\gamma$ decays, as well as the direct CP asymmetry A_{CP} and time-dependent CP asymmetry S_{CP} in various $b \to s\gamma$ decays, has yielded complementary insights into the corresponding Wilson coefficients C_7 and C_7'. At the CEPC, however, the FCNC-mediated radiative modes are yet to be explored, despite their scientific significance [83]. One such example is the decay of $B_s \to \phi\,(\to K^+K^-)\,\gamma$, illustrated in Figure 21. Achieving a high accuracy in reconstructing the signal B_s meson necessitates superior photon angular and momentum resolution. At the LHCb upgrade II, it is found that $\mathrm{BR}(B_s \to \phi\gamma)$ could be measured with a statistical uncertainty $\sim 0.1\%$, and the CP parameters can also be well-measured [17, 84]. These sensitivities are expected to be further improved at the CEPC due to the potentially high performance of its ECAL. This study can be extended to baryonic radiative decays of $b \to s\gamma$, such as $\Lambda_b \to \Lambda\gamma$ and $\Xi_b \to \Xi\gamma$, again with an expected sensitivity better than the LHCb one [85]. The study can be also extended to the $b \to d\gamma$ decays, which can broaden our understanding on the FCNC amplitudes and potentially refine the CKM matrix determination. Finally, if the ECAL of the CEPC allows an effective reconstruction of $\pi^0, \eta \to \gamma\gamma$ [31], the double-radiative decays of $B_{s,d} \to \gamma\gamma$ could be measured [86]. Theoretical studies show that the $\Lambda_{\mathrm{QCD}}/m_b$ power corrections in these channels are well under control, making them new benchmark probes of non-standard dynamics [87, 88]. The SM predictions for the their branching ratios are given by [87, 88]

$$\mathcal{B}(B_s \to \gamma\gamma) = (3.8^{+1.9}_{-2.1}) \times 10^{-7} \ , \ \mathcal{B}(B_d \to \gamma\gamma) = (1.9^{+1.1}_{-1.0}) \times 10^{-8} \ . \tag{4.4}$$

Belle II has estimated its relative sensitivities to be $\sim 23\%$ and $\sim 30\%$ [6], based on overestimated branching ratios [89].

5 CP Asymmetry in b Decays

In the SM, the intricate properties of flavor physics are all elegantly accounted for by the CKM matrix, particularly for what concerns CPV phenomena. In fact, the only source of CPV in hadronic EW interactions is the single phase of the CKM [4]. On the other hand, it is known that the matter-antimatter asymmetry observed in our universe requires additional sources CPV. This is one of the reasons why the investigation of CPV asymmetries is a field that attracts most efforts in flavor physics experiments. Such explorations
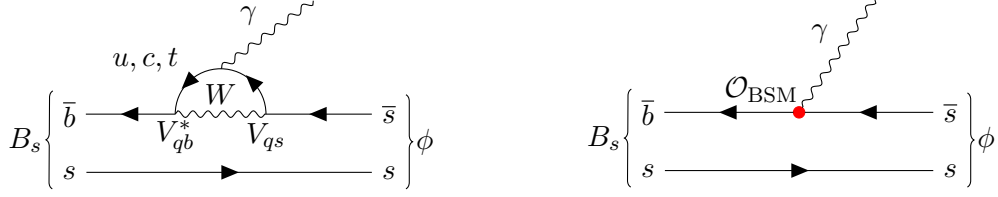
Figure 21: Illustrative Feynman diagrams for $B_s \to \phi\gamma$ decay. **LEFT**: SM example. **RIGHT**: BSM example.

at the CEPC will generally demand high statistics, low background interference, efficient hadron PID, and extreme displacement resolution. As customary, the observables, handled by proper analysis of amplitudes, can be then fed into the global fit of the CKM matrix, such that any deviation from CKM unitarity would be a smoking gun of CPV NP.

The CP asymmetry measurements are generically classified as time-integrated and time-dependent measurements, in complement to each other. The time-integrated measurements take place when the heavy particle to be investigated does not mix with its own CP conjugate and thus never oscillates. Alternatively, the measurements are forced to be time-integrated if an oscillating particle's decay lifetime can not be determined well. The effective statistics in this case are not only directly proportional to the overall signal rate but also to the effective efficiency in tagging the initiating heavy quark/lepton's charge. The effective efficiency ϵ_{eff} can be expressed as $\epsilon_{\mathrm{tag}}(1 - 2\omega)^2$, where ϵ_{tag} is the fraction of particle candidates that are assigned with a particular charge, and ω is the chance that this charge is misidentified. Currently, the time-integrated CP asymmetry plays a significant role in the determination of the CKM angle γ.

The time-dependent asymmetry measurements, conversely, occur when the heavy particle can mix with its own CP conjugate, and its decay lifetime can be uniquely identified. The neutral B^0 and B_s are relevant for most measurements, as their oscillations are apparent. Depending on the decay final states, the decay rate asymmetry as a function of time takes several forms which will not be elaborated upon here. However, the general pattern holds across different decay modes. The asymmetry will have non-oscillatory terms having the time scale of the decay width difference ($\Delta\Gamma$) between mass-eigenstates after mixing. Furthermore, there will be oscillatory terms with the period determined by the mass difference between mass eigenstates. In practice, the oscillatory terms are more crucial for CP asymmetry, since $\Delta m \gg \Delta\Gamma$ for both the B^0 and B_s^0 system [9]. The mistag probability ω could be significant in this case, as the algorithm must determine the initial b-quarks' charge after the oscillation happens; such techniques will be discussed below. Another factor affecting the overall precision is the decay lifetime resolution, which is mainly limited by the vertex resolution of the tracking system.

Tagging the initial b-quark charge is crucial and – in general – challenging, as the direct final states from $B_{(s)}^0$ are affected by oscillations and thus cannot be used directly. The algorithm must therefore rely on other particles like another produced b-hadron. In this case, if the other b-quark hadronizes into a non-oscillatory species, such as a $B^\pm$, and is subsequently identified, then the original b-quark's charge is identified as well. Alternatively,
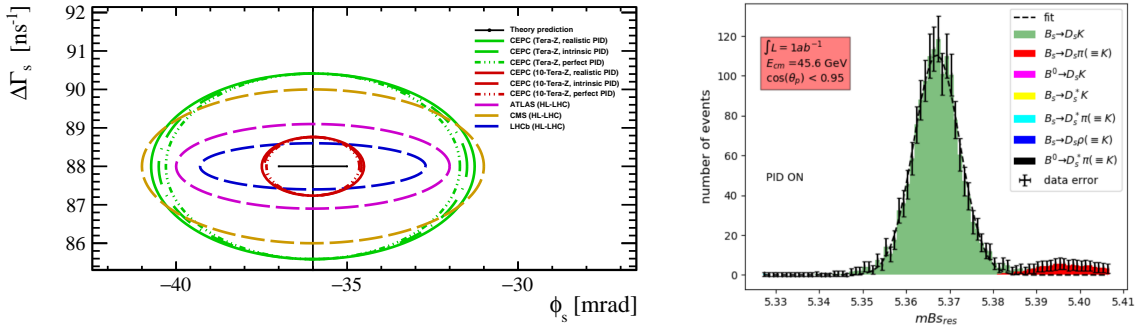
Figure 22: **LEFT:** Expected sensitivity (68% confidence level) of $\Delta\Gamma_s - \phi_s$ at various experiments [45]. The CEPC projections come from the time-dependent CP asymmetry measurement of $B_s \to J/\psi(\to \mu^+\mu^-)\phi(\to K^+K^-)$ decays. **RIGHT:** B_s mass resolutions in $B_s \to D_s^\pm(\to \phi\pi^\pm \to K^+K^-\pi^\pm)K^\mp$ decays at the Z pole [94]. A simple PID algorithm removes most combinatoric and misidentification-induced backgrounds, making a clean peak of signal events.

other particles produced from the QCD shower could also help, as they encode the original b-quark's charge from QCD interactions before any mixing could happen. For example, a B_s is often accompanied by a K^+ flying in the same direction, since strange quarks also need to be produced in pairs from QCD, and the s hadronizes to form B_s. The recent CEPC study with fast focusing on leading charged particles in the jet and the weighted jet charges [34]. As discussed in Section 2, the expected ϵ_{tag} for inclusive c or b hadrons can reach 39% and 20%, respectively. On the other hand, the value of effective tagging efficiency ϵ_{eff} at the CEPC using full simulation is still under evaluation, but is supposed to be better than the LEP ones [90–92]. A recent study [45] using particles accompanying the B_s meson also suggests that ϵ_{eff} will be $\gtrsim 20\%$ at the CEPC, higher than the typical 5% level at LHCb [93].

The decay lifetime resolution at the CEPC benefits from both a clean collision environment and the tracking system design; a study based on CEPC full simulation [45] reports a typical resolution of $\lesssim 5\,\text{fs}$ on the 4-prong $B_s \to J/\psi\phi \to \mu^+\mu^- K^+K^-$ decay, which is a fraction of the typical LHCb value of $\gtrsim 20 - 30\,\text{fs}$. The improved resolution would benefit all time-dependent CP asymmetry measurements, as well as the general parameters Δm and $\Delta\Gamma$ for $B^0_{(s)}$ oscillations. The latter two will be fundamental inputs to many CP asymmetry studies, as well as individual inputs to the global CKM fit. Results from another study in the FCC-ee context [94] suggest that the relative uncertainty of Δm for B_s can reach $\lesssim 3 \times 10^{-5}$, which is about an order of magnitude better than the current sensitivity. We hope that dedicated studies in the future could help validate such results and reveal the full potential of the CEPC for measuring these basic flavor physics inputs.

A few published works investigated CP asymmetry measurements at the CEPC or other Z-factories. As mentioned above, time-dependent measurements benefit from the high decay time resolution and high effective tagging efficiency. Significant strides were made in utilizing the $B_s \to J/\psi\phi \to \mu^+\mu^- K^+K^-$ channel as an essential benchmark for
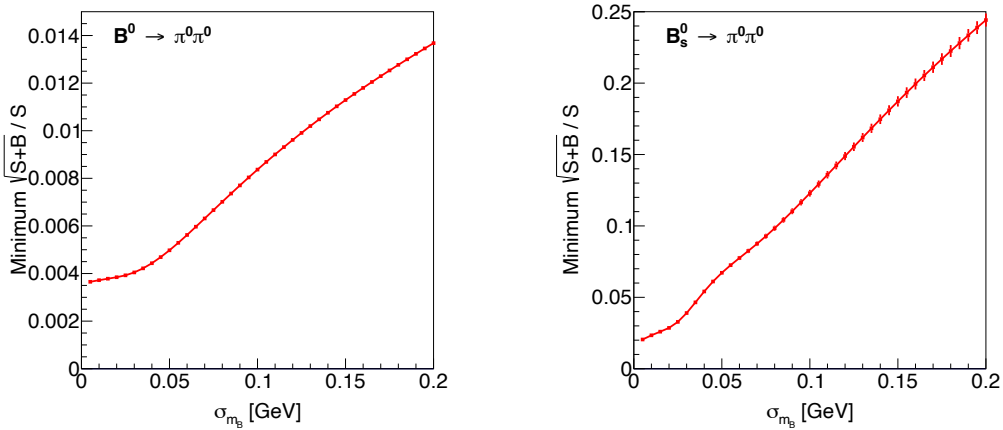
Figure 23: Relative statistical uncertainties of $\mathrm{BR}(B^0 \to \pi^0\pi^0)$ (left) and $\mathrm{BR}(B_s^0 \to \pi^0\pi^0)$ (right) versus B-meson mass resolution σ_{m_B} with four-photon final states. Plots taken from [31].

β_s measurement. According to the CEPC full simulation study, the uncertainty of β_s can be reduced to approximately 4×10^{-3} mrad [45], a significant improvement over the existing measurements. The relevant projected resolutions are displayed in the left panel of Figure 22. Similar resolutions were also achieved in [94], where the time-dependent CP asymmetry of $B_s \to D_s^\pm K^\mp$ and $B_s \to J/\psi\phi \to \mu\mu KK$ decays are simulated with fast simulation – see the right panel of Figure 22 for the obtained reconstruction of the B_s mass. It is anticipated that most combinatoric and misidentification-induced backgrounds can be removed if the proper PID is adopted in the analysis. With the correct theoretical interpretation, the angles of the sb unitarity triangle α_s and β_s could be measured with uncertainties of $0.4°$ and $0.035°$, respectively. These results will also be helpful in recovering the CKM angle γ.

In a recent study [95], it was proposed that there exists the so-called double-mixing CP violation in cascade decays involving two neutral mesons in the decay chain, induced by the interference of different meson oscillating paths. The double-mixing CP violation in channels like $B_s^0 \to \rho^0 K \to \rho^0(\pi^-\ell^+\nu)$ and $B^0 \to D^0 K \to D^0(\pi^+\ell^-\bar\nu)$ is supposed to be very significant. The asymmetry depends on two time variables, the oscillating time of $B_{(s)}^0$ and the oscillating time of K, so a two-dimensional time-dependent analysis can be performed through its measurements. The CEPC, with large $B_{(s)}^0$ production and good time resolution, can provide a good opportunity.

Interesting contributions to the assessment of time-integrated uncertainties were also present. Exploration of $B_{(s)}^0 \to \pi^0\pi^0 \to 4\gamma$ modes has been performed using a CEPC fast simulation [31]. The measurement is time-independent, as the decay lifetime of the fully-neutral final state is intractable. Figure 23 displays the relative uncertainties (statistical only) of $\mathrm{BR}(B^0 \to \pi^0\pi^0)$ and $\mathrm{BR}(B_s^0 \to \pi^0\pi^0)$ as a function of the B-meson mass resolution (σ_{m_B}), which is highly dependent on the ECAL performance. The resulting expected precision on the measurement of $\mathrm{BR}(B_s \to \pi^0\pi^0)$ and $\mathrm{BR}(B_d \to \pi^0\pi^0)$ at the Tera-Z
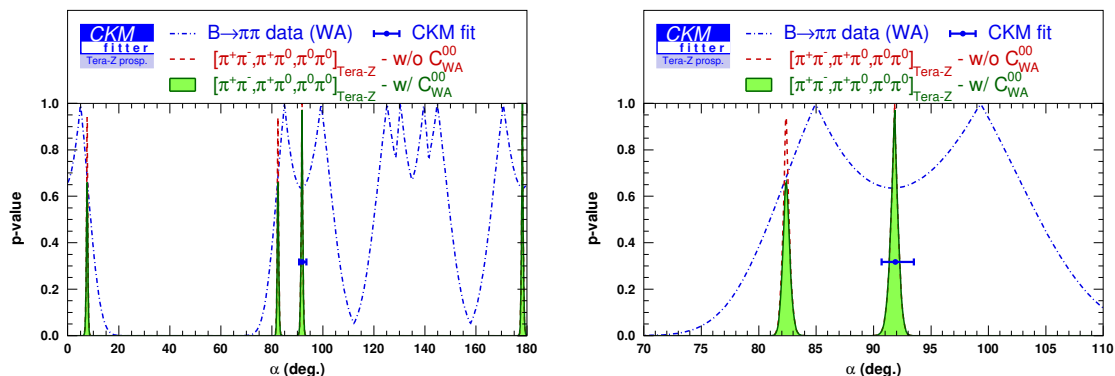
Figure 24: *p*-value for α from $B \to \pi\pi$ measurements. Three scenarios are compared: using the current world average (dotted-dashed blue), with improvement from both neutral and charged modes without (dashed red) and with (solid green) the measurement of C_{CP}^{00} at CEPC. We show the scan over the whole range of α (on the left) and around the value favored by the global CKM fit (on the right). See [31] for more details.
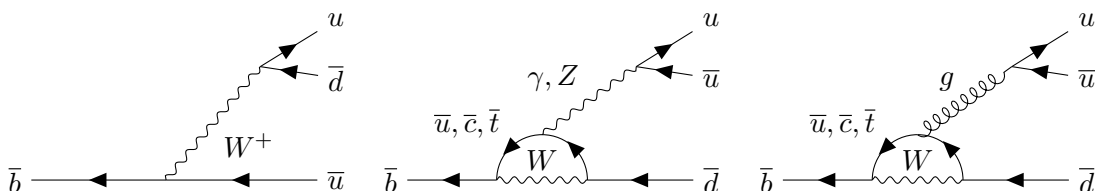

Figure 25: Illustrative Feynman diagrams for the $\bar{b} \to u\bar{u}\bar{d}$ transitions. **LEFT**: tree level. **MIDDLE**: EW penguin diagram. **RIGHT**: QCD penguin diagram.

phase are $\lesssim 10\%$ and $\lesssim 1\%$, respectively. Such high resolution on photon-only final states is only possible with a fully crystal ECAL [96]. We remark that this mode would play a key role in the measurement of the CKM angle α [97]. In this case, the time-integrated CP asymmetry observables are different from B-factory counterparts, as the two b-hadrons created by Z decay are not entangled, and the interaction point can be uniquely determined from other tracks. The result is thus complementary to future Belle II measurements [6], leading to a future sensitivity on α as small as $0.4°$ with Tera-Z luminosity (see Figure 24) – if the theoretical uncertainty could be resolved. Another study [98] contributed to the program by looking into the time-integrated CP asymmetry in $B^{\pm} \to D^0(\bar{D}^0)K^{\pm}$ decays. This work exploits the high acceptance and reconstruction of K_S^0 from $D^0 \to K_S^0\pi^0$ if the crystal ECAL is available. As a result, the angle γ_s from the sb unitarity triangle could be determined up to an uncertainty of $\mathcal{O}(1°)$ without assuming unitarity constraints..

Although the contributions introduced above significantly improve the understanding of the CEPC's potential in CPV measurements, the richness of hundreds of possible modes makes an exhaustive enumeration of the CEPC's CP asymmetry precision impractical. Even if only the minimal inputs for the CKM global fit are considered, there still remain many projections that need to be confirmed by MC simulations or solid recasting

Measurement	Current [105–107]	FCC [108]	CEPC prelim.	Comments
BR($Z \to \tau\mu$)	$< 6.5 \times 10^{-6}$	$\mathcal{O}(10^{-9})$	same [109]	$\tau\tau$ bkg, $\sigma(p_{\text{track}})$ & $\sigma(E_{\text{beam}})$ limited
BR($Z \to \tau e$)	$< 5.0 \times 10^{-6}$	$\mathcal{O}(10^{-9})$		
BR($Z \to \mu e$)	$< 7.5 \times 10^{-7}$	$10^{-8} - 10^{-10}$	1×10^{-9} [110]	PID limited

Table 7: Present limits on Z LFV decays and projected sensitivities at the Z-factory run of FCC-ee [108] and CEPC [109]. See also [110].

procedures. For example, the β angle is primarily determined by $b \to c\bar{c}s$ transitions via final states like $B^0 \to J/\psi K^0$ and their time-dependent CP asymmetries [9]. A dedicated simulation study may validate the projection in [18] or push it even further. The measurement of the angle α also receives contributions from other $b \to u\bar{u}d$ transitions (see Figure 25), $e.g.$, multiple $B \to \rho\rho$ and $B \to \rho\pi$ asymmetries.

The CP asymmetry measurements highlighted in this section employ well-established channels. At the same time, future studies considering alternative observables that might prove advantageous at the CEPC could be valuable. Such possibilities could involve channels with multiple photons in the final state, for instance, $\Lambda_b^0 \to p\rho^-(\to \pi^0\pi^-)$ [99]. Additionally, the CEPC enables measurements of other intriguing rare hadronic decay modes, which include, (but are not limited to), $B_s \to D^{(*)0}\bar{D}^{(*)0}$, $B_s \to \pi^0\eta'(\to \pi^+\pi^-\eta)$ [100], and $B_c^+ \to \pi^+\omega(\to \pi^+\pi^-\pi^0)$ [101]. Given the high detector acceptance and effective volume, modes with K_S^0 could also benefit from the high-quality reconstruction potential. Moreover, due to the low background level and substantial statistics at the CEPC, the Z pole run could offer an ideal setting for studying CP asymmetry in loop-suppressed rare decays. Even though they may not significantly contribute to the global CKM fit due to limited statistics, these decays are generally more sensitive to CPV NP [102, 103]. Interesting modes of $b \to s\nu\bar{\nu}$ and $b \to s\ell\ell$ rare decays are discussed in [103, 104].

6 Global Symmetry Tests in Z and b Decays

Aside from gauge symmetries, the SM also admits several global symmetries that are almost preserved, including lepton flavor symmetries (that is, the lepton family numbers), the total lepton number, and the baryon number. The only known violating effects for these symmetries are highly suppressed in collider environments; lepton family numbers are only violated by neutrino mixing and thus suppressed by the small neutrino mass differences; lepton and baryon numbers are only violated by the non-perturbative $SU(2)_L$ sphaleron that is exponentially suppressed at zero temperature. Therefore, observing Lepton Flavor Violation (LFV), Lepton Number Violation (LNV) or Baryon Number Violation (BNV) at the CEPC would be indisputable evidence for BSM physics. Although previous experimental bounds suggest that the rates of such processes, if any exist, should be extremely rare, these forbidden modes in the SM often give striking signals that are distinct from background events. The CEPC, with sufficient event statistics and a clean environment, may play a significant role at testing possible violations of the above global symmetries.
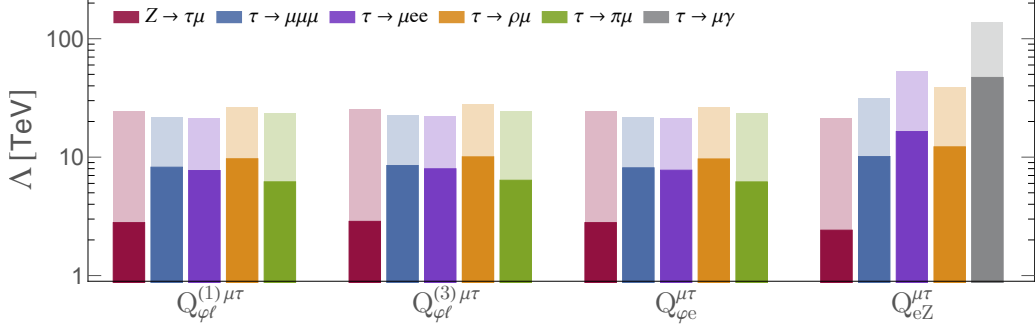
Figure 26: Sensitivity on the NP scale Λ associated to different LFV operators – cf. Eqs. (6.1, 6.2) – from the current bounds on various LFV observables (dark-colored bars) and future expected reach from searches for $Z \to \tau\mu$ at the CEPC and $\tau \to \mu$ transitions at Belle II with 50 ab^{-1} (light-colored bars). The Wilson coefficients are set equal to 1 for one operator at a time. From [111].

Recent research on the prospect of discovering NP at the CEPC and similar Z factory projects largely emphasizes the role of searches for LFV in Z decays. The current limits and projected sensitivities are shown in Table 7. An improvement no larger than one order of magnitude can be expected at the high-luminosity run of the LHC (HL-LHC), as a consequence of the large background from $Z \to \tau\tau$, which is difficult to deal with at hadron colliders. On other the hand, as outlined in [110, 111], searches for LFV Z decays at Tera Z factories can test plausible theoretical frameworks. It was found that although the allowed rates of $Z \to \mu e$ generally lie way beyond the expected sensitivity,[2] a Tera Z factory, with its $\mathcal{O}(10^{12})$ Z decays, holds promise for $Z \to \tau\ell$ decays, whose rates can be as large as BR$(Z \to \tau\ell) \approx 10^{-7}$ without being in conflict with the indirect limits set by LFV τ decays [111]. In particular, the CEPC could probe NP at a level comparable to future low-energy LFV observables. This is illustrated in Figure 26, where the possible reach of searches for a number of LFV τ decays at Belle II – assuming that the experiment will collect an integrated luminosity of 50 ab^{-1} – is compared with the CEPC sensitivity on the NP scale Λ associated to the dimension-6 SM EFT (SMEFT) operators $\mathcal{H}_{\text{SMEFT}} \supset \frac{1}{\Lambda^2} \sum_a C_a Q_a$ [112, 113] that can induce $Z \to \tau\mu$ at the tree level. These operators are defined as

$$Q_{\varphi\ell}^{(1)} \equiv i(\Phi^\dagger \overleftrightarrow{D}_\mu \Phi)(\bar{L}\gamma^\mu L), \quad Q_{\varphi\ell}^{(3)} \equiv i(\Phi^\dagger \tau^I \overleftrightarrow{D}_\mu \Phi)(\bar{L}\tau^I \gamma^\mu L), \quad Q_{\varphi e} \equiv i(\Phi^\dagger \overleftrightarrow{D}_\mu \Phi)(\bar{E}\gamma^\mu E),$$
$$(6.1)$$

$$Q_{eZ} \equiv (\sin\theta_w Q_{eB} + \cos\theta_w Q_{eW}) \quad \left[Q_{eB} \equiv (\bar{L}\sigma^{\mu\nu}E)\Phi B_{\mu\nu}, \; Q_{eW} \equiv (\bar{L}\sigma^{\mu\nu}E)\tau^I \Phi W_{\mu\nu}^I\right],$$
$$(6.2)$$

where L and E are respectively the SM doublet and singlet lepton fields (with flavor indices omitted), Φ is the Higgs doublet, $B_{\mu\nu}$ and $W_{\mu\nu}^I$ ($I = 1, 2, 3$) are respectively the $U(1)_Y$ and $SU(2)_L$ field strengths, τ^I are the Pauli matrices, and $\Phi^\dagger \overleftrightarrow{D}_\mu \Phi \equiv \Phi^\dagger(D_\mu\Phi) - (D_\mu\Phi)^\dagger\Phi$.

---

[2]Barring unlikely accidental cancellations among different contributions, searches for LFV muon decays set the indirect constraint BR$(Z \to \mu e) \lesssim 10^{-12}$ [111].

See [111] for details. As one can see from the figure, NP scales up to $20 - 30$ TeV can be probed by searches for $Z \to \tau\mu$ at the CEPC. Similar results are obtained for $Z \to \tau e$.

The study in [110] also considers an alternative probe: the non-resonant production of $\tau\mu$ at future electron-positron colliders. The CEPC and FCC-ee's expected sensitivity to $e^+e^- \to \tau\mu$ signals was examined. It was found that the signal exhibits a characteristic dependence on the center-of-mass energy, depending on which effective operator in the SMEFT is the dominant source of LFV. For instance, while the contributions of operators containing the Z boson are resonantly enhanced on the Z pole, contributions to the $e^+e^- \to \tau\mu$ cross-section from contact interactions – $i.e.$, 4-fermion operators such as $(\bar{e}\gamma_\mu P_X e)(\bar{\mu}\gamma^\mu P_Y \tau)$ $(X, Y = L, R)$ – increases linearly with the center-of-mass energy squared s. In contrast, dipole interactions as in Eq. (6.2) yield a cross-section that remains constant at large s, while the Higgs current interactions in Eq. (6.1) result in a cross-section that decreases as $1/s$ for large s. Overall, the Tera Z factories can test NP scales of the order of $\mathcal{O}(10 \text{ TeV})$, rivaling the sensitivity of searches for LFV tau decays at Belle II. The framework provided by this study enables the disentanglement of contributions from different operators, exploiting the complementarity of searches at various center-of-mass energies. Additional diagnostic measures could potentially be provided by measurements of forward-backward asymmetry or CP asymmetries. LFV searches at energies beyond the Z pole, in particular for LFV Higgs decays, were recently studied also in [114], with the conclusion that the statistical uncertainty on $\mathrm{BR}(h \to \tau\ell)$ can reach the 10^{-4} level. The sensitivity improves to the $\mathcal{O}(10^{-5})$ level when considering the $h \to \mu e$ decay. However, the rate of this process is indirectly constrained to be $\mathrm{BR}(h \to \mu e) \lesssim 10^{-8}$ by LFV muon decays [115].

A set of related observables is provided by the ratios of (flavor-conserving) leptonic Z decays. In fact, LFUV and LFV processes are often correlated and imply each others within explicit NP models [116]. Currently, the flavor universality of the Z boson couplings to leptons is probed at the per mil level [117]:

$$\frac{\mathrm{BR}(Z \to \mu^+\mu^-)}{\mathrm{BR}(Z \to e^+e^-)} = 1.0009 \pm 0.0028 \,, \quad \frac{\mathrm{BR}(Z \to \tau^+\tau^-)}{\mathrm{BR}(Z \to e^+e^-)} = 1.0019 \pm 0.0032 \,. \quad (6.3)$$

Despite being based on a combination of old data sets, (1.7×10^7 Z decays at LEP experiments, plus 6×10^5 Z decays with polarized beams at SLC), these tests were among the most challenging constraints on NP models aiming at a combined explanation of the anomalies in charged-current and neutral-current semileptonic B decays [118]. Improving on these observables would then probe LFUV NP with high precision. For instance, reaching a 10^{-4} level precision on the measurements of $\mathrm{BR}(Z \to \ell^+\ell^-)$ would be sensitive to the scale Λ of the flavor-conserving counterparts of the operators appearing in Figure 26 – see Eq. (6.1) – above ≈ 20 TeV, ($e.g.$, if NP couples dominantly to τ leptons). Similarly, a Z LFU test with such a level of precision would reach $\Lambda \approx 10$ TeV for the scale of a semileptonic charged-current operator comprising third generation fields that contributes to other LFUV observables such as $R_{D^{(*)}}$, cf. Eq. (3.5). We notice that at a Tera Z factory, these measurements are only limited by systematics, while statistical and systematic errors were of the same order at LEP. Hence further scrutiny is necessary in order to assess the CEPC

capability of performing tests of LFU in Z decays by reducing the systematic uncertainties on $\text{BR}(Z \to \ell^+\ell^-)$ substantially below the LEP level.

Investigations into LFV effects also extend to heavy hadron decays [119], such as $H_b \to H_{d/s}\tau\ell$, where H_f denotes a hadron of flavor f and ℓ an electron or a muon. These are significant not only in the context of flavor anomalies but also in their contribution to our understanding of flavor patterns relating the third generation of quarks and leptons. In the past, experimental efforts have primarily focused on the mode $B^+ \to K^+\mu\tau$, reaching upper limits at the 10^{-5} level [120]. Topological reconstruction techniques, employing a fast parametric simulation with momentum reconstruction resolutions and high-resolution vertex detector performance, have been implemented to simulate LFV signal events for $B^0 \to K^{*0}\mu\tau$ as well. Initial explorations have demonstrated the potential detector requirements, offering guidance for future design and performance goals for the vertex detector. As for LFV two-body decays, preliminary studies are showing that constraints from the CEPC on decays such as $B^0_{(s)} \to \mu^\pm e^\mp$ and $B^0_{(s)} \to \tau^\pm\mu^\mp$ could match the LHCb sensitivity [17], with a relatively more substantial improvement for $B^0_{(s)} \to \tau^\pm e^\mp$, due to the expected CEPC's excellent electron identification.

In addition to the LFV searches discussed above, the potential of several LFV, lepton number violation (LNV), and baryon number violation (BNV) searches remains to be evaluated at CEPC. For instance, analyses of LNV modes, such as $B^+ \to \pi^-(K^-)\ell^+\ell^+$, are fundamentally straightforward, with limitations primarily due to statistics and lepton charge identification. Unlike LHCb studies focused on same-sign di-muon modes [121, 122], the CEPC could yield considerable contributions to the same-sign di-electron cases, given the achievable low misidentification rates for electrons. On the other hand, BNV searches may feature signals including forbidden baryon-antibaryon oscillations [123] and explicit BNV decays. A typical example of the latter is $\Lambda^0_b \to h^-(h^0)\ell^+$, which can generated by dimension-6 $qq'q''\ell$ operators that conserve the $B - L$ charge.

7 Charm and Strange Physics

The high $\text{BR}(Z \to c\bar{c}) \simeq 12\%$ comparable to $\text{BR}(Z \to b\bar{b}) \sim 15\%$ makes the CEPC a c-factory as well. Charm physics studies enjoy the high luminosity, low background level, and good detector system at the CEPC. Unfortunately, few solid statements about charm physics are available at the current stage. On the other hand, the recent observation of CPV in charm decays [124–126] raises the necessity of further charm physics studies and constrains possible NP contributions.

Possible worthwhile avenues of investigation for charm physics at the CEPC, akin to the discussion in Section 3 and 4, include semileptonic c-hadron decays. Theoretical discussions were conducted for rare $c \to u\nu\bar{\nu}$ decays [127], yet the phenomenology at the Z pole remains elusive. In addition, hadronic c decay modes play key roles in both charm and b physics, given that the $b \to c + X$ EW transition is the dominant b decay mode. Decays involving neutral particles can enhance the c-hadron tagging efficiency, $e.g.$, $D^0 \to K^-\pi^+\pi^0$ with its BR=14.2% and its reconstructable decay vertex. Other similar modes include $D^0 \to K^0_S\pi^+\pi^-\pi^0$ (BR=5.1%) or $D^0 \to K^-2\pi^+\pi^-\pi^0$ (BR=4.2%). For D_s, reconstructions

like $D_s^+ \to K^+K^-\pi^+\pi^0$ (BR=6.3%), $D_s^+ \to \eta\rho^+$ (BR=8.9%), or $\eta'\rho^+$ (BR=5.8%) were considered. c-hadron to CP eigenstates, such as $D^0 \to K_S^0\pi^0, K_S^0\omega, K_S^0\phi$, were valuable for extracting CPV parameters from $B \to DK$ type decays and are hence important for determining the CKM γ angle [9], as stated in Section 5. Regarding direct CPV effects in charm decays, precision probes crucial in measuring the parameter $\Delta\mathcal{A}_{\rm CP} \equiv \mathcal{A}_{\rm CP}(K^+K^-) - \mathcal{A}_{\rm CP}(\pi^+\pi^-)$: for the sake of comparison the LHCb upgrade II prospect is $\sim 3 \times 10^{-4}$ [17]. Other decays useful for probing CPV include $D^+ \to \pi^+\pi^0$, $D^0 \to K_S^0\bar{K}_S^0$, and $D_{(s)}^+ \to K^+K_S^0\pi^+\pi^-$, among others.

A full-simulation study has showcased the excellent reconstruction quality for K_S^0 and Λ at the CEPC, featuring efficiencies $\gtrsim 30\%$ and purity $\sim 90\%$ [46]. These short-lived strange hadrons, with lifetimes of $\mathcal{O}(100)$ ps, are suitable for the CEPC's tracking system. In contrast, higher-intensity experiments like the kaon factories prioritize longer-lived $K^\pm$ and K_L^0 states, even in planned upgrades [128–130]. Hence, the exploration of the K_S^0 and Λ physics potential at CEPC is essential. With its PID-friendly environment, CEPC facilitates the investigation of rare K_S^0 or Λ decays with reduced background systematics as compared to LHCb [131]. A case in point is the rare decay $K_S^0 \to \mu\mu$, with the current limit being $\mathcal{O}(100)$ times greater than its SM prediction. With $\mathcal{O}(10^{12})$ K_S^0 produced at CEPC, this rare decay mode can be measured. Given that most strange quarks are pair-produced at the Z pole, initial strange quark sign tagging prior to $K^0 - \bar{K}^0$ mixing is achievable, analogous to b or c tagging. It was demonstrated that observing CPV in this mode enables extrapolation of $|V_{td}V_{ts}|\sin(\beta+\beta_s)$ [132, 133]. There also lies the CEPC potential for other rare decays involving neutral final states, like $K_S^0 \to \mu\mu\gamma$ or $K_S^0 \to \mu\mu\pi^0$, which require future investigations.

7.1 Null tests with rare charm decays

It is well-known that, due to the strong GIM suppression, the sensitivity of rare charm decays to NP is expected to be higher than that of the rare b decays [134–136]. Nevertheless, due to the large resonance contributions, it is much more challenging to control the hadronic effects in charm decays. Furthermore, the usually adopted heavy quark expansion methods in rare b decays become much less reliable when applied to the rare charm decays. Therefore, the short-distance physics in rare charm decays cannot be probed through simple observables like the branching ratios. Instead, we can consider the so-called "null tests", i.e., the observables that are strongly suppressed within the SM due to exact or approximate symmetries and largely free of hadronic uncertainties. Typical examples include potential deviations from the lepton flavor universality in semileptonic $c \to u\ell^+\ell^-$ decays [137], the lepton flavor violating decays like $D \to \pi e\mu$ and $D_s \to Ke\mu$ [138], the angular observables in semileptonic $c \to u\ell^+\ell^-$ decays [139, 140], as well as the di-neutrino decay modes like $D \to \pi\nu\bar{\nu}$ and $D_s \to K\nu\bar{\nu}$ [127, 141]. Any observation of a non-standard effect in these null tests would be a robust evidence of NP beyond the SM. The NP effects in rare charm decays could also be probed through measurements of the di-lepton production at high-energy colliders [142], as well as through the low-energy scattering processes $e + p \to e(\mu) + \Lambda_c$ [143–145].

Measurement	Current [150]	FCC [108]	CEPC prelim. [109]	Comments
Lifetime [sec]	$\pm 5 \times 10^{-16}$	$\pm 1 \times 10^{-18}$		from 3-prong decays, stat. limited
$\mathrm{BR}(\tau \to \ell\nu\bar{\nu})$	$\pm 4 \times 10^{-4}$	$\pm 3 \times 10^{-5}$		$0.1\times$ the ALEPH systematics
$\mathrm{m}(\tau)$ [MeV]	± 0.12	$\pm 0.004 \pm 0.1$		$\sigma(p_{\mathrm{track}})$ limited
$\mathrm{BR}(\tau \to \mu\mu\mu)$	$< 2.1 \times 10^{-8}$	$\mathcal{O}(10^{-10})$		
$\mathrm{BR}(\tau \to eee)$	$< 2.7 \times 10^{-8}$	$\mathcal{O}(10^{-10})$		
$\mathrm{BR}(\tau \to e\mu\mu)$	$< 2.7 \times 10^{-8}$	$\mathcal{O}(10^{-10})$	same	bkg free
$\mathrm{BR}(\tau \to \mu ee)$	$< 1.8 \times 10^{-8}$	$\mathcal{O}(10^{-10})$		
$\mathrm{BR}(\tau \to \mu\gamma)$	$< 4.4 \times 10^{-8}$	$\sim 2 \times 10^{-9}$	$\mathcal{O}(10^{-10})$	$Z \to \tau\tau\gamma$ bkg , $\sigma(p_\gamma)$ limited
$\mathrm{BR}(\tau \to e\gamma)$	$< 3.3 \times 10^{-8}$	$\sim 2 \times 10^{-9}$		

Table 8: Projected sensitivities for some τ physics measurements at the Z-factory run of FCC-*ee* [108] and CEPC [109]. Absolute instead of relative uncertainties are quoted. For the LFV modes $\tau \to eee$, $\tau \to \mu ee$, and $\tau \to e\mu\mu$, we assume that the sensitivity is similar to that of $\tau \to \mu\mu\mu$.

8 τ Physics

With $\mathrm{BR}(Z \to \tau\tau) \sim 3\%$ in the SM, the CEPC is anticipated to yield $\sim 10^{11}$ tau lepton pairs [1] (see Table 2). The machine could thus produce five orders of magnitude more τ leptons than the last generation Z factory, *i.e.*, the LEP [117]. The absence of accompanying showered particles and large boosts ($\gamma_\tau \sim 26$) in τ production at the Z pole renders these events particularly favorable for measurements and analyses. The amount of τ events at the CEPC is comparable to that produced at Belle II ($\sim 5 \times 10^{10}$ τ pairs) [6, 146], while the reconstruction efficiency of the τ lepton and the identification of some particular decay modes could be significantly better due to the larger boost of τ lepton and the particle flow oriented detector design at CEPC, with promising tagging efficiencies. Similarly, the τ event yield at the CEPC is anticipated to comparable to those at the proposed SCTF project ($\sim 3.5 \times 10^{10}$ τ pairs in 10 years) [25, 147]. These attributes make the CEPC an optimal environment for τ physics and contribute significantly to the future of τ physics. The preliminary study in [47] investigated the tagging efficiency of inclusive τ hadronic modes using CEPC full simulations, obtaining an efficiency times purity value of approximately 70%, ascertained from W^+W^- events. Concurrently, research is being undertaken to scrutinize the exclusive tagging of prominent τ decay modes with the dual-readout calorimeter at the Z pole [148]. Preliminary results suggest that the average τ-tagging accuracy of seven common decay modes is around 90%. Detector performances of τ-tagging at the Z pole with the aid of machine learning algorithms were also investigated in [149].

Recent τ physics projections and potential measurements at an e^+e^- collider running at the Z pole have been comprehensively summarized by [108]. This analysis, predominantly founded on rapid simulations within the FCC-*ee* context, provides valuable benchmarks. The study is comprehensive, focusing on precision decay time and mass measurements, LFU tests in leptonic τ decays, and LFV τ decays.
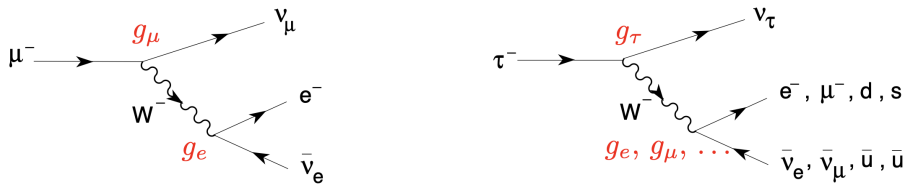
Figure 27: Illustrative Feynman diagrams for the muon and tau decays. In the SM, $g_e = g_\mu = g_\tau$ is predicted. Adapted from [154].

8.1 LFV τ Decays

The large number of τ pairs, high boost, and low background make Z-factories an ideal environment to study τ LFV decay modes. As discussed in Section 6, these decays are complementary to LFV observables at higher energy scales, which highlights the theoretical importance of these modes in discriminating among different NP models [151, 152]. Table 8 displays current limits compared with FCC-ee projections from [108] and CEPC preliminary estimates from [109] for a number of purely leptonic and radiative LFV modes. These limits should be also compared with the future reach of Belle II. Based on projections from existing Belle results, the prospects for over 50 distinct τ LFV decay modes have been presented in [6] and recently revised in [153]. With 50 ab^{-1} of collected data, Belle II is expected to set limits in the $10^{-10} - 10^{-9}$ range for most decay modes with the notable exception of the radiative decays, $\tau \to \ell\gamma$, whose BRs can not be constrained much below the 10^{-8} level, as a consequence of the difficult background from initial-state-radiation photons affecting e^+e^- colliders running at energies around the $\Upsilon(\text{nS})$ resonances. As we can see, Tera-Z factories can play a crucial role in discovering or constraining τ LFV searching for the radiative modes – and, more in general, it will be complementary to Belle II measurements, reaching a comparable sensitivity for the other modes displayed in Table 8. Clearly, in order to achieve that, the ECAL/PFA performance will be crucial, especially when the LFV final states have one or more neutral components. Besides the radiative decays, other examples of such a situation include $\tau \to \ell h^0$ with $h^0 = \pi^0(\to \gamma\gamma)$, $\eta(\gamma\gamma)$, $\eta'(\pi^+\pi^-\eta)$, etc. Additionally, since τ LFV decays do not feature neutrinos, the m_τ invariant mass peak reconstruction plays a crucial rule in suppressing large backgrounds from ordinary τ decays. For explicit discussions of the $\tau \to \ell\gamma$ phenomenology at Tera-Z factories, see [108, 109], while studies of the prospects for hadronic τ LFV decays are still lacking and will require future efforts. Finally, we notice that, in presence of a light NP boson a with LFV couplings to SM leptons, decays such as $\tau \to \ell a$ can also occur. We will discuss such exotic LFV τ decay modes involving light on-shell BSM states in Section 12.

8.2 LFU Tests in τ Decays

Table 8 also reports current accuracy and Tera-Z prospects of measurements of the τ mass, lifetime, and the BRs of standard leptonic τ decays. These are the crucial quantities to perform tests of LFU in τ and μ decays. The SM predicts LFU of weak charged currents, that is, that the three lepton families couple with the same strength to $W^\pm$ bosons, *i.e.*, $g_e = g_\mu = g_\tau = g$, where $g = e/\sin\theta_w$ is the $SU(2)_L$ gauge coupling, cf. Figure 27.

Inspecting the processes in the figure, one can see that the LFU prediction can be tested by measuring the following quantities:

$$\left(\frac{g_\mu}{g_e}\right)^2 = \frac{\mathrm{BR}(\tau \to \mu\nu\bar{\nu})}{\mathrm{BR}(\tau \to e\nu\bar{\nu})} \frac{f(m_e^2/m_\tau^2)}{f(m_\mu^2/m_\tau^2)} \frac{R_W^{\tau e}}{R_W^{\tau\mu}}, \tag{8.1}$$

$$\left(\frac{g_\tau}{g_\ell}\right)^2 = \frac{\tau_\mu}{\tau_\tau} \left(\frac{m_\mu}{m_\tau}\right)^5 \frac{\mathrm{BR}(\tau \to \ell\nu\bar{\nu})}{\mathrm{BR}(\mu \to e\nu\bar{\nu})} \frac{f(m_e^2/m_\mu^2)}{f(m_\ell^2/m_\tau^2)} \frac{R_W^{\mu e} R_\gamma^\mu}{R_W^{\tau\ell} R_\gamma^\tau}, \quad (\ell = e, \mu), \tag{8.2}$$

where $\tau_{\tau/\mu}$ is the decaying lepton lifetime, $f(x) = 1 - 8x + 8x^3 - x^4 - 12x^2 \log x$ is a phase-space factor, $R_W^{\ell'\ell} = 1 + \frac{3}{5}\frac{m_{\ell'}^2}{m_W^2} + \frac{9}{5}\frac{m_\ell^2}{m_W^2}$ and $R_\gamma^\ell = 1 + \frac{\alpha(m_\ell)}{2\pi}\left(\frac{25}{4} - \pi^2\right)$ are electroweak and QED radiative corrections respectively [9, 154].[3] Using the purely leptonic processes in Figure 27, the current experimental determination of the coupling ratios results to be compatible with LFU at the per mil level [9]:

$$\left(\frac{g_\mu}{g_e}\right) = 1.0009 \pm 0.0014, \quad \left(\frac{g_\tau}{g_e}\right) = 1.0027 \pm 0.0014, \quad \left(\frac{g_\tau}{g_\mu}\right) = 1.0019 \pm 0.0014. \tag{8.3}$$

As muon physics quantities are known with high precision, the above uncertainties only stem from measurements of τ leptonic BRs, lifetime and mass. The present relative uncertainties on $\mathrm{BR}(\tau \to e\nu\bar{\nu})$ and $\mathrm{BR}(\tau \to \mu\nu\bar{\nu})$ are respectively 2.2‰ and 2.3‰ [150], which have a ≈ 1.1‰ impact on the measurement of coupling ratios. As we can see, they constitute the major source of uncertainty at the moment. The impact of τ_τ on the uncertainty of g_τ/g_ℓ is at a comparable level, ≈ 0.9‰, given its current 1.7‰ relative precision [150]. On the other hand, the current world average for m_τ is substantially more precise, with a relative error of 6.7×10^{-5} [150], which contributes to the uncertainty of g_τ/g_ℓ only at the 0.2‰ level. As shown in Table 8, important contributions on the τ mass measurement are unlikely at a Tera-Z factory. However, m_τ is already known with enough precision to allow to test LFU in Eq. (8.2) below the per mil level. Moreover, substantial improvements on the determination of m_τ are to be expected at BESIII [155], Belle II [6] – which recently released the single most precise measurement [156] – and an STCF [25]. As suggested by the numbers in Table 8, Tera-Z factories can instead play a major role for what concerns the measurement of the BRs and lifetime. In fact, the world average for $\mathrm{BR}(\tau \to \ell\nu\bar{\nu})$ is still dominated by measurements at LEP experiments that were statistically limited, although the systematic errors are typically just a factor of two smaller than the statistical ones [150]. On the other hand, measurements of τ_τ at LEP had comparable statistical errors and systematic uncertainties, which were respectively twice and three times larger than those of the most precise measurement of τ_τ from Belle [157]. Given the large boost stemming from $m_Z \gg m_\tau$, lifetime measurements are simpler at a Tera-Z factory. Moreover, statistic is not going to be a limitation at the CEPC, hence the main challenge will be to control the systematics on τ_τ and $\mathrm{BR}(\tau \to \ell\nu\bar{\nu})$ at a level better than LEP. If about one order of magnitude improvement can be achieved, as indeed estimated in [108] (see

---

[3]Numerically one obtains $R_\gamma^\mu/R_\gamma^\tau - 1 \simeq 8.0 \times 10^{-5}$ [9], $R_W^{\tau e}/R_W^{\tau\mu} - 1 \simeq -\frac{9}{5}\frac{m_\tau^2}{m_W^2} \simeq -3.1 \times 10^{-6}$ and $R_W^{\mu e}/R_W^{\tau\ell} - 1 \simeq -\frac{3}{5}\frac{m_\tau^2}{m_W^2} \simeq -2.9 \times 10^{-4}$.

Table 8), the precision in Eq. (8.3) will reach $\approx \pm 1 \times 10^{-4}$. This would make CEPC very sensitive to LFUV NP scenarios, such as those discussed in the literature in the context of the $R_{D^{(*)}}$ anomaly [9], as one can see, *e.g.*, in [118], where it was shown that tests of LFU in the τ sector are already providing important constraints on such models. As another example of the discovery potential of these measurements, we can consider the SMEFT operator $\frac{1}{\Lambda^2} i (\Phi^\dagger \tau^I \overset{\leftrightarrow}{D}_\mu \Phi)(\bar{L}_3 \tau^I \gamma^\mu L_3)$ (with $L_3 \equiv (\nu_\tau, \ \tau_L)^T$), which only involves (left-handed) τ leptons and is the flavor-conserving counterpart of the operators discussed in Section 6 that gives rise to Z LFV decays. The presence of such an operator would induce the shift $g_\tau = g \left(1 + \frac{v^2}{\Lambda^2}\right)$ [61], where $v \simeq 246$ GeV is the vacuum expectation value of the Higgs field. A 0.1‰ level precision in the determination of g_τ / g_ℓ would then test a NP sector generating such an operator (but not the corresponding ones involving muons or electrons) up to about $\Lambda \approx 20$ TeV.

8.3 Hadronic τ Decays and Other Opportunities

Other significant aspects of τ physics at the CEPC are yet to be fully explored, for instance, the precise measurements of various (SM-allowed) hadronic τ decays. Historically, during the LEP era, precision in these measurements was constrained by systematic limitations [158, 159]. In fact, the systematic uncertainties of LEP measurements of τ hadronic decays are often comparable to the statistical ones. The CEPC's performance in these measurements, especially in processes with relatively high hadron multiplicity (*e.g.*, from τ decays into 3 and 5 hadrons) and in the large hadron m^2 region, is expected to exceed the results obtained at LEP. In turn, it is promising that LEP experiments still provide the most precise measurements for a significant portion of inclusive and exclusive hadronic τ decay channels [150], which highlights the advantage of high-energy e^+e^- colliders over other flavor factories in this field. Nevertheless, reaching better sensitivities at the CEPC will further challenge the calorimeter system and PID performance. We remind that inclusive hadronic decays are crucial for the extraction of the strong coupling constant $\alpha_s(m_\tau)$ [154], which is currently limited by the uncertainties in the large-recoil region. Another potential topic worth investigation is the measurement of the $\tau \to K(+X)$ decay modes, which turns out to be useful in both the determination of $|V_{us}|$ and the kaon decay constant f_K. Additionally, polarization measurements of the τ leptons produced in Z decays can provide additional handles to study LFU and add relevant input to the EWPT global fit [160], which is often led by $\tau \to \rho\nu$ and $\tau \to \pi\nu$ hadronic decays. For more theoretical insights and details on hadronic τ decays, see [154, 161].

Finally, we remark that hadronic τ decays at the CEPC could be employed to improve the measurements of the τ electric dipole moment (d_τ) and the currently weakly-constrained τ anomalous magnetic moment (a_τ), *e.g.*, along the lines of the studies in [162, 163] performed in the context of Belle II. Interestingly, the current best limit on the magnetic moment $- -0.052 < a_\tau < 0.013$ at 95% CL – was set by the DELPHI experiment at LEP studying $\tau^+\tau^-$ production in photon-photon collisions at energies larger than the Z pole [164]. As we can see, the above limit is still one order of magnitude larger than the SM prediction, $a_\tau^{\mathrm{SM}} = 0.00117721(5)$ [165], while Belle II could test BSM contributions to

a_τ at the 10^{-6} level [162, 163]. The possible role of future high-energy e^+e^- colliders in this endeavor needs to be evaluated.

8.4 CPV in hadronic τ decays

The hadronic τ decays, besides serving as a clean laboratory to study the low-energy aspect of strong interaction [154, 161, 166], are also a good place to study CPV both within the SM and beyond [167–171]. Interestingly, when the well-established CP asymmetry in $K^0 - \bar{K}^0$ mixing is taken into account, a non-zero CPV of $\mathcal{O}(10^{-3})$ can arise in the processes involving a K_S or a K_L meson in the final state [172, 173]. Therefore, any significant excess of CP asymmetry beyond the SM expectation can be served as a clear hint of NP. Assuming that the hadronic τ decays receive an additional contribution from some NP, which carries different weak and strong phases from that of the SM term, one can then construct CP-violating observables in terms of the interference between the SM and NP amplitudes. Being of linear dependence on the potential NP amplitude, these observables show a higher sensitivity to NP than do other SM-forbidden ones, such as the $\tau \to \mu\gamma$ decay rate and the electric dipole moment (EDM) of leptons, which are usually quadratic in the NP amplitude [170]. For this purpose, possible CPV in $\tau \to K_S\pi\nu_\tau$ decays has been searched for by several experiments. After the initial null results from CLEO [174, 175] and Belle [176], a non-zero CP asymmetry was reported for the first time by the BaBar collaboration [177], by measuring the decay-rate difference between τ^+ and τ^- decays. However, such a measurement is in conflict with the SM prediction [172, 173, 178] at the level of 2.8σ, which has motivated many NP explanations by including the extra contribution from non-standard tensor interactions [178–180].

Another interesting observable is the CP asymmetry in the angular distributions of $\tau \to K_S\pi\nu_\tau$ decays, which can be measured for unpolarized single τ's even if their rest frame cannot be reconstructed [168]. Following the same notation as adopted in Ref. [6], we can write the CP-violating observable as

$$A_i^{CP} = \frac{\int_{s_{1,i}}^{s_{2,i}} \int_{-1}^{1} \cos\alpha \left[\frac{d^2\Gamma(\tau^- \to K_S\pi^-\nu_\tau)}{ds\,d\cos\alpha} - \frac{d^2\Gamma(\tau^+ \to K_S\pi^+\bar\nu_\tau)}{ds\,d\cos\alpha} \right] ds\,d\cos\alpha}{\frac{1}{2}\int_{s_{1,i}}^{s_{2,i}} \int_{-1}^{1} \left[\frac{d^2\Gamma(\tau^- \to K_S\pi^-\nu_\tau)}{ds\,d\cos\alpha} + \frac{d^2\Gamma(\tau^+ \to K_S\pi^+\bar\nu_\tau)}{ds\,d\cos\alpha} \right] ds\,d\cos\alpha} \,, \qquad (8.4)$$

which is defined as the difference between the differential τ^- and τ^+ decay widths weighted by $\cos\alpha$, with α being the angle between the directions of K and τ in the $K\pi$ rest frame, and can be evaluated in different bins of the $K\pi$ invariant mass squared s, with the i-th bin given by the interval $[s_{1,i}, s_{2,i}]$ [176]. As a K_S meson is involved in the final state, the well-established CPV in $K^0 - \bar{K}^0$ mixing can also induce a non-zero CP asymmetry in the angular distributions even within the SM [181, 182]. Direct CPV in the angular distributions of $\tau \to K_S\pi\nu_\tau$ decays can be induced by the interference between the S-wave from exotic scalar-exchange and the P-wave from SM W-exchange diagrams, provided the couplings of exotic scalars to fermions are complex, and has been studied for both polarized and unpolarized beams [167, 168]. While being still plagued by large experimental uncertainties, the current constraints will be improved with more precise measurements from the Belle II experiment [6], as well as the future Tera-Z [161] and STCF [183] facilities.

Measurement	Current Limit [150]	CEPC prelim.	Comments
$\mathrm{BR}(Z \to \pi^+\pi^-)$	-	$\mathcal{O}(10^{-10})$	$\sigma(\vec{p}_{\mathrm{track}})$ limited, good PID
$\mathrm{BR}(Z \to \pi^+\pi^-\pi^0)$	-	$\mathcal{O}(10^{-9})$	$\tau\tau$ bkg
$\mathrm{BR}(Z \to J/\psi\gamma)$	$< 1.4 \times 10^{-6}$	$10^{-9} - 10^{-10}$	$\ell\ell\gamma + \tau\tau\gamma$ bkg
$\mathrm{BR}(Z \to \rho\gamma)$	$< 2.5 \times 10^{-5}$	$\mathcal{O}(10^{-9})$	$\tau\tau\gamma$ bkg, $\sigma(p_{\mathrm{track}})$ limited

Table 9: Preliminary Tera-Z limits on several exclusive hadronic Z decay modes. The limits come from the previous study [109] using CEPC full simulation samples. The exact numbers and systematic effects remain to be fully validated.

9 Exclusive Hadronic Z Decays

During the Tera-Z phase of CEPC, precise measurements can be made for various Z decay channels. Apart from the well-known decay channels involving lepton pairs and quark-jet pairs, which allow for the determination of the Z coupling to leptons and quarks, and the LFV channels for probing NP, there are also exciting opportunities to explore exclusive $Z \to$ hadron decay modes such as $J/\psi\gamma$ and $\pi\pi$, which have never been observed before. These decays, occurring at the typical electroweak scale and having better convergence behaviors, offer distinct advantages compared to traditional heavy flavor physics at the b- or c-mass scales.

In the pursuit of exploring flavor physics at the Z-mass scale, the measurements of exclusive $Z \to$ hadron decay modes intersect with QCD inquiries, particularly in the examination of factorization formalisms for exclusive processes. While the factorization formalisms for exclusive decays [184–187] are standard frameworks for theoretically calculating B meson decays, their applications to B decays are hindered by large power corrections of $\mathcal{O}(\Lambda_{\mathrm{QCD}}^n/m_b^n)$ due to the insufficiently large b quark mass. This dilemma, however, can be circumvented in exclusive Z decays, as the large Z mass significantly suppresses the inverse mass power corrections. Therefore, the leading-power factorization of exclusive Z decays, with smaller uncertainties and precise measurements, can serve as a touchstone for the examination of factorization formalisms. The example channel $Z \to J/\psi\,\gamma$, with a BR of $\sim 10^{-7}$ [188], has a good chance to be precisely measured at the CEPC [109] as compared to the current limit of $< 1.4 \times 10^{-6}$ [189]. Moreover, the Z decays into two mesons are expected to be exceptionally rare, with branching fractions of the order of 10^{-11} or smaller [190, 191]. Investigating this in the LHC era, or even the HE-LHC era, is unattainable, thereby positioning the CEPC as a vital entity.

In practical terms, the radiative $Z \to M\gamma$ decays can serve as a mean to investigate the internal structures of the involved light mesons, which are crucial theoretical inputs to factorization formulas, typically formulated by the light-cone distribution amplitudes (LCDAs). While the parton-distribution function (PDF) of the proton can be precisely determined by high-energy inclusive processes, a comparable comprehensive experimental determination of meson LCDAs is still lacking. However, the $Z \to M\gamma$ processes provide an ideal platform for extracting the leading-power LCDAs of mesons. This is due not only

to the involvement of only one meson in the process, but also because the large Z mass once again significantly suppresses power corrections, resulting in a clean environment. As illustrated in Table 9, the CEPC will feature a promising chance for determining the LCDAs of mesons such as J/ψ and ρ by accurately measuring their corresponding radiative decays.

Flavor-specific examples also encompass the Higgs exclusive hadronic decays, believed to be more sensitive to NP, especially to non-standard Yukawa couplings of the Higgs boson [192]. Such decays can be examined within the Higgs factory mode of the CEPC, and are thus primarily limited by statistics rather than systematic uncertainties. Despite the challenging nature of measuring these rare processes, exclusive decays $h \to V\gamma$ of the Higgs boson at the LHC, the high luminosity run of the LHC and the CEPC could provide the much-needed platform to investigate these processes. These measurements could be vital for testing the QCD factorization approach and extracting valuable information about the LCDAs of various mesons.

10 Flavor Physics beyond Z Pole

In preceding sections, flavor physics studies' prospects for the CEPC, primarily within the context of b, c, and τ decays, have been examined. Once the narrow resonance is formed, the outcomes exhibit limited sensitivity to the production details of heavy-flavored particles. Nonetheless, possibilities for scrutinizing the SM and seeking NP also reside at higher scales $\gg m_{b,c,\tau}$. Typically, sensitivity to NP increases with the energy scale, provided a consistent level of precision is maintained. An instance of this concept can be traced back to the LFV searches discussed in Section 6. Furthermore, the transition to a perturbative state in QCD with increasing scale significantly alters the physics paradigm. As an integral component of the flavor physics proposition, it is recommended that the CEPC exploit phases beyond the Tera-Z run, operating at energies up to the $2m_t$ threshold. During these runs, the CEPC can produce EW gauge bosons, Higgs, and top quarks directly, thereby enabling a deeper inspection of flavor physics at energies considerably surpassing $m_{b,c,\tau}$ to provide opportunities to probe NP.

10.1 $|V_{cb}|$ and W Decays

An essential measurement at higher energy scales turns out to be examining the CKM matrix elements' amplitudes from on-shell W decays, particularly $|V_{cb}|$. Recently, a discrepancy was identified between inclusive and exclusive B meson decays at the 3σ level [9]. This discrepancy, however, is not indicative of BSM physics, as both methods rely on semileptonic b-hadron decays and consequently are susceptible to theoretical uncertainties from non-perturbative QCD [9]. At higher energies, these non-perturbative effects are heavily suppressed, thereby improving the theoretical predictability [194]. Previous studies suggested that WW pair production from W factory runs could yield the most precise $|V_{cb}|$ measurement in future investigations [66]. This indication necessitates further comprehensive analysis for validation. Preliminary studies indicate that the Higgs factory mode significantly contributes to the precision of $|V_{cb}|$, given the sizeable $\sigma(e^+e^- \to WW) \simeq 17$ pb
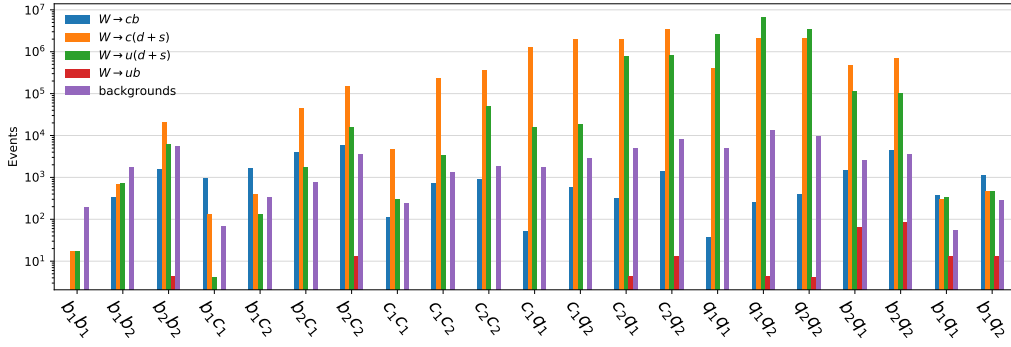
Figure 28: Event yields after basic selection at the Higgs factory run at the CEPC, with the signal being $ee \to W(\to cb)W(\to \mu\nu)$. Different jet flavor-tagging based signal regions are listed in horizontal axis. The most relevant signal regions are b_1c_1 and b_1c_2.
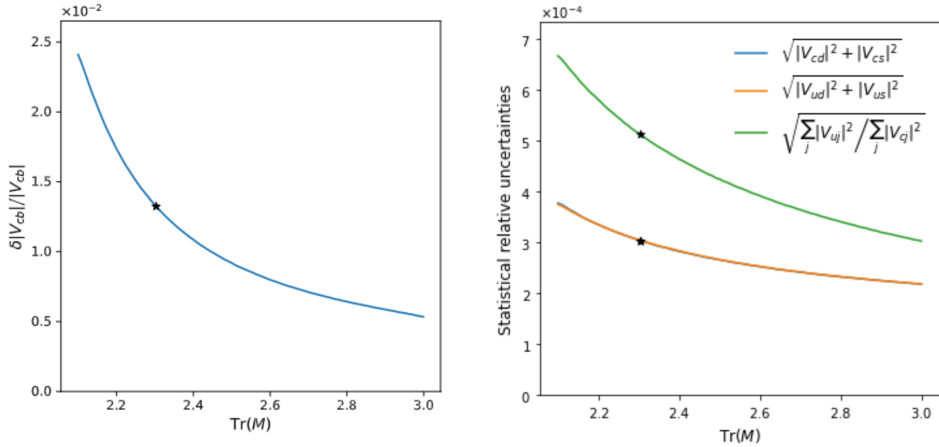

Figure 29: **LEFT:** the relative statistical uncertainties of $|V_{cb}|$ versus the trace of the migration matrix. **RIGHT:** statistical precision of $W \to c(d+s)$ and unitarity test versus the trace of the migration matrix. The stars indicate the CEPC baseline. Both plots are adapted from [193].

when $\sqrt{s} = 240$ GeV. Furthermore, W decay flavor physics studies bear similarities with Z decays and can delve into topics such as W exclusive hadronic decays [188].

By examining the full simulation of the CEPC baseline design, the precision of $|V_{cb}|$ in $\mu\nu qq$ and $\tau(\to \mu\nu\bar{\nu})\nu qq$ processes can be projected. The projected statistical error for $|V_{cb}|$ was determined to be $\lesssim 0.5\%$ [193] after extrapolating to the combined analysis of $ee \to WW \to qq\mu\nu$ at $\sqrt{s} = 240$ GeV with $L = 20$ ab^{-1}, providing accuracy on par with that from b-hadrons decay. The relevant simulation details are shown in Figures 28 and 29. The event statistics will further increase if the electron mode $ee \to WW \to qq\mu\nu$, shown in Figure 30, and the WW threshold scan data are included. On the other hand, the final performance of $|V_{cb}|$ determination relies on controlling systematic uncertainties, especially the flavor tagging efficiency and mistag rates, which remain to be fully evaluated in later
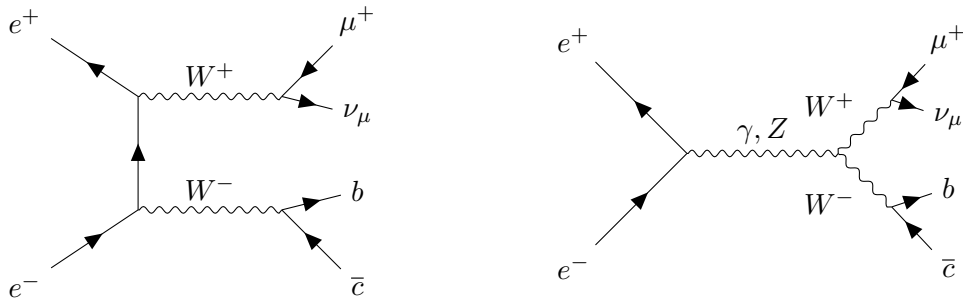
Figure 30: Illustrative Feynman diagrams for the $e^+e^- \to W^+W^- \to cb\mu\nu$ processes.

studies.

10.2 Higgs Exotic and FCNC

The study of flavor physics can also be conducted on the Higgs boson, such as via FCNC hadronic Higgs decays $H \to sb, sd, db, uc$ [4] These processes are forbidden in SM at tree level, but can have branching ratios up to 10^{-7} due to loop contribution. Since the final state is different species of quarks, it is crucial to identify the correct quark types. Using the machine learning, the study [32] develops a jet origin identification tool and estimates the upper limits of FCNC ($H \to sb, sd, db, uc$) and rare ($H \to ss, uu, dd$) hadronic Higgs decays. With the CEPC nominal parameters, these Higgs decay branching ratios can be measured with a typical upper limit of 0.02%—0.1% at 95% confidence level. Detailed simulation results are shown in Figure 31. For the $H \to ss$ decay, its upper limit exceeds the standard model prediction by a factor of three.

The SM predicts these FCNC hadronic Higgs decay processes to have extremely small branching ratios, however, several BSM theories, such as models with multiple Higgs doublets or supersymmetry[195], could enhance the rates of these decays. Therefore, any observation of Higgs hadronic FCNC decays at rates significantly above the SM predictions would be a strong indication of new physics.

10.3 Top FCNC

The top quark plans an important role in the electroweak symmetry breaking mechanism [196]. While the CEPC can potentially be upgraded to run at the $t\bar{t}$ production energy of 360 GeV, there are other possibilities to study the top quark physics below the $t\bar{t}$ production threshold.

The top quark FCNC can be studied at the CEPC Higgs factory operation mode via single top quark production process $e^+e^- \to t(\bar{t})j$. This process is highly suppressed by GIM in the SM, and any observation would be a clear sign of NP. The single top FCNC production can happen via a two-fermion interaction through an s-channel Z or photon, or via a contact four-fermion interaction, as shown in Figure 32.

The LHC TOP Working Group note [197] provides a complete and systematic description of the top quark FCNC based on SMEFT. In total, a full set of 56 independent

---

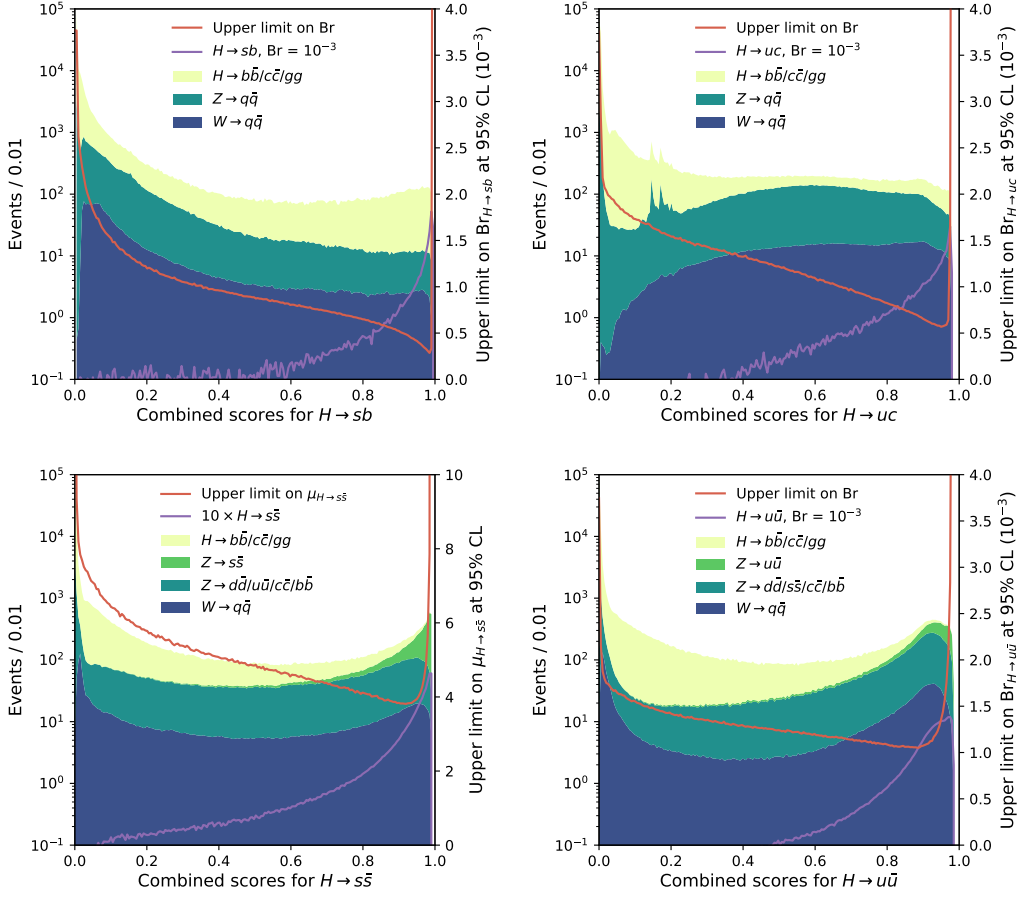[4]Here sb denotes $s\bar{b}$, and similarly for sd, db, and uc.

Figure 31: The distributions of combined scores for signal and SM backgrounds, where the signals are $H \to sb$ (upper left panel), $H \to uc$ (upper right panel), $H \to s\bar{s}$ (lower left panel), and $H \to u\bar{u}$ (lower right panel), respectively, in the $\nu\bar{\nu}H$ process, with CEPC nominal parameters [32].

operators are relevant for the single top quark production process $e^+e^- \to t(\bar{t})j$. For each quark generation a ($a = 1, 2$), the 28 coefficients can be written as follows [198]:

$$
\begin{array}{ccccccc}
c_{\varphi q}^{-(3+a)} & c_{uZ}^{(a3)} & c_{uA}^{(a3)} & c_{lq}^{-(1,3+a)} & c_{eq}^{(1,3+a)} & c_{lequ}^{S(1,a3)} & c_{lequ}^{T(1,a3)} \\
c_{\varphi u}^{(3+a)} & c_{uZ}^{(3a)} & c_{uA}^{(3a)} & c_{lu}^{(1,3+a)} & c_{eu}^{(1,3+a)} & c_{lequ}^{S(1,3a)} & c_{lequ}^{T(1,3a)} \\
c_{\varphi q}^{-I(3+a)} & c_{uZ}^{I(a3)} & c_{uA}^{I(a3)} & c_{lq}^{-I(1,3+a)} & c_{eq}^{I(1,3+a)} & c_{lequ}^{SI(1,a3)} & c_{lequ}^{TI(1,a3)} \\
c_{\varphi u}^{I(3+a)} & c_{uZ}^{I(3a)} & c_{uA}^{I(3a)} & c_{lu}^{I(1,3+a)} & c_{eu}^{I(1,3+a)} & c_{lequ}^{SI(1,3a)} & c_{lequ}^{TI(1,3a)}
\end{array}
\tag{10.1}
$$

The first three columns come from the two-fermion operators. $c_{\varphi q}^-$ and $c_{\varphi u}$ give rise to tqZ coupling with a vector-like Lorentz structure, while c_{uA} and c_{uZ} give rise to the $tq\gamma$ and tqZ dipole interactions. The last four columns come from the four-fermion operators. c_{lq}^-, c_{lu}, c_{eq}, and c_{eu} give rise to interactions between two vector currents, while c_{lequ}^S and c_{lequ}^T to interactions between two scalar and two tensor currents, respectively. The interference between coefficients from different rows vanishes in the limit of massless quark. The first row (second row) and the third row (fourth row) only differ by a CP phase and give identical
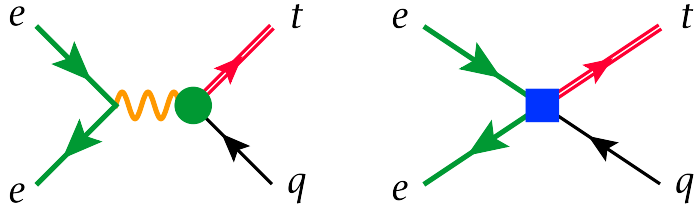
Figure 32: Feynman diagrams of the flavor-changing single top production process at e^+e^- collider. The green dot represents the two-fermion operator. The blue square represents the four-fermion operator.

signatures in experiment due to the absence of an SM amplitude interfering with the FCNC coefficients, and thus it is sufficient to consider only the first two rows in analysis.

Currently, the best constraints on the two-fermion FCNC are from the LHC [199–203], while the best constraints on the four-fermion FCNC are still from LEP2 [204, 205].

The prospect of top FCNC constraints at CEPC is studied in Ref. [198] based on a CEPC operation scenario with a center-of-mass energy E_{cm} =240 GeV and an integrated luminosity of 5.6 ab^{-1}, and assuming a detector performance as described in the CEPC Conceptual Design Report [1]. Consider the semileptonic decay of the top quark, the final state signature contains a b-jet, an up or charm quark jet, a charged lepton and a neutrino. The dominant background comes from the W pair production with one W boson decaying hadronically and the other leptonically. Figure 33 shows some key kinematic distributions of two benchmark signals and the background after reconstruction. The background can be suppressed by requiring exactly one b-tagged jet, an untagged jet with energy less than 60 GeV, the di-jet mass greater than 100 GeV and the top candidate mass not exceeding 180 GeV. A basic analysis with the cuts above can already provide good constraints on top quark FCNC, improving the limits on the four-fermion operator coefficients by one to two orders of magnitude comparing to the current best bounds from the LEP2 data. Figure 34 shows the expected constraints from CEPC comparing with the existing LHC+LEP2 bounds and the projected limits from HL-LHC+LEP2 and FCC-ee. Additional, the analysis sensitivity can be further improved by exploiting more features of the FCNC signal. Imposing a c-tagging requirement together with b-tagging can further suppress the background and improve the the sensitivity to FCNC interactions induced by second generation quark operators. The top quark scattering angle can help to lift the degeneracy between coefficients and pinpoint the coefficient that gives rise to the excess if an FCNC signal is observed.

11 Spectroscopy and Exotics

Spectroscopy of hadrons is critical to understand mass generation in QCD, given the persisting mystery of color confinement. Although exotic hadrons, extending beyond conventional quark-antiquark mesons and three-quark baryons, have been postulated for a long time, their unambiguous confirmation has only recently been confirmed since the discovery of the $D_{s0}^*(2317)$ meson by BaBar [206] and the $X(3872)$ meson, also known as $\chi_{c1}(3872)$ [150],
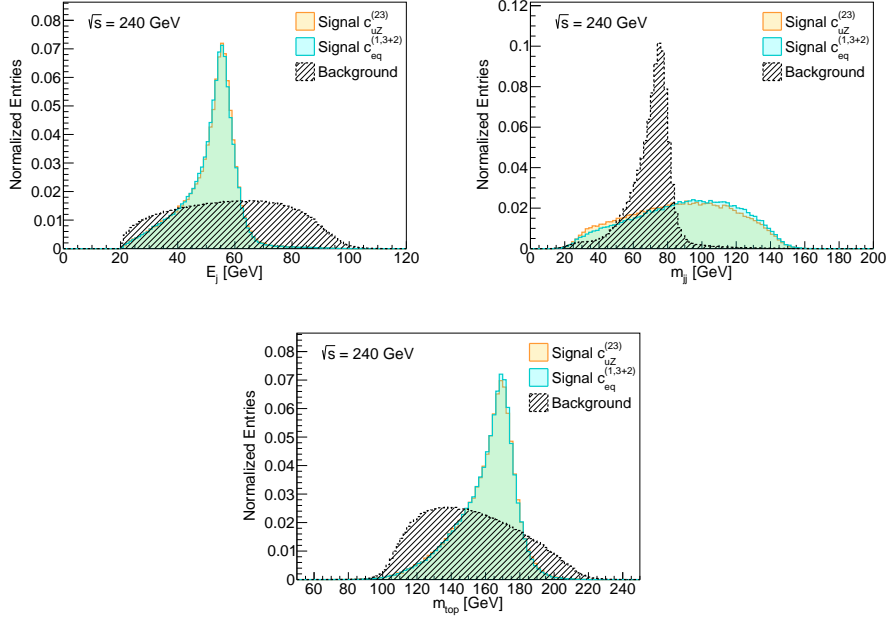
Figure 33: Reconstructed signal and background before selection. See [198] for details.
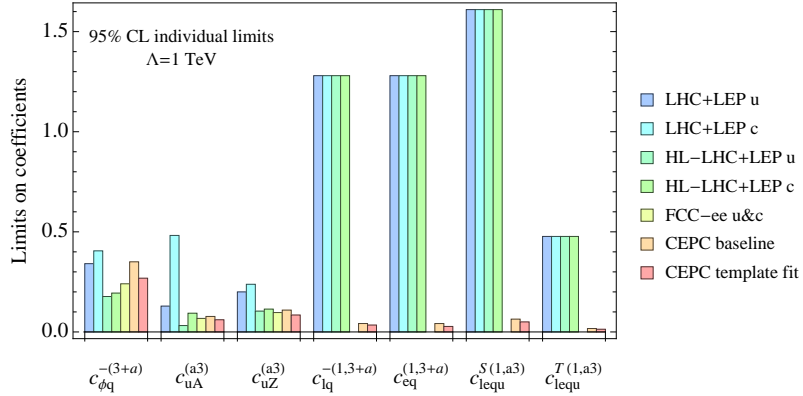

Figure 34: Expected constraints from CEPC comparing with the existing LHC+LEP2 bounds and the projected limits from HL-LHC+LEP2 and FCC-ee See [198] for details.

by Belle [207]. Dozens of exotic states, with a noteworthy characteristic of narrow states located near the threshold of a pair of open-flavor hadrons, have been identified following the line. In particular, intriguing resonant structures, that are explicitly exotic, were observed, such as the $Z_c(3900)^{\pm}$ by BESIII [208] and Belle [209], hidden-charm P_c pentaquarks [210, 211] and double-charm $T_{cc}(3875)^{+}$ tetraquark [212] by LHCb, and hidden-charm strange tetraquark Z_{cs} candidates by BESIII [213] and LHCb [214]. It is evident from Figure 35 that most of the newly observed states in the charmomnium mass region go beyond the charmonium spectrum predicted by the quark model (*e.g.*, the Godfrey-Isgur
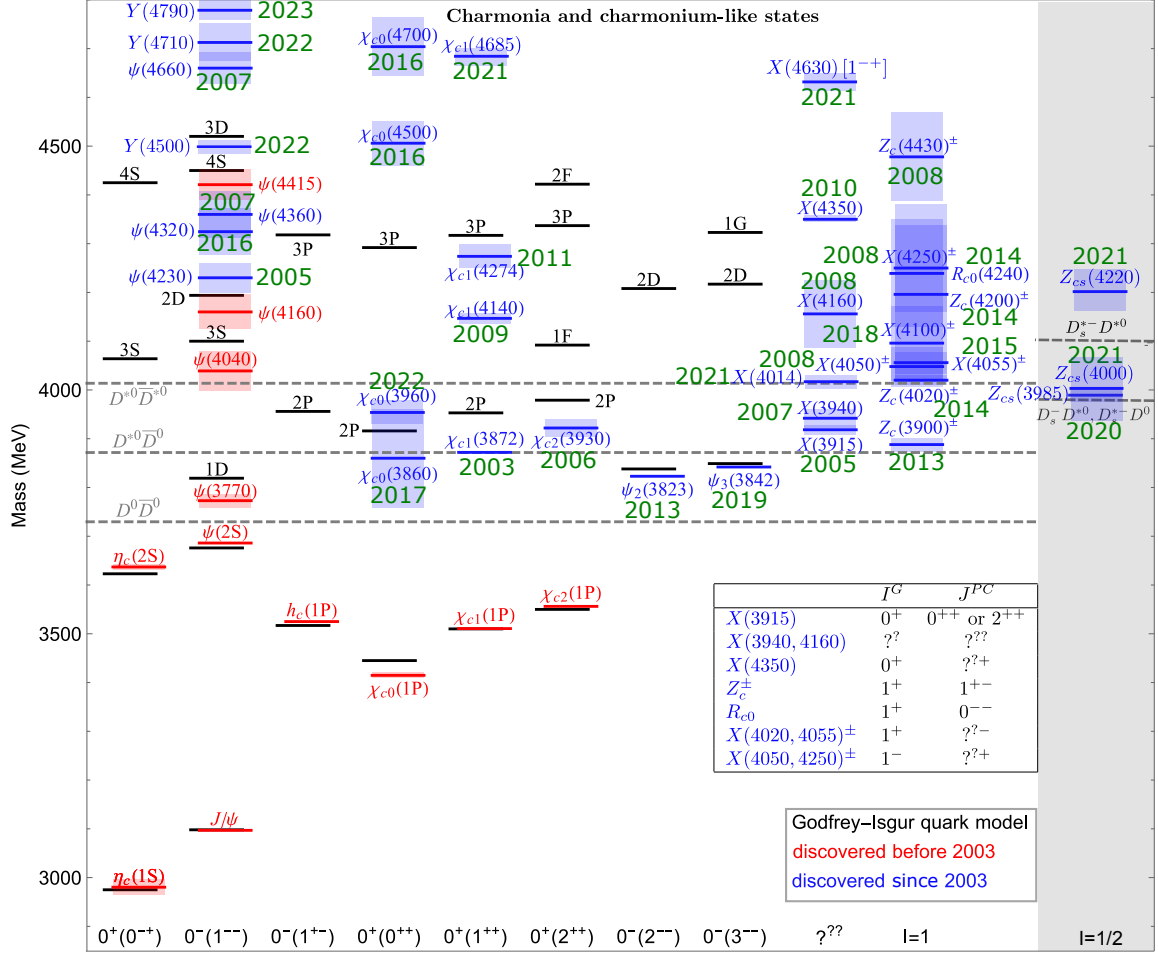
Figure 35: Spectrum of the charmonium and charmonium-like states. Black lines represent the masses in the Godfrey-Isgur quark model [215]. The red and blue lines represent the states observed experimentally before 2003 and since 2003, respectively. For the latter, the years when the states were observed are labeled in green. The height of each shadow indicates the width of the corresponding state. We also show a few two-body open-charm thresholds as dashed lines.

quark model [215]). These discoveries spur plenty of efforts in trying to reveal the nature of the new hadrons and to gain deeper understanding of nonperturbative strong interactions; for recent reviews, see [216–227]. A wide spectrum of potential new resonances and a multitude of observables make hadron spectroscopy a promising avenue for discoveries at CEPC. This is particularly relevant considering the current lack of understanding about hadronic states beyond simple quark model configurations.

Despite numerous works, a comprehensive understanding and classification of these novel structures remain elusive. Thereby, experimental data is paramount for further theoretical development. At CEPC, the production of exotic states from either b-hadron decays or directly from the Z decays is expected. For example, the hidden-charm exotic
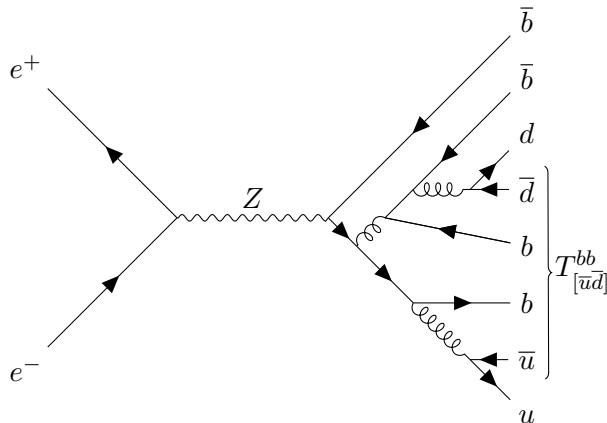
Figure 36: An illustrative Feynman diagram for the production of tetraquark state $T^{bb}_{[\bar{u}b]}$ from the $Z \to bb\bar{b}\bar{b}$ decay.

states such as $X(3872)$ and $P_c(4450)$ can be produced at CEPC via $b \to c\bar{c}s$ transitions after b-flavored hadrons are formed. Given the extensive production of heavy quark pairs (*e.g.*, the branching fraction of $Z \to b\bar{b}$ is $(15.12 \pm 0.05)\%$ [150]), a considerable amount of exotic hadrons, including known ones and new states, will be generated. Investigation of conventional heavy-flavor mesons and baryons will also be significant, including excited hadrons and multi-heavy baryons such as Ξ_{bb}.

At CEPC, another significant source of exotic or multi-flavored hadrons at the Z pole comes from $Z \to q\bar{q}q'\bar{q}'$. The multiple heavy quarks produced, either of the same or opposite signs, could hadronize into various (exotic) species if their relative velocity is low enough. The process is highly relevant to the B_c physics studies since B_c from the Z pole mainly comes from $Z \to b\bar{b}c\bar{c}$ decays [228–231]. In addition, the measurement of many inclusive rates of new resonances occur for the first time, and the confirmation of numerous new decay modes is anticipated. With regards to doubly-heavy baryons (bbq, bcq and ccq) and doubly-heavy exotic states (for instance, the double-charm tetraquark $T_{cc}(3875)^+$ [212, 232], double-bottom tetraquarks [233–236] and hidden-bottom pentaquarks [237]), the high mass threshold necessitates Z inclusive decays as their main production mechanism. An example of Feynman diagrams contributing to the production of a double-bottom tetraquark is shown in Figure 36.

Simplified assumptions and parton-level simulations were employed to deduce the inclusive decay rates: $\mathrm{BR}(Z \to X + T^{cc}_{[\bar{q}\bar{q}']}) \sim \mathcal{O}(10^{-6})$, $\mathrm{BR}(Z \to X + \Xi_{cc}) \sim 1 \times 10^{-5}$, and $\mathrm{BR}(Z \to X + \Omega_{cc}) \sim 5 \times 10^{-5}$ at the Z pole [238]. Additionally, $\mathrm{BR}(Z \to X + T^{bb}_{[\bar{q}\bar{q}']}) \sim \mathcal{O}(10^{-6})$ was also calculated [239].

One may also estimate the inclusive production cross section double-charm tetraquarks of the hadronic molecular type by combining Monte Carlo event generators and nonrelativistic effective field theory (NREFT). Such method can successfully reproduce the inclusive cross section of the $X(3872)$ at hadron colliders [241–243]. Using Pythia 8.3 [244]
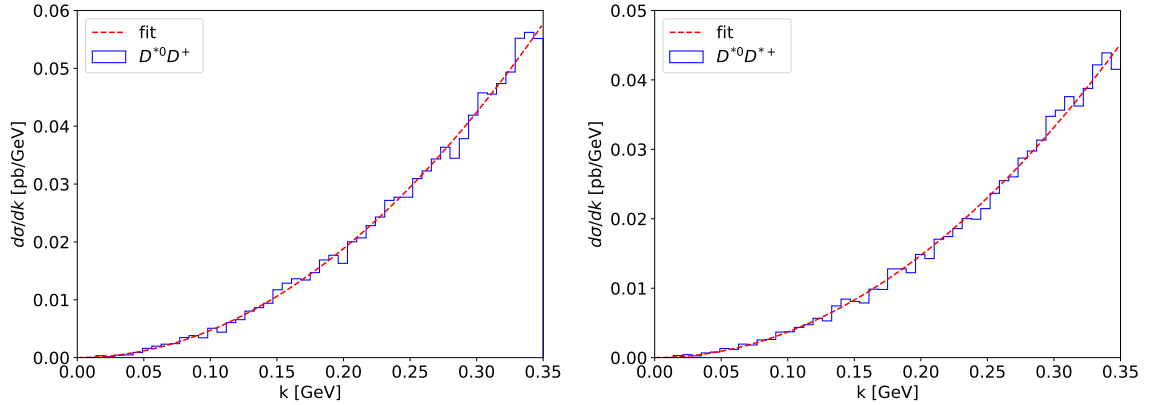
Figure 37: Differential cross sections of $e^+e^- \to Z^0 \to D^{*0}D^+$ and $D^{*0}D^{*+}$ generated using Pythia (histograms) and fit with $d\sigma/dk \propto k^2$ (dashed curves) [240].

to generate differential distributions of the $D^{(*)}D^*$ pairs with low relative momenta (see Figure 37) and using NREFT to compute the effective couplings of the $T_{cc}(3875)$ to DD^* and its hypothesized spin partner T'_{cc} to D^*D^* [245], one finds that both the inclusive cross section for the $T_{cc}(3875)$ and T'_{cc} at the Z pole are at the order of a few to 10 fb [240]. Given the expected integrated luminosity of 100 ab^{-1} at the Z pole at CEPC (see Table 1), one expects $10^5 - 10^6$ T_{cc} and T'_{cc} to be produced, consistent with the estimate in Ref. [239]. Events of these states can be reconstructed from the $DD\pi(\pi)$ final states.

Due to the high uncertainties in their differential rates and decay final states, the MC simulation of such exotic hadron events and reconstructing their resonance are impractical without more advanced theoretical calculations or analysis algorithms. On the other hand, more recent efforts aiming doubly-flavored baryons, *i.e.*, Ξ_{cc}, Ξ_{bc}, and Ξ_{bb} have been predicted at the Z pole with differential distributions available [246, 247].

12 Light BSM States from Heavy Flavors

Light NP states are widely predicted in BSM scenarios involving dark sectors and feebly interacting particles [248], and may couple to lepton and quark sectors. Candidates for such particles include axions and axion-like-particles (ALPs) a [249–252], dark photons A' and light Z' bosons [253], heavy neutral leptons (HNL) [254–256], hidden valley hadrons such as the dark pion $\hat{\pi}$ [257], etc. As a handy example, an ALP a can couple with the SM fermions via the dimension-5 operators

$$\mathcal{L} \supset \frac{\partial_\mu a}{2f_a} \left(c^A_{ff'} \, \bar{f}\gamma^\mu\gamma^5 f' + c^V_{ff'} \, \bar{f}\gamma^\mu f' \right) , \tag{12.1}$$

where f and f' are SM fermions, $c^{A,V}_{ff'}$ are dimensionless couplings, (with the vector ones c^V_{ff} being unphysical if $f = f'$), and f_a is the ALP decay constant that can be regarded as a measure of the NP energy scale. These light BSM states could thus be explored in flavor-physics experiments if their production via lepton and/or quark radiation or decay is turned on. Interestingly, the production in the former case does not conserve lepton flavor
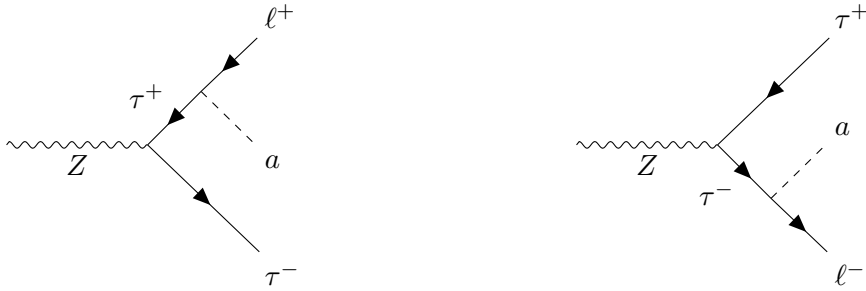
Figure 38: Illustrative Feynman diagrams for the ALP production via $Z \to \tau^{\pm}\ell^{\mp}a$, where lepton flavor is violated.
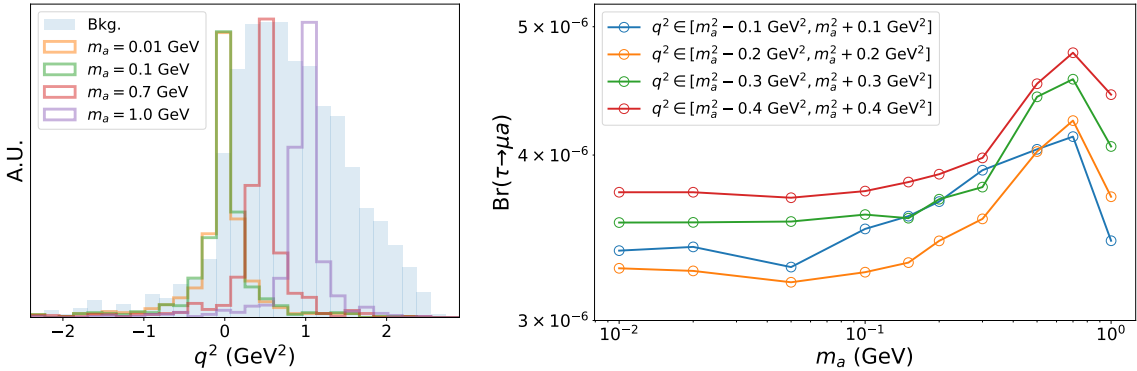

Figure 39: Preliminary sensitivity analysis for searching for an invisible ALP in the $Z \to \tau(\to \mu a)\tau(\to 3\pi\nu)$ events at the CEPC. **LEFT:** Reconstruction of $q^2 \equiv (p_\tau - p_\mu)^2$. **RIGHT:** Upper limits on $\mathrm{BR}(\tau \to \mu a)$ with 95% C.L., where four q^2 windows have been considered.

and is usually heightened by the narrow width of the SM fermions. Owing to their feebly-interacting nature, (so as for them to remain undetected so far), the produced BSM particles tend to be long-lived. They are often subject to displaced decays or they contribute to missing energy directly. Both kinematic features being used as collider signatures of light BSM particles have been widely studied. Note that the heavy-flavored particles in the SM are also long-lived; in order to enable their identification, detectors have often been designed for reconstructing the tracking/vertexing information with high quality. Even if the light BSM particle in question is invisible, the techniques for reconstructing the missing energy at the Z pole can facilitate the reconstruction of its invariant mass. Therefore, the exploration of light BSM states in this context is naturally expected. Below, let us consider the detection of light BSM states which are produced via the decays of heavy-flavored leptons and quarks, using the ALP and dark pion as respective examples.

12.1 Lepton Sector

As discussed in Sections 3, 4, and 8, the CEPC has a strong potential for carrying out τ-related searches, due to the excellent performance of its tracker. A prominent example
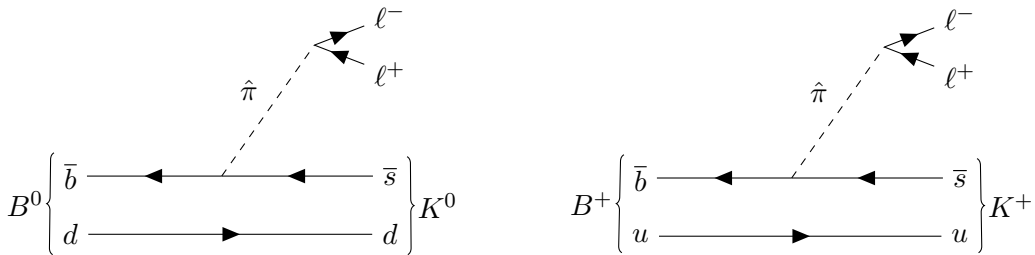
Figure 40: Illustrative Feynman diagrams for the production of a light dark pion $\hat{\pi}$ via heavy-flavored quark decays. **LEFT**: $B^0 \to K^0 \hat{\pi}(\to \mu^+\mu^-)$. **RIGHT**: $B^+ \to K^+ \hat{\pi}(\to \mu^+\mu^-)$. The flavor-changing interaction between the SM quarks and $\hat{\pi}$ can arise either at the tree level or through an EW loop.

is the LFV decay $\tau \to \ell a$ (see Figure 38) with the ALP a being invisible [258]. The major backgrounds then arise from the $\tau \to \ell\nu\nu$ decays, which share the signal signature of one visible object and missing energy. Let us consider a full reconstruction of the $Z \to \tau\tau$ event. Indeed, the 3- or 5-prong decays of the second τ in the $Z \to \tau\tau$ event can yield an efficient determination for the τ momentum direction. Combing this result with some other kinematic constraints, such as the τ mass on-shell condition and energy-momentum conservation, we are able to reconstruct the invisible mass $q^2 \equiv (p_\tau - p_\ell)^2 = m_a^2$ accurately. Consequently, the pseudo rest frame approximation employed in Belle II [259] is no longer necessary. The results from a preliminary sensitivity analysis are presented in Figure 39, where the events are simulated with non-zero spatial beam spread, initial state radiation, and finite tracking/calorimetry resolution. As shown in the left panel, the reconstructed q^2 for the signal events sharply peaks at m_a, in contrast to that of the backgrounds. The right panel shows the expected CEPC 95% C.L upper limits on BR($\tau \to \mu a$). Compared with the current Belle II bound, *i.e.*, BR($\tau \to \mu a$) $\lesssim 7 \times 10^{-4}$, for a massless ALP [259], these limits are about two orders of magnitude stronger. In terms of the interactions in Eq. (12.1), this implies that a NP scale as high as $\mathcal{O}(10^8)$ GeV (for $c_{\tau\mu}^{A,V} \sim \mathcal{O}(1)$) could be probed at the CEPC.

The light ALPs can be also searched for by their lepton-flavor-conserving radiation, such as that in the $Z \to \tau\tau a$ process [251]. Currently, the ALP coupling with τ leptons is essentially yet unconstrained. For the case of $Z \to \mu\mu a$, where the dynamics is relatively simple, it has been shown [251] that the CEPC has the potential to reach BR($Z \to \mu\mu a$) $\lesssim 3 \times 10^{-11}$, yielding a limit to the ALP coupling with muons of $f_a/c_{\mu\mu}^A \gtrsim 1$ TeV.

Moreover, both Dirac and Majorana HNLs can be produced via LFV processes. The HNLs might be responsible for the origin of neutrino mass, the puzzle of dark matter and even the cosmic baryon asymmetry. Their mixing with neutrinos allows them to be produced via τ decays such as $\tau \to \ell\nu N$ and $\tau \to \pi N$, if they are lighter than the τ lepton. This provides an alternative to the $Z \to \nu N$ decays in searching for HNLs at the Z pole [260]. Nevertheless, the relevant sensitivity analysis is yet to be explored.
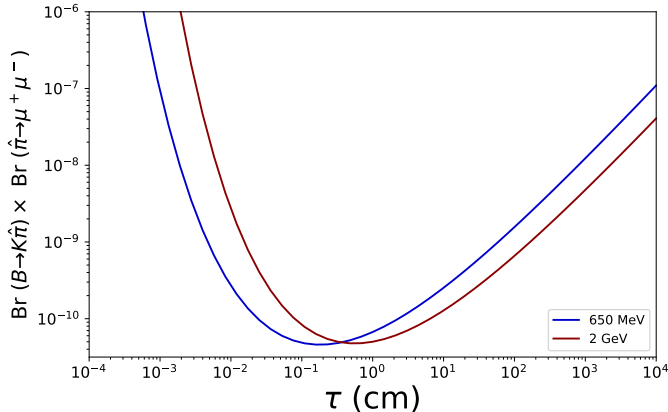
Figure 41: Preliminary limits for searching for a long-lived dark pion in $B \to K\hat{\pi}(\to \mu\mu)$ events at the CEPC [261].

12.2 Quark Sector

Light BSM particles can be also produced in heavy-flavored quark decays [79, 257, 261–265]. As an example, let us consider a dark pion from the strong dynamics of a hidden sector, where this dark pion also couples with the SM leptons, yielding a signature of a displaced dilepton vertex from its decay (see Figure 40) [257]. The reconstruction of a narrow dilepton resonance away from the primary vertex with high quality then allows for the efficient distinction of the signal events from the backgrounds. Figure 41 demonstrates preliminary limits for searching for a long-lived dark pion in $B \to K\hat{\pi}(\to \mu\mu)$ events at the CEPC [261]. The strongest constraints, namely $\mathrm{BR}(B \to K\hat{\pi}(\to \mu\mu)) \lesssim 10^{-10}$, are achieved while the proper lifetime of $\hat{\pi}$ is $\sim 0.1 - 10$ cm. Since the dark pion, a composite pseudoscalar, also admits an effective coupling like an ALP, as in Eq. (12.1), one can also interpret the above constraints as a probe of the decay constant f_a of a (composite) ALP through its coupling with quarks. Even when the FCNC couplings are absent at tree level, they will be generated at one loop by EW interactions. In the case where the couplings to all fermions are close to unity ($c_{ff}^A \sim \mathcal{O}(1)$), the constraint on f_a by the CEPC will be up to $\sim \mathcal{O}(10^7)$ GeV [257]. If a large FCNC coupling $c_{bs}^V \sim 1$ presents at tree level, the constraints on f_a will be even higher, though all such limits will also depend on other parameters that control the dark pion lifetime, such as $m_{\hat{\pi}}$.

Finally, we remark that this strategy can be applied in searching for other long-lived light BSM bosons, if they are produced and decay in a similar way. Also, it is interesting to extend this study to the case where these particles decay outside the detector and hence contribute to the missing energy directly. In the latter case, the CLEO analysis performed about twenty years ago [266] still provides the current strongest constraints of $\mathrm{BR}(B^\pm \to \pi^\pm/K^\pm + X) < 4.9 \times 10^{-5}$ These constraints can be interpreted as $f_a \gtrsim 10^8$ GeV in the relevant QCD axion scenarios [265]. However, the sensitivity prospect for such a measurement at the CEPC is still missing.

13 Summary and Outlook

The electron-positron Higgs factory is identified as the highest priority for future collider projects, for it could significantly enhance the discovery potential for new physics compared to existing facilities, including LHC and Super-KEKB. Several electron-positron Higgs factories are therefore proposed, supported by intensive physics study as well as critical design and technology R&D studies. These proposed facilities are expected to produce millions of Higgs bosons in an extremely clean collision environment. The electron-positron Higgs factory would not only improve the precision of Higgs boson property measurements by approximately an order of magnitude compared to the ultimate precision achievable by the LHC, but also generates huge statistic of massive SM particles. These facilities open new avenues for exploring new physics principles through multiple observational windows, making a significant leap forward in the field of high energy physics.

Among the proposed facilities, the CEPC and FCC are two circular colliders that could deliver Teras of Z bosons, surpassing the Z boson yields of the LEP-I operation by at least five orders of magnitude. In fact, the instantaneous luminosity of CEPC/FCC is so high that it could produce the entire statistic of LEP-I data in roughly 1 minute. This enormous Z-boson sample, together with samples acquired at higher center-of-mass energies, provides an unprecedented opportunity for flavor physics measurements, EW precision measurements, etc.

This manuscript delineates the flavor physics landscape at the CEPC, while the main findings is also applicable to FCC. Our investigation encompasses approximately 10 topics, including rare/exotic b decays, LFU/LFV, CPV, exotic states, etc, depicted in different sections. We have accumulated accuracy estimations from 36 different benchmark studies, as detailed in Table 10. These benchmark studies are processed with different methodologies, i.e. full simulation using Geant4 [271] toolkit, fast simulation based on detector performance modelling [272], and guesstimate/extrapolation from existing relevant studies. These benchmark studies conclude that the CEPC or Tera-Z factory, **could access to new physics at energy up to 10 TeV or even higher.**

As summarized in Table 10, a Tera-Z collider could reveal many previously unobserved physics processes that is of strong interests for flavor physics studies (e.g. item 18-19 of Table 10), and boost precisions of many critical measurements by orders of magnitudes. On top of the Tera-Z, the CEPC also provides intriguing flavor physics measurements at higher center-of-mass energies, for instance the measurements of Higgs rare/FCNC hadronic decay and top quark FCNC decay at the Higgs factory mode ($\sqrt{s} = 240$ GeV), and the $|V_{cb}|$ measurement from direct W boson decay at $\sqrt{s}$ of 160 GeV (for W boson mass measurement) and 240 GeV.

Compared to existing flavor physics platforms, especially the LHCb and Belle II, the CEPC has significant comparative advantages, providing unique opportunities for many measurements and **serving as a highly complementary platform for flavor physics programs.** In contrast to hadron colliders, the CEPC intrinsically possesses much cleaner collision environment as well as the precise and controllable initial state. On top of the collision environment, the PFA oriented design of CEPC detector and the potential imple-

No.	Process	$\sqrt{s}$ (GeV)	Parameter of interest	Observable	Current precision	CEPC Precision	Estimation method	Key detector performance	Relevant Section
1	$Z \to \mu\mu a$	91.2	-	BR upper limit	-	$\lesssim 3 \times 10^{-11}$ [251]	Fast simulation	Tracker Missing energy	12
2	$B \to K\hat{\pi}(\to \mu\mu)$	91.2	-	BR upper limit	-	$\lesssim 10^{-10}$ [261]	Fast simulation	Tracker Vertex	12
3	$Z \to \pi^+\pi^-$	91.2	-	BR upper limit	-	$\mathcal{O}(10^{-10})$ [109]	Guesstimate	Tracker PID	9
4	$Z \to \pi^+\pi^-\pi^0$	91.2	-	BR upper limit	-	$\mathcal{O}(10^{-9})$ [109]	Guesstimate	Tracker PID ECAL	9
5	$b \to s\tau^+\tau^-$	91.2	-	BR upper limit	-	$B^0 \to K^{*0}\tau^+\tau^- \sim \mathcal{O}(10^{-6})$ $B_s \to \phi\tau^+\tau^- \sim \mathcal{O}(10^{-6})$ $B^+ \to K^+\tau^+\tau^- \sim \mathcal{O}(10^{-6})$ $B_s \to \tau^+\tau^-\ \mathcal{O}(10^{-5})$ [71]	Fast simulation	Tracker Vertex Jet origin ID	4
6	$Z \to \rho\gamma$	91.2	-	BR upper limit	$< 2.5 \times 10^{-5}$ [150]	$\mathcal{O}(10^{-9})$ [109]	Guesstimate	Tracker PID ECAL	9
7	$Z \to J/\psi\gamma$	91.2	-	BR upper limit	$< 1.4 \times 10^{-6}$ [150]	$10^{-9} - 10^{-10}$ [109]	Guesstimate	Tracker PID ECAL	9
8	$Z \to \tau\mu$	91.2	-	BR upper limit	$< 6.5 \times 10^{-6}$ [105–107]	$\mathcal{O}(10^{-9})$ [108, 109] $\mathcal{O}(10^{-9})$ [108, 109] 1×10^{-9} [110]	Guesstimate	$E_{\rm beam}$ Tracker PID	6
9	$Z \to \tau e$	91.2	-	BR upper limit	$< 5.0 \times 10^{-6}$ [105–107]	$\mathcal{O}(10^{-9})$ [108, 109] $\mathcal{O}(10^{-9})$ [108, 109] 1×10^{-9} [110]	Guesstimate	$E_{\rm beam}$ Tracker PID	6
10	$Z \to \mu e$	91.2	-	BR upper limit	$< 7.5 \times 10^{-7}$ [105–107]	$\mathcal{O}(10^{-9})$ [108, 109] $\mathcal{O}(10^{-9})$ [108, 109] 1×10^{-9} [110]	Guesstimate	$E_{\rm beam}$ Tracker PID	6
11	$\tau \to \mu a$	91.2	-	BR upper limit	$\lesssim 7 \times 10^{-4}$ [259]	$\lesssim 3\text{–}5 \times 10^{-6}$	Fast simulation	Tracker Missing energy	12
12	$\tau \to \mu\mu\mu$	91.2	-	BR upper limit	$< 2.1 \times 10^{-8}$ [150]	$\mathcal{O}(10^{-10})$ [108, 109]	Guesstimate	Tracker Lepton ID	8
13	$\tau \to eee$	91.2	-	BR upper limit	$< 2.7 \times 10^{-8}$ [150]	$\mathcal{O}(10^{-10})$ [108, 109]	Guesstimate	Tracker Lepton ID	8
14	$\tau \to e\mu\mu$	91.2	-	BR upper limit	$< 2.7 \times 10^{-8}$ [150]	$\mathcal{O}(10^{-10})$ [108, 109]	Guesstimate	Tracker Lepton ID	8
15	$\tau \to \mu ee$	91.2	-	BR upper limit	$< 1.8 \times 10^{-8}$ [150]	$\mathcal{O}(10^{-10})$ [108, 109]	Guesstimate	Tracker Lepton ID	8
16	$\tau \to \mu\gamma$	91.2	-	BR upper limit	$< 4.4 \times 10^{-8}$ [150]	$\mathcal{O}(10^{-10})$ [108, 109]	Guesstimate	Tracker Lepton ID ECAL	8
17	$\tau \to e\gamma$	91.2	-	BR upper limit	$< 3.3 \times 10^{-8}$ [150]	$\mathcal{O}(10^{-10})$ [108, 109]	Guesstimate	Tracker Lepton ID ECAL	8
18	$B_c \to \tau\nu$	91.2	$|V_{cb}|$	$\sigma(\mu)/\mu$	BR$\lesssim 30\%$ [267]	$\mathcal{O}(1\%)$ [63]	Full simulation	Tracker Lepton ID Missing energy Jet origin ID	3
19	$B_s \to \phi\nu\bar{\nu}$	91.2	-	$\sigma(\mu)/\mu$	BR $< 5.4 \times 10^{-3}$ [150]	$\lesssim 2\%$ [35]	Full simulation	Tracker Vertex Missing energy PID	4
20		91.2		τ_τ (s) lifetime	$\pm 5 \times 10^{-16}$ [150]	$\pm 1 \times 10^{-18}$ [108]	Guesstimate	-	8
21		91.2		m_τ (MeV)	± 0.12 [150]	$\pm 0.004 \pm 0.1$ [108]	Guesstimate	-	8
22	$\tau \to \ell\nu\bar{\nu}$	91.2	-	BR	$\pm 4 \times 10^{-4}$ [150]	$\pm 3 \times 10^{-5}$ [108]	Guesstimate	Tracker Lepton ID Missing energy	8
23	$b \to c\ell\nu$	91.2	-	R_{H_c}	$R_{J/\psi} = 0.71 \pm 0.17 \pm 0.18$ [268] $R_{\Lambda_c} = 0.242 \pm 0.076$ [269]	relative (stat. only) $R_{J/\psi} \lesssim 5\%$ $R_{D_c^{(*)}} \lesssim 0.4\%$ $R_{\Lambda_c} \sim 0.1\%$ [38]	Fast simulation	Tracker Vertex	3
24	$B_s \to J/\psi\phi$	91.2	$\phi_s\ (= -2\beta_s)$	$\Gamma_s, \Delta\Gamma_s$	$\Gamma_s = 657.3 \pm 2.3$ ns^{-1} [150] $\Delta\Gamma_s = 65.7 \pm 4.3 \pm 3.7$ ns^{-1} [270] $\phi_s = -87 \pm 36 \pm 21$ mrad [270]	$\sigma(\Gamma_s) = 0.072$ ns^{-1} $\sigma(\Delta\Gamma_s) = 0.24$ ns^{-1} $\sigma(\phi_s) = 4.3$ mrad [45]	Full simulation	Tracker Vertex Lifetime resolution Jet origin ID	5
25	$B^0 \to \pi^0\pi^0$	91.2	α	BR, A_{CP}	$BR^{00} = (1.59 \pm 0.26) \times 10^{-6}$ (16%) [150] $C_{CP}^{00} = -0.33 \pm 0.22$	$\sigma(BR)/BR^{00} = 0.45\%$ $\sigma(a_{CP}^{00}) = \pm (0.014\text{-}0.018)$ [31]	Fast simulation	ECAL Jet origin ID	5
26	$B^0 \to \pi^+\pi^-$	91.2	α	BR	$BR^{+0} = (5.5 \pm 0.4) \times 10^{-6}$ (7%) [150]	$\sigma(BR)/BR^{+0} = 0.19\%$ [31]	Fast simulation	ECAL Tracker Jet origin ID	5
27	$B^+ \to \pi^+\pi^0$	91.2	α	BR, A_{CP}	$BR^{+-} = (5.12 \pm 0.19) \times 10^{-6}$ (4%) $C_{CP}^{+-} = -0.314 \pm 0.030$ [150] $S_{CP}^{+-} = -0.670 \pm 0.030$	$\sigma(BR)/BR^{+-} = 0.18\%$ $\sigma(C_{CP}^{+-}) = \pm (0.004\text{-}0.005)$ $\sigma(S_{CP}^{+-}) = \pm (0.004\text{-}0.005)$ [31]	Fast simulation	ECAL Tracker Vertex Jet origin ID	5
28	$H \to sb$	240	-	BR upper limit	-	$0.02\%\text{—}0.1\%$ [32]	Full simulation	Jet origin ID	10
29	$H \to sd$	240	-	BR upper limit	-	$0.02\%\text{—}0.1\%$ [32]	Full simulation	Jet origin ID	10
30	$H \to db$	240	-	BR upper limit	-	$0.02\%\text{—}0.1\%$ [32]	Full simulation	Jet origin ID	10
31	$H \to uc$	240	-	BR upper limit	-	$0.02\%\text{—}0.1\%$ [32]	Full simulation	Jet origin ID	10
32	$H \to ss$	240	-	BR upper limit	-	0.1% [32]	Full simulation	Jet origin ID	10
33	$H \to uu$	240	-	BR upper limit	-	0.1% [32]	Full simulation	Jet origin ID	10
34	$H \to dd$	240	-	BR upper limit	-	0.1% [32]	Full simulation	Jet origin ID	10
35	$e^+e^- \to t(\bar{t})j$	240	-	FCNC constraint coefficients	two-fermion, LHC [199–203] four-fermion, LEP2 [204, 205]	1–2 orders of magnitude improvement compared to LEP2 [198]	Fast simulation	Tracker Missing energy Jet origin ID	10
36	$WW \to \mu\nu qq$ $WW \to \tau(\to \mu\nu\nu)\nu qq$	240	$|V_{cb}|$	$|V_{cb}|$	$(38.9 \pm 0.53) \times 10^{-3}$ relative $\sim 1.4\%$ [9]	$\lesssim 0.5\%$ [193]	Full simulation	Jet origin ID	10

Table 10: Summary of flavor physics benchmarks.

mentation of high precision calorimeter system enable a precise reconstruction of neutral and missing final states. Thus, the CEPC could focus on the physics measurements with photon, neutral pion, lepton, and neutrino final states, which is highly complementary to LHCb measurements. With well-defined initial state of decay processes and less pile-up of events, the CEPC can access radiative or leptonic decays, therefore sensitive to FCNC processes, LFV and LFU tests in τ decays, and many other rare decay modes. Compared to B and C-factories [6, 25], the objective heavy hadrons/taus generated at CEPC has much higher kinematic energies and thus larger boosted vertices, which are beneficial for precise measurements of lifetime and secondary vertex, especially for time-dependent CP measurements. The wide energy coverage of the CEPC also opens up to hadron states that could not be produced directly at Belle II, such as B_c, Λ_b, and many exotic hadronic states, see Section 11. On the other hand, the CEPC uniquely enables precise measurements of FCNC processes and offers direct assessment of CKM matrix elements through the decay of W bosons.

The CEPC's extensive flavor physics program consequently imposes stringent and multifaceted requirements on detector performance, which becomes one of the key challenges in the design and optimization of the CEPC detector. Multiple physics benchmark analyses presented in this manuscript also serve as references for detector requirement and optimization studies, as these analyses quantify the correlations between anticipated accuracies and critical detector performances. These studies indicate that a suitable detector for the CEPC flavor physics measurements should:

- provide large acceptance of nearly 4π solid angle coverage, low P_T threshold for tracks, and low energy thresholds for photons and neutral hadrons.

- separate clearly final state particles, or in other words, provide excellent Particle Flow Reconstruction. The separation power is essential for CEPC flavor physics, because it could provide better reconstruction of the energy/momentum of the hadronic system, and therefore provide better measurement of missing energy and momentum. The PFA performance can be quantified by the Boson Mass Resolution (BMR). The CEPC Higgs physics program requires BMR < 4%, and its flavor physics program is actually more demanding on the PFA performance. More importantly, it's essential to identify the corresponding physics objects in a physics event or even inside a jet. For example, reconstructing leptons (including taus) inside jet is crucial for physics measurements with semileptonic heavy hadrons (b/c semileptonic decay) [44, 63], and reconstructing π^0 in $e^+e^- \to \tau^+\tau^-$ events is key for measuring tau decay branching ratios.

- distinguish different species of charged final state particles, especially charged kaons. Quantitatively, the CEPC detector should provide π/K separation better than $3\,\sigma$ [35, 45]. This PID requirement can be satisfied by different technologies. For example, the CEPC CDR baseline detector employs TPC as its main tracker, which could provide dE/dx or even dN/dx measurement. The dE/dx (or dN/dx) measurement is then required to reach a relative accuracy of 3%, at which, together with a TOF

measurement of 50 ps at cluster level [40], the reconstruction efficiency and purity of inclusive charged kaons in the hadronic Z pole sample can reach higher than 95%.

- pursue excellent intrinsic resolution of sub-detectors. For instance, an ECAL energy resolution better than $3\%/\sqrt{E} \oplus 0.3\%$ is required by the separation of B^0/B_s^0 once these mesons decay into photons [31]. Similarly, the tracker momentum resolution should reach per mille level in the barrel region, and the vertex position resolution should be better than 5 μm and be placed closer enough to the interaction point.

- be extremely stable. Many of the physics measurements, including a set of the flavor physics measurements [32, 38, 193], would be limited by systematic uncertainties. To have a stable detector is a prerequisite for controlling the systematics, yet, more quantitative studies are needed.

A very fundamental, but yet highly non-trivial, requirement for the detector is to be suited to the collision environment. This requirement is twofold: first of all, the detector design must be able to sustain the beam induced background and limit its impact on physics measurements to a tolerable level. To meet this requirement, dedicated design and optimization studies are needed in areas such as the machine-detector interface, integration study, and machine protection design, all of which still need significant effort. Secondly, the CEPC detector should be capable of reconstructing physics events with extremely high efficiency, while keeping the noise contamination in the data to an acceptable level, such as 10% of the total data size. Given the physics event rate of 10^5 Hz at the Z pole, the study and design of a dedicated Trigger-DAQ system are necessary to fulfill this requirement (as known as the triggerless equivalent scenario). In addition, the on-line and off-line time building is highly non-trivial, because the event rate at the CEPC Z pole is so high, and different sub-detectors take time to response (for instance TPC and calorimeters — the neutron induced hits may occur at milliseconds later after the collision), causing the overlap of physics events in time. It is impossible to separate the physics events using only time information. Therefore, new reconstruction technologies are required not only to reconstruct low-level physics objects (e.g. tracks, clusters, etc) with high efficiency and purity, but also to correctly associate them with different vertices. For example, particle flow algorithm using both spatial and time information is probably the needed technology to address this requirement.

These requirements need to be addressed by intensive detector design and R&D studies. Meanwhile, these requirements should also be considered coherently, since many of these requirements are correlated and can even be contradictory. For example, while the incorporation of TOF systems can significantly enhance PID performance, it concurrently introduces additional upstream material, which can adversely affect the intrinsic ECAL energy resolution.

On the other hand, the progress of advanced reconstruction algorithms, especially those based on machine learning and large language models, injects significant thrust to the CEPC physics and detector studies. An alive example would be the jet origin identification presented in Section 2, which shows that using the CEPC CDR baseline detector

and ParticleNet algorithm, 11 different types of jets (induced by u, d, s, c, b, their corresponding anti-quarks, and gluons) can be efficiently separated. In other word, the jet origin identification combines the jet flavor tagging, jet charge measurement, s-tagging, gluon-tagging, and even u/d-jet identification all together.

The jet origin identification gives a strong boost to the precision in measurements of Higgs rare/exotic hadronic decays — by roughly 3 times to 2 orders of magnitude — and in $|V_{cb}|$ measurement from W boson decays, see Section 10. It will also enhance the precisions of time-dependent CP measurements [45] and weak-mixing angle measurements [273]. These new technologies will certainly alter the detector design and optimization studies. For instance, a recent study [274] shows that new algorithms, even with a much worse detector, could still have performance surpassing the conventional algorithm with a much better detector. Of course, these new progresses also impose other challenges, for example, it would be essential to understand and to interpret the performance of these advanced algorithms, while the calibration and relevant systematic control certainly become critical, which are also highly non-trivial.

It should be remarked that the flavor physics program at the CEPC, or FCC, is so rich that this manuscript is by no means to be inclusive. Many interesting topics remain to be explored and quantified in the future. For instance, it would be valuable to quantify the impact of Tera-Z, on top of existing facilities, in terms of the CKM global fit. The physics measurements using $e^+e^- \to \tau^+\tau^-$ events, as well as those related to charm/strange physics, are also of interest. It is essential to control theoretical uncertainties, especially the QCD related ones. Furthermore, the relevant detector design and optimization studies, along with the development and exploration of new tools and new algorithms, need to continue and probably with much large paces.

To conclude, the flavor physics program holds immense scientific merit. It provides the access to new physics beyond SM at an energy scale of 10 TeV or even higher, and is highly complementary to existing flavor facilities. It is also very challenging to fully realize its potential, which needs dedicated detector design and critical R&D, as well as theoretical studies. We hope that the flavor physics studies for the CEPC will not only serve as a reference for the evaluation of CEPC physics potential and its detector design, but will also inspire innovative ideas towards new physics measurements, new technologies, new algorithms, and new tools.

References

[1] CEPC STUDY GROUP collaboration, *CEPC Conceptual Design Report: Volume 2 - Physics & Detector*, 1811.10545.

[2] CEPC ACCELERATOR STUDY GROUP collaboration, *Snowmass2021 White Paper AF3-CEPC*, 2203.09451.

[3] N. Cabibbo, *Unitary Symmetry and Leptonic Decays*, *Phys. Rev. Lett.* **10** (1963) 531.

[4] M. Kobayashi and T. Maskawa, *CP Violation in the Renormalizable Theory of Weak Interaction*, *Prog. Theor. Phys.* **49** (1973) 652.

[5] F. An et al., *Precision Higgs physics at the CEPC*, *Chin. Phys. C* **43** (2019) 043002 [1810.09037].

[6] Belle-II collaboration, *The Belle II Physics Book*, *PTEP* **2019** (2019) 123C01 [1808.10567].

[7] LHCb collaboration, *Measurement of the b-quark production cross-section in 7 and 13 TeV pp collisions*, *Phys. Rev. Lett.* **118** (2017) 052002 [1612.05140].

[8] LHCb collaboration, *Measurement of b hadron fractions in 13 TeV pp collisions*, *Phys. Rev. D* **100** (2019) 031102 [1902.06794].

[9] Heavy Flavor Averaging Group, HFLAV collaboration, *Averages of b-hadron, c-hadron, and τ-lepton properties as of 2021*, *Phys. Rev. D* **107** (2023) 052008 [2206.07501].

[10] X.-C. Zheng, C.-H. Chang, T.-F. Feng and X.-G. Wu, *QCD NLO fragmentation functions for c or $\bar{b}$ quark to B_c or B_c^* meson and their application*, *Phys. Rev. D* **100** (2019) 034004 [1901.03477].

[11] LHCb collaboration, *Measurement of the B_c^- meson production fraction and asymmetry in 7 and 13 TeV pp collisions*, *Phys. Rev. D* **100** (2019) 112006 [1910.13404].

[12] L. Gladilin, *Fragmentation fractions of c and b quarks into charmed hadrons at LEP*, *Eur. Phys. J. C* **75** (2015) 19 [1404.3888].

[13] DELPHI collaboration, *A Measurement of D meson production in Z0 hadronic decays*, *Z. Phys. C* **59** (1993) 533.

[14] ALEPH collaboration, *Production of charmed mesons in Z decays*, *Z. Phys. C* **62** (1994) 1.

[15] OPAL collaboration, *A Measurement of the production of D*+- mesons on the Z0 resonance*, *Z. Phys. C* **67** (1995) 27.

[16] A. Boehrer, *Inclusive particle production in hadronic decays of the Z boson at LEP-1*, *Phys. Rept.* **291** (1997) 107.

[17] LHCb collaboration, *Physics case for an LHCb Upgrade II - Opportunities in flavour physics, and beyond, in the HL-LHC era*, 1808.08865.

[18] FCC collaboration, *FCC Physics Opportunities*, *Eur. Phys. J.* **C79** (2019) 474.

[19] G. Bernardi et al., *The Future Circular Collider: a Summary for the US 2021 Snowmass Process*, 2203.06520.

[20] LCC Physics Working Group collaboration, *Tests of the Standard Model at the International Linear Collider*, 1908.11299.

[21] N. Bacchetta et al., *CLD – A Detector Concept for the FCC-ee*, 1911.12230.

[22] IDEA collaboration, *A proposal of a drift chamber for the IDEA experiment for a future e^+e^- collider*, *PoS* **ICHEP2020** (2021) 877.

[23] BaBar collaboration, *The BaBar detector*, *Nucl. Instrum. Meth. A* **479** (2002) 1 [hep-ex/0105044].

[24] BESIII collaboration, *Design and Construction of the BESIII Detector*, *Nucl. Instrum. Meth. A* **614** (2010) 345 [0911.4960].

[25] M. Achasov et al., *STCF Conceptual Design Report: Volume I - Physics & Detector*, 2303.15790.

[26] LHCв collaboration, *The LHCb Detector at the LHC*, *JINST* **3** (2008) S08005.

[27] ALEPH, CDF, D0, DELPHI, L3, OPAL, SLD, LEP ELECTROWEAK WORKING GROUP, TEVATRON ELECTROWEAK WORKING GROUP, SLD ELECTROWEAK WORKING GROUP, SLD HEAVY FLAVOR GROUP collaboration, *Precision Electroweak Measurements and Constraints on the Standard Model*, 0911.2604.

[28] T. Sjöstrand, S. Ask, J. R. Christiansen, R. Corke, N. Desai, P. Ilten et al., *An introduction to PYTHIA 8.2*, *Comput. Phys. Commun.* **191** (2015) 159 [1410.3012].

[29] M. Ruan and H. Videau, *Arbor, a new approach of the Particle Flow Algorithm*, in *International Conference on Calorimetry for the High Energy Frontier*, pp. 316–324, 2013, 1403.4784.

[30] J. S. Marshall and M. A. Thomson, *Pandora Particle Flow Algorithm*, in *International Conference on Calorimetry for the High Energy Frontier*, pp. 305–315, 2013, 1308.4537.

[31] Y. Wang, S. Descotes-Genon, O. Deschamps, L. Li, S. Chen, Y. Zhu et al., *Prospects for $B^0_{(s)} \to \pi^0\pi^0$ and $B^0_{(s)} \to \eta\eta$ modes and corresponding CP asymmetries at Tera-Z*, *JHEP* **12** (2022) 135 [2208.08327].

[32] H. Liang, Y. Zhu, Y. Wang, Y. Che, C. Zhou, H. Qu et al., *Jet origin identification and measurement of rare hadronic decays of Higgs boson at e^+e^- collider*, 2310.03440.

[33] LHCв collaboration, *Measurement of b-hadron branching fractions for two-body decays into charmless charged hadrons*, *JHEP* **10** (2012) 037 [1206.2794].

[34] H. Cui, M. Zhao, Y. Wang, H. Liang and M. Ruan, *Jet charge identification in ee-Z-qq process at Z pole operation*, 2306.14089.

[35] L. Li, M. Ruan, Y. Wang and Y. Wang, *Analysis of $B_s \to \phi\nu\nu$ at CEPC*, *Phys. Rev. D* **105** (2022) 114036 [2201.07374].

[36] Y. Zhu, S. Chen, H. Cui and M. Ruan, *Requirement analysis for dE/dx measurement and PID performance at the CEPC baseline detector*, *Nucl. Instrum. Meth. A* **1047** (2023) 167835 [2209.14486].

[37] F. Cuna, N. De Filippis, F. Grancagnolo and G. F. Tassielli, *Simulation of particle identification with the cluster counting technique*, in *International Workshop on Future Linear Colliders*, 5, 2021, 2105.07064.

[38] T. S. M. Ho, X.-H. Jiang, T. H. Kwok, L. Li and T. Liu, *Testing Lepton Flavor Universality at Future Z Factories*, 2212.02433.

[39] F. Bedeschi, M. Caccia, R. Ferrari, P. Giacomelli, F. Grancagnolo, P. Azzi et al., "IDEA detector Letter of Intent." https://www.snowmass21.org/docs/files/summaries/EF/SNOWMASS21-EF1_EF4-IF3_IF6-096.pdf, 2021.

[40] Y. Che, V. Boudry, H. Videau, M. He and M. Ruan, *Cluster time measurement with CEPC calorimeter*, *Eur. Phys. J. C* **83** (2023) 93 [2209.02932].

[41] R. Manqi, "The CEPC simulation and tools: software and performance." http://ias.ust.hk/program/shared_doc/2019/201901hep/conf/20190121_4042_pm_Manqi%20Ruan.pdf, 2019.

[42] Y. Shen, H. Xiao, H. Li, S. Qin, Z. Wang, C. Wang et al., *Photon Reconstruction Performance at the CEPC baseline detector*, 1908.09062.

[43] P.-Z. Lai, M. Ruan and C.-M. Kuo, *Jet performance at the circular electron-positron collider*, *JINST* **16** (2021) P07037 [2104.05029].

[44] D. Yu, T. Zheng and M. Ruan, *Lepton identification performance in Jets at a future electron positron Higgs Z factory*, 2105.01246.

[45] X. Li, M. Ruan and M. Zhao, *Prospect for measurement of CP-violation phase ϕ_s study in the $B_s \to J/\Psi\phi$ channel at future Z factory*, 2205.10565.

[46] T. Zheng, J. Wang, Y. Shen, Y.-K. E. Cheung and M. Ruan, *Reconstructing K_S^0 and Λ in the CEPC baseline detector*, *Eur. Phys. J. Plus* **135** (2020) 274.

[47] D. Yu, M. Ruan, V. Boudry, H. Videau, J.-C. Brient, Z. Wu et al., *The measurement of the $H \to \tau\tau$ signal strength in the future e^+e^- Higgs factories*, *Eur. Phys. J. C* **80** (2020) 7.

[48] CEPC CALORIMETRY WORKING GROUP collaboration, *High-granularity crystal calorimetry: conceptual designs and first studies*, *JINST* **15** (2020) C04056.

[49] M. T. Lucchini, L. Pezzotti, G. Polesello and C. G. Tully, *Particle flow with a hybrid segmented crystal and fiber dual-readout calorimeter*, *JINST* **17** (2022) P06008 [2202.01474].

[50] Z. Xiao and Z. Huaqiao, "Performance study of cross-crystal Fan Ecal for CEPC.." https://indico.ihep.ac.cn/event/16906/contributions/50989/attachments/24588/27822/cross-crystal_fan_Ecal.pptx, 2022.

[51] B. Qi and Y. Liu, *R&D of a Novel High Granularity Crystal Electromagnetic Calorimeter*, *Instruments* **6** (2022) 40.

[52] A. Ronzhin, S. Los, E. Ramberg, A. Apresyan, S. Xie, M. Spiropulu et al., *Study of the timing performance of micro-channel plate photomultiplier for use as an active layer in a shower maximum detector*, *Nucl. Instrum. Meth. A* **795** (2015) 288.

[53] J. Va'vra, *PID Techniques: Alternatives to RICH Methods*, *Nucl. Instrum. Meth. A* **876** (2017) 185 [1611.01713].

[54] X. She et al., *Development of Time Projection Chamber prototype integrated with UV laser tracks for the future circular e^+e^- collider*, *JINST* **18** (2023) C07015.

[55] H. Qu and L. Gouskos, *ParticleNet: Jet Tagging via Particle Clouds*, *Phys. Rev. D* **101** (2020) 056019 [1902.08570].

[56] CEPC STUDY GROUP collaboration, "CEPC Software Homepage." http://cepcsoft.ihep.ac.cn/.

[57] F. U. Bernlochner, Z. Ligeti, M. Papucci and D. J. Robinson, *Combined analysis of semileptonic B decays to D and D^*: $R(D^{(*)})$, $|V_{cb}|$, and new physics*, *Phys. Rev. D* **95** (2017) 115008 [1703.05330].

[58] W. Altmannshofer, S. Gori, M. Pospelov and I. Yavin, *Quark flavor transitions in $L_\mu - L_\tau$ models*, *Phys. Rev. D* **89** (2014) 095033 [1403.1269].

[59] D. Buttazzo, A. Greljo, G. Isidori and D. Marzocca, *Toward a coherent solution of diphoton and flavor anomalies*, *JHEP* **08** (2016) 035 [1604.03940].

[60] I. Doršner, S. Fajfer, A. Greljo, J. F. Kamenik and N. Košnik, *Physics of leptoquarks in precision experiments and at particle colliders*, *Phys. Rept.* **641** (2016) 1 [1603.04993].

[61] E. E. Jenkins, A. V. Manohar and P. Stoffer, *Low-Energy Effective Field Theory below the Electroweak Scale: Operators and Matching*, *JHEP* **03** (2018) 016 [1709.04486].

[62] M. Fedele, C. Helsens, D. Hill, S. Iguro, M. Klute and X. Zuo, *Prospects for B_c^+ and $B^+ \to \tau^+ \nu_\tau$ at FCC-ee*, 2305.02998.

[63] T. Zheng, J. Xu, L. Cao, D. Yu, W. Wang, S. Prell et al., *Analysis of $B_c \to \tau\nu_\tau$ at CEPC*, *Chin. Phys. C* **45** (2021) 023001 [2007.08234].

[64] Y. Amhis, M. Hartmann, C. Helsens, D. Hill and O. Sumensari, *Prospects for $B_c^+ \to \tau^+ \nu_\tau$ at FCC-ee*, *JHEP* **12** (2021) 133 [2105.13330].

[65] F. U. Bernlochner, Z. Ligeti and D. J. Robinson, *Model independent analysis of semileptonic B decays to D^{**} for arbitrary new physics*, *Phys. Rev. D* **97** (2018) 075011 [1711.03110].

[66] J. Charles, S. Descotes-Genon, Z. Ligeti, S. Monteil, M. Papucci, K. Trabelsi et al., *New physics in B meson mixing: future sensitivity and limitations*, *Phys. Rev. D* **102** (2020) 056023 [2006.04824].

[67] Y. Grossman and Z. Ligeti, *Theoretical challenges for flavor physics*, *Eur. Phys. J. Plus* **136** (2021) 912 [2106.12168].

[68] M. Artuso, G. Borissov and A. Lenz, *CP violation in the B_s^0 system*, *Rev. Mod. Phys.* **88** (2016) 045002 [1511.09466].

[69] P. Chang, K.-F. Chen and W.-S. Hou, *Flavor Physics and CP Violation*, *Prog. Part. Nucl. Phys.* **97** (2017) 261 [1708.03793].

[70] W. Altmannshofer and F. Archilli, *Rare decays of b and c hadrons*, in *Snowmass 2021*, 6, 2022, 2206.11331.

[71] L. Li and T. Liu, *$b \to s\tau^+\tau^-$ physics at future Z factories*, *JHEP* **06** (2021) 064 [2012.00665].

[72] S. Bifani, S. Descotes-Genon, A. Romero Vidal and M.-H. Schune, *Review of Lepton Universality tests in B decays*, *J. Phys.* **G46** (2019) 023001 [1809.06229].

[73] J. F. Kamenik, S. Monteil, A. Semkiv and L. V. Silva, *Lepton polarization asymmetries in rare semi-tauonic $b \to s$ exclusive decays at FCC-ee*, *Eur. Phys. J. C* **77** (2017) 701 [1705.11106].

[74] LHCв collaboration, *Test of lepton universality with $\Lambda_b^0 \to pK^-\ell^+\ell^-$ decays*, *JHEP* **05** (2020) 040 [1912.08139].

[75] LHCв collaboration, *Branching fraction measurements of the rare $B_s^0 \to \phi\mu^+\mu^-$ and $B_s^0 \to f_2'(1525)\mu^+\mu^-$ decays*, 2105.14007.

[76] LHCв collaboration, *Measurement of the $B_s^0 \to \mu^+\mu^-$ branching fraction and effective lifetime and search for $B^0 \to \mu^+\mu^-$ decays*, *Phys. Rev. Lett.* **118** (2017) 191801 [1703.05747].

[77] S. Descotes-Genon, M. Novoa-Brunet and K. K. Vos, *The time-dependent angular analysis of $B_d \to K_S\ell\ell$, a new benchmark for new physics*, *JHEP* **02** (2021) 129 [2008.08000].

[78] R. Fleischer, E. Malami, A. Rehult and K. K. Vos, *Fingerprinting cp-violating new physics with $b \to k\mu^+\mu^-$.*, *JHEP* **03** (2023) 113 [2212.09575].

[79] B. Batell, M. Pospelov and A. Ritz, *Multi-lepton Signatures of a Hidden Sector in Rare B Decays*, *Phys. Rev. D* **83** (2011) 054005 [0911.4938].

[80] J. A. Dror, R. Lasenby and M. Pospelov, *Dark forces coupled to nonconserved currents*, *Phys. Rev. D* **96** (2017) 075036 [1707.01503].

[81] B. Bhattacharya, A. Datta, D. London and S. Shivashankara, *Simultaneous Explanation of the R_K and $R(D^{(*)})$ Puzzles*, *Phys. Lett. B* **742** (2015) 370 [1412.7164].

[82] L. Calibbi, A. Crivellin and T. Ota, *Effective Field Theory Approach to $b \to s\ell\ell^{(')}$, $B \to K^{(*)}\nu\bar\nu$ and $B \to D^{(*)}\tau\nu$ with Third Generation Couplings*, *Phys. Rev. Lett.* **115** (2015) 181801 [1506.02661].

[83] D. Hill, "*First steps with flavour physics studies at FCC-ee.*" *Talk at the 4th FCC Physics and Experiments Workshop*, 2020.

[84] LHCb collaboration, *Measurement of CP-violating and mixing-induced observables in $B_s^0 \to \phi\gamma$ decays*, *Phys. Rev. Lett.* **123** (2019) 081802 [1905.06284].

[85] LHCb collaboration, *First Observation of the Radiative Decay $\Lambda_b^0 \to \Lambda\gamma$*, *Phys. Rev. Lett.* **123** (2019) 031801 [1904.06697].

[86] C. Bobeth and U. Haisch, *New Physics in Γ_{12}^s: $(\bar{s}b)(\bar\tau\tau)$ Operators*, *Acta Phys. Polon. B* **44** (2013) 127 [1109.1826].

[87] Q. Qin, Y.-L. Shen, C. Wang and Y.-M. Wang, *Deciphering the Long-Distance Penguin Contribution to $B^-{d,s} \to \gamma\gamma$ Decays*, *Phys. Rev. Lett.* **131** (2023) 091902 [2207.02691].

[88] Y.-L. Shen, Y.-M. Wang and Y.-B. Wei, *Precision calculations of the double radiative bottom-meson decays in soft-collinear effective theory*, *JHEP* **12** (2020) 169 [2009.02723].

[89] S. W. Bosch and G. Buchalla, *The Double radiative decays $B \longrightarrow gamma\ gamma$ in the heavy quark limit*, *JHEP* **08** (2002) 054 [hep-ph/0208202].

[90] ALEPH collaboration, *Limit on $B_{(s)}^0$ oscillation using a jet charge method*, *Phys. Lett. B* **356** (1995) 409.

[91] OPAL collaboration, *A Study of B meson oscillations using hadronic Z^0 decays containing leptons*, *Z. Phys. C* **76** (1997) 401 [hep-ex/9707009].

[92] DELPHI collaboration, *Search for B(s)0 anti-B(s)0 oscillations*, *Phys. Lett. B* **414** (1997) 382.

[93] LHCb collaboration, *Flavour Tagging in the LHCb experiment*, *PoS* **LHCP2018** (2018) 230.

[94] R. Aleksan, L. Oliver and E. Perez, *CP violation and determination of the bs flat unitarity triangle at an FCC-ee*, *Phys. Rev. D* **105** (2022) 053008 [2107.02002].

[95] Y.-F. Shen, W.-J. Song and Q. Qin, *CP violation induced by neutral meson mixing interference*, 2301.05848.

[96] M. T. Lucchini, W. Chung, S. C. Eno, Y. Lai, L. Lucchini, M.-T. Nguyen et al., *New perspectives on segmented crystal calorimeters for future colliders*, *JINST* **15** (2020) P11005 [2008.00338].

[97] J. Charles, O. Deschamps, S. Descotes-Genon and V. Niess, *Isospin analysis of charmless B-meson decays*, *Eur. Phys. J. C* **77** (2017) 574 [1705.02981].

[98] R. Aleksan, L. Oliver and E. Perez, *Study of CP violation in $B^\pm$ decays to $\overline{D^0}(D^0)K^\pm$ at FCCee*, 2107.05311.

[99] Y. K. Hsiao and C. Q. Geng, *Direct CP violation in Λ_b decays*, *Phys. Rev. D* **91** (2015) 116007 [1412.1899].

[100] Z.-J. Xiao, Y. Li, D.-T. Lin, Y.-Y. Fan and A.-J. Ma, $\bar{B}_s^0 \to (\pi^0 \eta^{(*)}, \eta^{(*)} \eta^{(*)})$ decays and the effects of next-to-leading order contributions in the perturbative QCD approach, *Phys. Rev. D* **90** (2014) 114028 [`1410.5274`].

[101] Z.-J. Xiao and X. Liu, *The two-body hadronic decays of B_c meson in the perturbative QCD approach: A short review*, *Chin. Sci. Bull.* **59** (2014) 3748 [`1401.0151`].

[102] W. Altmannshofer and P. Stangl, *New physics in rare B decays after Moriond 2021*, *Eur. Phys. J. C* **81** (2021) 952 [`2103.13370`].

[103] S. Descotes-Genon, S. Fajfer, J. F. Kamenik and M. Novoa-Brunet, *Probing CP violation in exclusive $b \to s\nu\bar{\nu}$ transitions*, *Phys. Rev. D* **107** (2023) 013005 [`2208.10880`].

[104] D. Bečirević, G. Piazza and O. Sumensari, *Revisiting $B \to K^{(*)}\nu\bar{\nu}$ decays in the Standard Model and beyond*, *Eur. Phys. J. C* **83** (2023) 252 [`2301.06990`].

[105] ATLAS collaboration, *Search for the lepton flavor violating decay $Z \to e\mu$ in pp collisions at $\sqrt{s}$ TeV with the ATLAS detector*, *Phys. Rev. D* **90** (2014) 072010 [`1408.5774`].

[106] ATLAS collaboration, *Search for charged-lepton-flavour violation in Z-boson decays with the ATLAS detector*, *Nature Phys.* **17** (2021) 819 [`2010.02566`].

[107] ATLAS collaboration, *Search for lepton-flavor-violation in Z-boson decays with τ-leptons with the ATLAS detector*, *Phys. Rev. Lett.* **127** (2022) 271801 [`2105.12491`].

[108] M. Dam, *Tau-lepton Physics at the FCC-ee circular e^+e^- Collider*, *SciPost Phys. Proc.* **1** (2019) 041 [`1811.09408`].

[109] D. Yu, "*Lepton identification and backgrounds for flavor studies at the CEPC.*" *Talk at the 2021 International CEPC Workshop*, 2021.

[110] W. Altmannshofer, P. Munbodh and T. Oh, *Probing Lepton Flavor Violation at Circular Electron-Positron Colliders*, `2305.03869`.

[111] L. Calibbi, X. Marcano and J. Roy, *Z lepton flavour violation as a probe for new physics at future e^+e^- colliders*, *Eur. Phys. J. C* **81** (2021) 1054 [`2107.10273`].

[112] W. Buchmuller and D. Wyler, *Effective Lagrangian Analysis of New Interactions and Flavor Conservation*, *Nucl. Phys. B* **268** (1986) 621.

[113] B. Grzadkowski and J. F. Gunion, *Using decay angle correlations to detect CP violation in the neutral Higgs sector*, *Phys. Lett.* **B350** (1995) 218 [`hep-ph/9501339`].

[114] Q. Qin, Q. Li, C.-D. Lü, F.-S. Yu and S.-H. Zhou, *Charged lepton flavor violating Higgs decays at future e^+e^- colliders*, *Eur. Phys. J. C* **78** (2018) 835 [`1711.07243`].

[115] R. Harnik, J. Kopp and J. Zupan, *Flavor Violating Higgs Decays*, *JHEP* **03** (2013) 026 [`1209.1397`].

[116] S. L. Glashow, D. Guadagnoli and K. Lane, *Lepton Flavor Violation in B Decays?*, *Phys. Rev. Lett.* **114** (2015) 091801 [`1411.0565`].

[117] ALEPH, DELPHI, L3, OPAL, SLD, LEP Electroweak Working Group, SLD Electroweak Group, SLD Heavy Flavour Group collaboration, *Precision electroweak measurements on the Z resonance*, *Phys. Rept.* **427** (2006) 257 [`hep-ex/0509008`].

[118] F. Feruglio, P. Paradisi and A. Pattori, *On the Importance of Electroweak Corrections for B Anomalies*, *JHEP* **09** (2017) 061 [`1705.00929`].

[119] M. Chrzaszcz, R. G. Suarez and S. Monteil, *Hunt for rare processes and long-lived particles at FCC-ee*, *Eur. Phys. J. Plus* **136** (2021) 1056 [2106.15459].

[120] BaBar collaboration, *A search for the decay modes $B^{+-} \to h^{+-}\tau^{+-}l$*, *Phys. Rev. D* **86** (2012) 012004 [1204.2852].

[121] LHCb collaboration, *Search for the lepton number violating decays $B^+ \to \pi^-\mu^+\mu^+$ and $B^+ \to K^-\mu^+\mu^+$*, *Phys. Rev. Lett.* **108** (2012) 101601 [1110.0730].

[122] LHCb collaboration, *Search for Majorana neutrinos in $B^- \to \pi^+\mu^-\mu^-$ decays*, *Phys. Rev. Lett.* **112** (2014) 131802 [1401.5361].

[123] LHCb collaboration, *Search for Baryon-Number Violating Ξ_b^0 Oscillations*, *Phys. Rev. Lett.* **119** (2017) 181807 [1708.05808].

[124] LHCb collaboration, *Evidence for CP violation in time-integrated $D^0 \to h^-h^+$ decay rates*, *Phys. Rev. Lett.* **108** (2012) 111602 [1112.0938].

[125] CDF collaboration, *Measurement of the difference of CP–violating asymmetries in $D^0 \to K^+K^-$ and $D^0 \to \pi^+\pi^-$ decays at CDF*, *Phys. Rev. Lett.* **109** (2012) 111801 [1207.2158].

[126] LHCb collaboration, *Observation of CP Violation in Charm Decays*, *Phys. Rev. Lett.* **122** (2019) 211803 [1903.08726].

[127] R. Bause, H. Gisbert, M. Golz and G. Hiller, *Rare charm $c \to u\nu\bar{\nu}$ dineutrino null tests for e^+e^- machines*, *Phys. Rev. D* **103** (2021) 015033 [2010.02225].

[128] NA62 collaboration, *The Beam and detector of the NA62 experiment at CERN*, *JINST* **12** (2017) P05025 [1703.08501].

[129] KOTO collaboration, *Search for the $K_L \to \pi^0\nu\bar{\nu}$ and $K_L \to \pi^0X^0$ decays at the J-PARC KOTO experiment*, *Phys. Rev. Lett.* **122** (2019) 021802 [1810.09655].

[130] E. Goudzovski et al., *New physics searches at kaon and hyperon factories*, *Rept. Prog. Phys.* **86** (2023) 016201 [2201.07805].

[131] A. A. Alves Junior et al., *Prospects for Measurements with Strange Hadrons at LHCb*, *JHEP* **05** (2019) 048 [1808.03477].

[132] A. Dery, M. Ghosh, Y. Grossman and S. Schacht, *$K \to \mu^+\mu^-$ as a clean probe of short-distance physics*, *JHEP* **07** (2021) 103 [2104.06427].

[133] A. Dery, M. Ghosh, Y. Grossman, T. Kitahara and S. Schacht, *A precision relation between $\Gamma(K \to \mu^+\mu^-)(t)$ and $\mathcal{B}(K_L \to \mu^+\mu^-)/\mathcal{B}(K_L \to \gamma\gamma)$*, *JHEP* **03** (2023) 014 [2211.03804].

[134] G. Burdman, E. Golowich, J. L. Hewett and S. Pakvasa, *Rare charm decays in the standard model and beyond*, *Phys. Rev. D* **66** (2002) 014009 [hep-ph/0112235].

[135] S. de Boer and G. Hiller, *Flavor and new physics opportunities with rare charm decays into leptons*, *Phys. Rev. D* **93** (2016) 074001 [1510.00311].

[136] S. Fajfer and N. Košnik, *Prospects of discovering new physics in rare charm decays*, *Eur. Phys. J. C* **75** (2015) 567 [1510.00965].

[137] R. Bause, M. Golz, G. Hiller and A. Tayduganov, *The new physics reach of null tests with $D \to \pi\ell\ell$ and $D_s \to K\ell\ell$ decays*, *Eur. Phys. J. C* **80** (2020) 65 [1909.11108].

[138] D. Guadagnoli and P. Koppenburg, *Lepton-flavor violation and lepton-flavor-universality violation in b and c decays*, in *Snowmass 2021*, 7, 2022, 2207.01851.

[139] S. De Boer and G. Hiller, *Null tests from angular distributions in $D \to P_1 P_2 l^+ l^-$, $l = e, \mu$ decays on and off peak*, *Phys. Rev. D* **98** (2018) 035041 [1805.08516].

[140] M. Golz, G. Hiller and T. Magorsch, *Pinning down $|\Delta c| = |\Delta u| = 1$ couplings with rare charm baryon decays*, *Eur. Phys. J. C* **82** (2022) 357 [2202.02331].

[141] BESIII collaboration, *Search for the decay $D^0 \to \pi^0 \nu \bar{\nu}$*, *Phys. Rev. D* **105** (2022) L071102 [2112.14236].

[142] J. Fuentes-Martin, A. Greljo, J. Martin Camalich and J. D. Ruiz-Alvarez, *Charm physics confronts high-p_T lepton tails*, *JHEP* **11** (2020) 080 [2003.12421].

[143] L.-F. Lai, X.-Q. Li, X.-S. Yan and Y.-D. Yang, *Prospects for discovering new physics in charm sector through low-energy scattering processes e-$p \to e$-$(\mu$-$)\Lambda c$*, *Phys. Rev. D* **105** (2022) 035007 [2111.01463].

[144] L.-F. Lai, X.-Q. Li, X.-S. Yan and Y.-D. Yang, *Searching and identifying leptoquarks through low-energy polarized scattering processes e-$p \to e$-Λc*, *Phys. Rev. D* **105** (2022) 115025 [2203.17104].

[145] Y.-R. Kong, L.-F. Lai, X.-Q. Li, X.-S. Yan and Y.-D. Yang, *Probing new physics with polarized τ and Λ_c in quasielastic $\nu_\tau + n \to \tau^- + \Lambda_c$ scattering process*, 2307.07239.

[146] S. Banerjee, *Searches for Lepton Flavor Violation in Tau Decays at Belle II*, *Universe* **8** (2022) 480 [2209.11639].

[147] X.-D. Shi, X.-R. Zhou, X.-S. Qin and H.-P. Peng, *A fast simulation package for STCF detector*, *JINST* **16** (2021) P03029 [2011.01654].

[148] R. Ferrari, *"PID with Dual-readout Calorimeters." Talk at the 2021 IAS Program on Particle Physics*, 2021.

[149] S. Giagu, L. Torresi and M. Di Filippo, *Tau Lepton Identification With Graph Neural Networks at Future Electron–Positron Colliders*, *Front. in Phys.* **10** (2022) 909205.

[150] PARTICLE DATA GROUP collaboration, *Review of Particle Physics*, *PTEP* **2022** (2022) 083C01.

[151] A. Celis, V. Cirigliano and E. Passemar, *Model-discriminating power of lepton flavor violating τ decays*, *Phys. Rev. D* **89** (2014) 095014 [1403.5781].

[152] L. Calibbi and G. Signorelli, *Charged Lepton Flavour Violation: An Experimental and Theoretical Introduction*, *Riv. Nuovo Cim.* **41** (2018) 71 [1709.00294].

[153] S. Banerjee et al., *Snowmass 2021 White Paper: Charged lepton flavor violation in the tau sector*, 2203.14919.

[154] A. Pich, *Precision Tau Physics*, *Prog. Part. Nucl. Phys.* **75** (2014) 41 [1310.7922].

[155] BESIII collaboration, *Future Physics Programme of BESIII*, *Chin. Phys. C* **44** (2020) 040001 [1912.05983].

[156] BELLE-II collaboration, *Measurement of the τ-lepton mass with the Belle˜II experiment*, 2305.19116.

[157] BELLE collaboration, *Measurement of the τ-lepton lifetime at Belle*, *Phys. Rev. Lett.* **112** (2014) 031801 [1310.8503].

[158] OPAL collaboration, *Measurement of the strong coupling constant alpha(s) and the vector*

and axial vector spectral functions in hadronic tau decays, *Eur. Phys. J. C* **7** (1999) 571 [`hep-ex/9808019`].

[159] ALEPH collaboration, *Branching ratios and spectral functions of tau decays: Final ALEPH measurements and physics implications*, *Phys. Rept.* **421** (2005) 191 [`hep-ex/0506072`].

[160] R. Tenchini, *Asymmetries at the Z pole: The Quark and Lepton Quantum Numbers*, *Adv. Ser. Direct. High Energy Phys.* **26** (2016) 161.

[161] A. Pich, *Challenges for tau physics at the TeraZ*, *Eur. Phys. J. Plus* **136** (2021) 1117 [`2012.07099`].

[162] X. Chen and Y. Wu, *Search for the Electric Dipole Moment and anomalous magnetic moment of the tau lepton at tau factories*, *JHEP* **10** (2019) 089 [`1803.00501`].

[163] A. Crivellin, M. Hoferichter and J. M. Roney, *Toward testing the magnetic moment of the tau at one part per million*, *Phys. Rev. D* **106** (2022) 093007 [`2111.10378`].

[164] DELPHI collaboration, *Study of tau-pair production in photon-photon collisions at LEP and limits on the anomalous electromagnetic moments of the tau lepton*, *Eur. Phys. J. C* **35** (2004) 159 [`hep-ex/0406010`].

[165] S. Eidelman and M. Passera, *Theory of the tau lepton anomalous magnetic moment*, *Mod. Phys. Lett. A* **22** (2007) 159 [`hep-ph/0701260`].

[166] M. Davier, A. Hocker and Z. Zhang, *The Physics of hadronic tau decays*, *Rev. Mod. Phys.* **78** (2006) 1043 [`hep-ph/0507078`].

[167] Y. S. Tsai, *Search for new mechanism of CP violation through tau decay and semileptonic decay of hadrons*, *Nucl. Phys. B Proc. Suppl.* **55** (1997) 293 [`hep-ph/9612281`].

[168] J. H. Kuhn and E. Mirkes, *CP violation in semileptonic tau decays with unpolarized beams*, *Phys. Lett.* **B398** (1997) 407 [`hep-ph/9609502`].

[169] D. Kimura, K. Y. Lee, T. Morozumi and K. Nakagawa, *CP violation in tau decays*, in *Heavy Quarks and Leptons 2008 (HQ&L08)*, 5, 2009, `0905.1802`.

[170] I. I. Bigi, *CP Violation in τ Decays at SuperB & Super-Belle II Experiments - like Finding Signs of Dark Matter*, *Nucl. Phys. Proc. Suppl.* **253-255** (2014) 91 [`1210.2968`].

[171] K. Kiers, *CP violation in hadronic τ decays*, *Nucl. Phys. Proc. Suppl.* **253-255** (2014) 95 [`1212.6921`].

[172] I. I. Bigi and A. I. Sanda, *A 'Known' CP asymmetry in tau decays*, *Phys. Lett.* **B625** (2005) 47 [`hep-ph/0506037`].

[173] Y. Grossman and Y. Nir, *CP Violation in $\tau \to \nu \pi K_S$ and $D \to \pi K_S$: The Importance of $K_S - K_L$ Interference*, *JHEP* **04** (2012) 002 [`1110.3790`].

[174] CLEO collaboration, *First search for CP violation in tau lepton decay*, *Phys. Rev. Lett.* **81** (1998) 3823 [`hep-ex/9805027`].

[175] CLEO collaboration, *Search for CP violation in tau —> K pi tau-neutrino decays*, *Phys. Rev. Lett.* **88** (2002) 111803 [`hep-ex/0111095`].

[176] BELLE collaboration, *Search for CP violation in $\tau \to K_S^0 \pi \nu_\tau$ decays at Belle*, *Phys. Rev. Lett.* **107** (2011) 131801 [`1101.0349`].

[177] BABAR collaboration, *Search for CP Violation in the Decay $\tau^- -> \pi^- K_S^0 (>= 0\pi^0)\nu_t au$*, *Phys. Rev. D* **85** (2012) 031102 [`1109.1527`].

[178] F.-Z. Chen, X.-Q. Li, Y.-D. Yang and X. Zhang, *CP asymmetry in $\tau \to K_S \pi \nu_\tau$ decays within the Standard Model and beyond*, *Phys. Rev. D* **100** (2019) 113006 [1909.05543].

[179] V. Cirigliano, A. Crivellin and M. Hoferichter, *A no-go theorem for non-standard explanations of the $\tau \to K_S \pi \nu_\tau$ CP asymmetry*, *Phys. Rev. Lett.* **120** (2018) 141803 [1712.06595].

[180] J. Rendón, P. Roig and G. Toledo Sánchez, *Effective-field theory analysis of the $\tau^- \to (K\pi)^- \nu_\tau$ decays*, *Phys. Rev.* **D99** (2019) 093005 [1902.08143].

[181] F.-Z. Chen, X.-Q. Li and Y.-D. Yang, *CP asymmetry in the angular distribution of $\tau \to K_S \pi \nu_\tau$ decays*, *JHEP* **05** (2020) 151 [2003.05735].

[182] F.-Z. Chen, X.-Q. Li, S.-C. Peng, Y.-D. Yang and H.-H. Zhang, *CP asymmetry in the angular distributions of $\tau \to K_S \pi \nu_\tau$ decays. Part II. General effective field theory analysis*, *JHEP* **01** (2022) 108 [2107.12310].

[183] H. Sang, X. Shi, X. Zhou, X. Kang and J. Liu, *Feasibility study of CP violation in $\tau \to K_S \pi \nu_\tau$ decays at the Super Tau Charm Facility*, *Chin. Phys. C* **45** (2021) 053003 [2012.06241].

[184] M. Beneke, G. Buchalla, M. Neubert and C. T. Sachrajda, *QCD factorization for $B \to \pi\pi$ decays: Strong phases and CP violation in the heavy quark limit*, *Phys. Rev. Lett.* **83** (1999) 1914 [hep-ph/9905312].

[185] M. Beneke, G. Buchalla, M. Neubert and C. T. Sachrajda, *QCD factorization for exclusive, nonleptonic B meson decays: General arguments and the case of heavy light final states*, *Nucl. Phys. B* **591** (2000) 313 [hep-ph/0006124].

[186] Y. Y. Keum, H.-N. Li and A. I. Sanda, *Penguin enhancement and $B \to K\pi$ decays in perturbative QCD*, *Phys. Rev. D* **63** (2001) 054008 [hep-ph/0004173].

[187] C.-D. Lu, K. Ukai and M.-Z. Yang, *Branching ratio and CP violation of $B \to \pi\pi$ decays in perturbative QCD approach*, *Phys. Rev. D* **63** (2001) 074009 [hep-ph/0004213].

[188] Y. Grossman, M. König and M. Neubert, *Exclusive Radiative Decays of W and Z Bosons in QCD Factorization*, *JHEP* **04** (2015) 101 [1501.06569].

[189] CMS collaboration, *Search for rare decays of Z and Higgs bosons to J/ψ and a photon in proton-proton collisions at $\sqrt{s} = 13$ TeV*, *Eur. Phys. J. C* **79** (2019) 94 [1810.10056].

[190] S. Cheng and Q. Qin, *$Z \to \pi^+\pi^-, K^+K^-$: A touchstone of the perturbative QCD approach*, *Phys. Rev. D* **99** (2019) 016019 [1810.10524].

[191] L. Bergstrom and R. W. Robinett, *ON the rare decays $Z \to VV$ and $Z \to VP$*, *Phys. Rev. D* **41** (1990) 3513.

[192] M. König and M. Neubert, *Exclusive Radiative Higgs Decays as Probes of Light-Quark Yukawa Couplings*, *JHEP* **08** (2015) 012 [1505.03870].

[193] H. Liang, Y. Zhu and M. Ruan, *"Measurement of V_{cb} from $WW \to \mu\nu qq$ at the CEPC."* *Talk at CEPC Flavor Physics Discussion*, 2023.

[194] S. Descotes-Genon, A. Falkowski, M. Fedele, M. González-Alonso and J. Virto, *The CKM parameters in the SMEFT*, *JHEP* **05** (2019) 172 [1812.08163].

[195] N. Escudero, C. Muñoz and A. M. Teixeira, *Flavor changing neutral currents in supersymmetric multi-higgs doublet models*, *Phys. Rev. D* **73** (2006) 055015.

[196] C. T. Hill and E. H. Simmons, *Strong Dynamics and Electroweak Symmetry Breaking*, *Phys. Rept.* **381** (2003) 235 [hep-ph/0203079].

[197] D. Barducci et al., *Interpreting top-quark LHC measurements in the standard-model effective field theory*, 1802.07237.

[198] L. Shi and C. Zhang, *Probing the top quark flavor-changing couplings at CEPC*, *Chin. Phys. C* **43** (2019) 113104 [1906.04573].

[199] ATLAS collaboration, *Search for single top-quark production via flavour-changing neutral currents at 8 TeV with the ATLAS detector*, *Eur. Phys. J. C* **76** (2016) 55 [1509.00294].

[200] ATLAS collaboration, *Search for flavor-changing neutral currents in top quark decays $t \to Hc$ and $t \to Hu$ in multilepton final states in proton-proton collisions at $\sqrt{s} = 13$ TeV with the ATLAS detector*, *Phys. Rev. D* **98** (2018) 032002 [1805.03483].

[201] ATLAS collaboration, *Search for flavour-changing neutral current top-quark decays $t \to qZ$ in proton-proton collisions at $\sqrt{s} = 13$ TeV with the ATLAS detector*, *JHEP* **07** (2018) 176 [1803.09923].

[202] CMS collaboration, *Search for Anomalous Single Top Quark Production in Association with a Photon in pp Collisions at $\sqrt{s} = 8$ TeV*, *JHEP* **04** (2016) 035 [1511.03951].

[203] CMS collaboration, *Search for anomalous Wtb couplings and flavour-changing neutral currents in t-channel single top quark production in pp collisions at $\sqrt{s} = 7$ and 8 TeV*, *JHEP* **02** (2017) 028 [1610.03545].

[204] G. Durieux, F. Maltoni and C. Zhang, *Global approach to top-quark flavor-changing interactions*, *Phys. Rev. D* **91** (2015) 074017 [1412.7166].

[205] A. Cerri et al., *Report from Working Group 4: Opportunities in Flavour Physics at the HL-LHC and HE-LHC*, *CERN Yellow Rep. Monogr.* **7** (2019) 867 [1812.07638].

[206] BaBar collaboration, *Observation of a narrow meson decaying to $D_s^+ \pi^0$ at a mass of 2.32-GeV/c^2*, *Phys. Rev. Lett.* **90** (2003) 242001 [hep-ex/0304021].

[207] Belle collaboration, *Observation of a resonance-like structure in the $pi^\pm \psi'$ mass distribution in exclusive $B \to K\pi^\pm \psi'$ decays*, *Phys. Rev. Lett.* **100** (2008) 142001 [0708.1790].

[208] BESIII collaboration, *Observation of a Charged Charmoniumlike Structure in $e^+e^- \to \pi^+\pi^- J/\psi$ at $\sqrt{s}$ =4.26 GeV*, *Phys. Rev. Lett.* **110** (2013) 252001 [1303.5949].

[209] Belle collaboration, *Study of $e^+e^- \to \pi^+\pi^- J/\psi$ and Observation of a Charged Charmoniumlike State at Belle*, *Phys. Rev. Lett.* **110** (2013) 252002 [1304.0121].

[210] LHCb collaboration, *Observation of $J/\psi p$ Resonances Consistent with Pentaquark States in $\Lambda_b^0 \to J/\psi K^- p$ Decays*, *Phys. Rev. Lett.* **115** (2015) 072001 [1507.03414].

[211] LHCb collaboration, *Observation of a narrow pentaquark state, $P_c(4312)^+$, and of two-peak structure of the $P_c(4450)^+$*, *Phys. Rev. Lett.* **122** (2019) 222001 [1904.03947].

[212] LHCb collaboration, *Observation of an exotic narrow doubly charmed tetraquark*, *Nature Phys.* **18** (2022) 751 [2109.01038].

[213] BESIII collaboration, *Observation of a Near-Threshold Structure in the K^+ Recoil-Mass Spectra in $e^+e^- \to K^+(D_s^- D^{*0} + D_s^{*-} D^0)$*, *Phys. Rev. Lett.* **126** (2021) 102001 [2011.07855].

[214] LHCв collaboration, *Observation of New Resonances Decaying to $J/\psi K^+ +$ and $J/\psi\phi$*, *Phys. Rev. Lett.* **127** (2021) 082001 [2103.01803].

[215] S. Godfrey and N. Isgur, *Mesons in a Relativized Quark Model with Chromodynamics*, *Phys. Rev. D* **32** (1985) 189.

[216] H.-X. Chen, W. Chen, X. Liu and S.-L. Zhu, *The hidden-charm pentaquark and tetraquark states*, *Phys. Rept.* **639** (2016) 1 [1601.02092].

[217] A. Hosaka, T. Iijima, K. Miyabayashi, Y. Sakai and S. Yasui, *Exotic hadrons with heavy flavors: X, Y, Z, and related states*, *PTEP* **2016** (2016) 062C01 [1603.09229].

[218] H.-X. Chen, W. Chen, X. Liu, Y.-R. Liu and S.-L. Zhu, *A review of the open charm and open bottom systems*, *Rept. Prog. Phys.* **80** (2017) 076201 [1609.08928].

[219] A. Esposito, A. Pilloni and A. D. Polosa, *Multiquark Resonances*, *Phys. Rept.* **668** (2017) 1 [1611.07920].

[220] R. F. Lebed, R. E. Mitchell and E. S. Swanson, *Heavy-Quark QCD Exotica*, *Prog. Part. Nucl. Phys.* **93** (2017) 143 [1610.04528].

[221] F.-K. Guo, C. Hanhart, U.-G. Meißner, Q. Wang, Q. Zhao and B.-S. Zou, *Hadronic molecules*, *Rev. Mod. Phys.* **90** (2018) 015004 [1705.00141].

[222] A. Ali, J. S. Lange and S. Stone, *Exotics: Heavy Pentaquarks and Tetraquarks*, *Prog. Part. Nucl. Phys.* **97** (2017) 123 [1706.00610].

[223] S. L. Olsen, T. Skwarnicki and D. Zieminska, *Nonstandard heavy mesons and baryons: Experimental evidence*, *Rev. Mod. Phys.* **90** (2018) 015003 [1708.04012].

[224] Y.-R. Liu, H.-X. Chen, W. Chen, X. Liu and S.-L. Zhu, *Pentaquark and Tetraquark states*, *Prog. Part. Nucl. Phys.* **107** (2019) 237 [1903.11976].

[225] N. Brambilla, S. Eidelman, C. Hanhart, A. Nefediev, C.-P. Shen, C. E. Thomas et al., *The XYZ states: Experimental and theoretical status and perspectives*, *Phys. Rep.* **873** (2020) 1 [1907.07583].

[226] F.-K. Guo, X.-H. Liu and S. Sakai, *Threshold cusps and triangle singularities in hadronic reactions*, *Prog. Part. Nucl. Phys.* **112** (2020) 103757 [1912.07030].

[227] H.-X. Chen, W. Chen, X. Liu, Y.-R. Liu and S.-L. Zhu, *An updated review of the new hadron states*, *Rept. Prog. Phys.* **86** (2023) 026201 [2204.02649].

[228] C.-H. Chang and Y.-Q. Chen, *The Production of $B_{(c)}$ or $\bar{B}_{(c)}$ meson associated with two heavy quark jets in Z^0 boson decay*, *Phys. Rev.* **D46** (1992) 3845.

[229] OPAL collaboration, *Search for the B_c meson in hadronic Z^0 decays*, *Phys. Lett. B* **420** (1998) 157 [hep-ex/9801026].

[230] DELPHI collaboration, *Search for the B(c) Meson*, *Phys. Lett. B* **398** (1997) 207.

[231] ALEPH collaboration, *Search for the B_c meson in hadronic Z decays*, *Phys. Lett. B* **402** (1997) 213.

[232] LHCв collaboration, *Study of the doubly charmed tetraquark T_{cc}^+*, *Nature Commun.* **13** (2022) 3351 [2109.01056].

[233] J. P. Ader, J. M. Richard and P. Taxil, *DO NARROW HEAVY MULTI - QUARK STATES EXIST?*, *Phys. Rev. D* **25** (1982) 2370.

[234] A. V. Manohar and M. B. Wise, *Exotic Q Q anti-q anti-q states in QCD*, *Nucl. Phys. B* **399** (1993) 17 [hep-ph/9212236].

[235] M. Karliner and J. L. Rosner, *Discovery of doubly-charmed Ξ_{cc} baryon implies a stable $(bb\bar{u}\bar{d})$ tetraquark*, *Phys. Rev. Lett.* **119** (2017) 202001 [1707.07666].

[236] E. J. Eichten and C. Quigg, *Heavy-quark symmetry implies stable heavy tetraquark mesons $Q_iQ_j\bar{q}_k\bar{q}_l$*, *Phys. Rev. Lett.* **119** (2017) 202002 [1707.09575].

[237] J.-J. Wu, L. Zhao and B. S. Zou, *Prediction of super-heavy N^* and Λ^* resonances with hidden beauty*, *Phys. Lett. B* **709** (2012) 70 [1011.5743].

[238] Q. Qin, Y.-F. Shen and F.-S. Yu, *Discovery potentials of double-charm tetraquarks*, *Chin. Phys. C* **45** (2021) 103106 [2008.08026].

[239] A. Ali, A. Y. Parkhomenko, Q. Qin and W. Wang, *Prospects of discovering stable double-heavy tetraquarks at a Tera-Z factory*, *Phys. Lett. B* **782** (2018) 412 [1805.02535].

[240] Z.-S. Jia, P.-P. Shi, Z.-H. Zhang, G. Li and F.-K. Guo, *Production of hadronic molecules at the Z pole (in preparation)*, 2023.

[241] P. Artoisenet and E. Braaten, *Estimating the Production Rate of Loosely-bound Hadronic Molecules using Event Generators*, *Phys. Rev. D* **83** (2011) 014019 [1007.2868].

[242] F.-K. Guo, U.-G. Meißner, W. Wang and Z. Yang, *Production of the bottom analogs and the spin partner of the X(3872) at hadron colliders*, *Eur. Phys. J. C* **74** (2014) 3063 [1402.6236].

[243] M. Albaladejo, F.-K. Guo, C. Hanhart, U.-G. Meißner, J. Nieves, A. Nogga et al., *Note on X(3872) production at hadron colliders and its molecular structure*, *Chin. Phys. C* **41** (2017) 121001 [1709.09101].

[244] C. Bierlich et al., *A comprehensive guide to the physics and usage of PYTHIA 8.3*, 2203.11601.

[245] M.-L. Du, V. Baru, X.-K. Dong, A. Filin, F.-K. Guo, C. Hanhart et al., *Coupled-channel approach to T_{cc}^+ including three-body effects*, *Phys. Rev. D* **105** (2022) 014024 [2110.13765].

[246] X. Luo, Y.-Z. Jiang, G.-Y. Zhang and Z. Sun, *Doubly-charmed baryon production in Z boson decay*, 2206.05965.

[247] J.-J. Niu, J.-B. Li, H.-Y. Bi and H.-H. Ma, *Production of Excited Doubly Heavy Baryons at the Super-Z Factory*, 2305.15362.

[248] C. Antel et al., *Feebly Interacting Particles: FIPs 2022 workshop report*, in *Workshop on Feebly-Interacting Particles*, 5, 2023, 2305.01715.

[249] M. Bauer, M. Neubert and A. Thamm, *Collider Probes of Axion-Like Particles*, *JHEP* **12** (2017) 044 [1708.00443].

[250] J. Liu, X. Ma, L.-T. Wang and X.-P. Wang, *ALP explanation to the muon (g-2) and its test at future Tera-Z and Higgs factories*, *Phys. Rev. D* **107** (2023) 095016 [2210.09335].

[251] L. Calibbi, Z. Huang, S. Qin, Y. Yang and X. Yin, *Testing axion couplings to leptons in Z decays at future e+e- colliders*, *Phys. Rev. D* **108** (2023) 015002 [2212.02818].

[252] K. Cheung and C. J. Ouseph, *Axion Like Particle Search at Higgs Factories*, 2303.16514.

[253] M. He, X.-G. He, C.-K. Huang and G. Li, *Search for a heavy dark photon at future e^+e^- colliders*, *JHEP* **03** (2018) 139 [1712.09095].

[254] FCC-EE STUDY TEAM collaboration, *Search for Heavy Right Handed Neutrinos at the FCC-ee*, *Nucl. Part. Phys. Proc.* **273-275** (2016) 1883 [`1411.5230`].

[255] J.-N. Ding, Q. Qin and F.-S. Yu, *Heavy neutrino searches at future Z-factories*, *Eur. Phys. J. C* **79** (2019) 766 [`1903.02570`].

[256] Y.-F. Shen, J.-N. Ding and Q. Qin, *Monojet search for heavy neutrinos at future Z-factories*, *Eur. Phys. J. C* **82** (2022) 398 [`2201.05831`].

[257] H.-C. Cheng, L. Li and E. Salvioni, *A theory of dark pions*, *JHEP* **01** (2022) 122 [`2110.10691`].

[258] L. Calibbi, D. Redigolo, R. Ziegler and J. Zupan, *Looking forward to lepton-flavor-violating ALPs*, *JHEP* **09** (2021) 173 [`2006.04795`].

[259] BELLE-II collaboration, *Search for Lepton-Flavor-Violating τ Decays to a Lepton and an Invisible Boson at Belle II*, *Phys. Rev. Lett.* **130** (2023) 181803 [`2212.03634`].

[260] A. Blondel et al., *Searches for long-lived particles at the future FCC-ee*, *Front. in Phys.* **10** (2022) 967881 [`2203.05502`].

[261] H.-C. Cheng, X. Jiang, L. Li and E. Salvioni, "Phenomenology of Electroweak Portal Dark Shower: High Energy Direct Probes and Low Energy Complementarity (In Preparation)." 2023.

[262] J. F. Kamenik and C. Smith, *FCNC portals to the dark sector*, *JHEP* **03** (2012) 090 [`1111.6402`].

[263] L. Calibbi, F. Goertz, D. Redigolo, R. Ziegler and J. Zupan, *Minimal axion model from flavor*, *Phys. Rev. D* **95** (2017) 095009 [`1612.08040`].

[264] D. Aloni, C. Fanelli, Y. Soreq and M. Williams, *Photoproduction of Axionlike Particles*, *Phys. Rev. Lett.* **123** (2019) 071801 [`1903.03586`].

[265] J. Martin Camalich, M. Pospelov, P. N. H. Vuong, R. Ziegler and J. Zupan, *Quark Flavor Phenomenology of the QCD Axion*, *Phys. Rev. D* **102** (2020) 015023 [`2002.04623`].

[266] CLEO collaboration, *Search for the familon via B+- —> pi+- X0, B+- —> K+- X0, and B0 —> K0(S)X0 decays*, *Phys. Rev. Lett.* **87** (2001) 271801 [`hep-ex/0106038`].

[267] A. Akeroyd and C.-H. Chen, *Constraint on the branching ratio of $B_c \to \tau\bar{\nu}$ from LEP1 and consequences for $R(D^{(*)})$ anomaly*, *Phys. Rev. D* **96** (2017) 075011 [`1708.04072`].

[268] LHCB collaboration, *Measurement of the ratio of branching fractions $\mathcal{B}(B_c^+ \to J/\psi\tau^+\nu_\tau)/\mathcal{B}(B_c^+ \to J/\psi\mu^+\nu_\mu)$*, *Phys. Rev. Lett.* **120** (2018) 121801 [`1711.05623`].

[269] LHCB collaboration, *Observation of the decay $\Lambda_b^0 \to \Lambda_c^+\tau^-\overline{\nu}_\tau$*, *Phys. Rev. Lett.* **128** (2022) 191803 [`2201.03497`].

[270] ATLAS collaboration, *Measurement of the CP-violating phase ϕ_s in $B_s^0 \to J/\psi\phi$ decays in ATLAS at 13 TeV*, *Eur. Phys. J. C* **81** (2021) 342 [`2001.07115`].

[271] GEANT4 collaboration, *GEANT4–a simulation toolkit*, *Nucl. Instrum. Meth. A* **506** (2003) 250.

[272] DELPHES 3 collaboration, *DELPHES 3, A modular framework for fast simulation of a generic collider experiment*, *JHEP* **02** (2014) 057 [`1307.6346`].

[273] Z. Zhao, S. Yang, M. Ruan, M. Liu and L. Han, *Measurement of the effective weak mixing angle at the CEPC**, *Chin. Phys. C* **47** (2023) 123002 [2204.09921].

[274] Y. Zhu, H. Liang, Y. Wang, H. Qu, C. Zhou and M. Ruan, *ParticleNet and its application on CEPC Jet Flavor Tagging*, 2309.13231.